A Dissertation for the Degree of Doctor of Philosophy

Estimation of Total Phenolic Contents Based on UV-B Radiation Interception in Three-Dimensional Structure of Kale Leaves under Controlled Environment

제어 환경 하에서 재배한 케일의 3차원 구조 내
자외선-B 수광량 기반 총 페놀 함량 추정

BY

HYO IN YOON

FEBRUARY, 2022

MAJOR IN HORTICULTURAL SCIENCE AND BIOTECHNOLOGY
DEPARTMENT OF AGRICULTURE, FORESTRY, AND BIORESOURCES
THE GRADUATE SCHOOL OF SEOUL NATIONAL UNIVERSITY

Estimation of Total Phenolic Contents Based on UV-B Radiation Interception in Three-Dimensional Structure of Kale Leaves under Controlled Environment

UNDER THE DIRECTION OF DR. JUNG EEK SON
SUBMITTED TO THE FACULTY OF THE GRADUATE SCHOOL
OF SEOUL NATIONAL UNIVERSITY

BY

HYO IN YOON

MAJOR IN HORTICULTURAL SCIENCE AND BIOTECHNOLOGY
DEPARTMENT OF AGRICULTURE, FORESTRY, AND BIORESOURCES

FEBRUARY, 2022

APPROVED AS A QUALIFIED DISSERTATION OF HYO IN YOON
FOR THE DEGREE OF DOCTOR OF PHILOSOPHY
BY THE COMMITTEE MEMBERS

CHAIRMAN
_____
EUN JIN LEE, PH.D.

VICE-CHAIRMAN
_____
JUNG EEK SON, PH.D.

MEMBER
_____
HEE JAE LEE, PH.D.

MEMBER
_____
MYUNG-MIN OH, PH.D.

MEMBER
_____
JONGYUN KIM, PH.D.

Estimation of Total Phenolic Contents Based on UV-B Radiation Interception in Three-Dimensional Structure of Kale Leaves under Controlled Environment

Hyo In Yoon

Department of Agriculture, Forestry, and Bioresources

The Graduate School of Seoul National University

ABSTRACT

Ultraviolet-B (UV-B, 280-315 nm) radiation has been used as a photo-elicitor to enhance the accumulation of bioactive compounds in plants. Local accumulation of phenolics, due to uneven UV-B exposure at leaf position and age-dependent sensitivity to UV-B radiation, is unpredictable in plant structures. This study aimed to analyze the relationship between the UV-B-induced phenolic contents and UV-B radiation interception in plant structures, to develop statistical models for estimating the distribution of phenolic contents, and to evaluate the UV-B light-emitting diodes (LEDs) lighting system with simulation-based scenario analysis in plant factories. Kale (*Brassica oleracea* L. var. *acephala*) plants grown under a plant factory for 3, 4, and 5 weeks were exposed to UV-B LEDs with a peak at 310 nm for 12 h per day for 1 or 2 days

right before harvest. Spatial distribution of UV-B radiation interception (UVR$_{int}$) in kale plants was quantified using ray-tracing simulation with three-dimensional-scanned plant model. According to three harvest time, multiple regression models for phenolic content were developed based on daily UVR$_{int}$ and developmental age of individual leaves using a second-order multi-polynomial equation. Two UV-B LED arrangements were used to estimate model parameters. Scenario analysis was performed with lighting system factors, such as vertical or horizontal lighting distance and lighting angle of UV-B LED bars. The pre-harvest UV-B radiation did not cause noticeable changes in growth, photochemical activity, or chlorophyll content. Total phenolic content (TPC), total flavonoid content (TFC), UV-absorbing pigment content, and antioxidant capacity were significantly higher in UV-B exposed leaves. At a whole plant level, the intraindividual distributions of TPC or TFC could be determined by daily UVR$_{int}$ and leaf order, and were more heterogeneous than those without UV-B radiation. The developed models predicted accurately with $R^2 > 0.78$ and normalized root mean squared error of about 30% in the test data. From the models, the dependence of UV-B energy yield on plant and leaf developmental age was confirmed. In most scenario results, the uniformity and efficiency were opposite for both total phenolic and flavonoid production. These results suggest that the prediction model using UV-B radiation interception can be used to improve UV-B radiation use efficiency and to optimize the lighting system. These results will contribute to increasing

the commercial application of UV-B radiation for bioactive compound production in plant factories.

Additional keywords: abiotic stress, antioxidants, bioactive compounds, flavonoids, plant factory, ray-tracing simulation, secondary metabolites

Student number: 2018-35422

CONTENTS

Chapter 1. Quantitative Analysis of UV-B Radiation Interception in Three-Dimensional Structures of Kale Leaves and Intraindividual Distribution of Phenolic Contents

Chapter 2. Prediction of Total Phenolic Contents in Three-Dimensional Structure of Kale Leaves According to UV-B Radiation Interception and Developmental Age

Chapter 3. Evaluation of UV-B Lighting Design for Phenolic Production in Kale Leaves Using Optical Simulation with Three-Dimensional Plant Models in Plant Factories

LIST OF TABLES

LIST OF FIGURES

GENERAL INTRODUCTION

Plant factory is a novel plant production system that controls the environment independently of the external environment and addresses the demands of consumers (SharathKumar et al., 2020). The plant factories can provide appropriate environments for the stable production of highly functional/high-value-added plants, such as medicinal plants and functional vegetables (Kozai, 2018). Kale (*Brassica oleracea* L. var. *acephala*) is a functional vegetable that benefits human health and is a rich source of health-promoting phytochemicals with antioxidant capacity (Šamec et al., 2019). Accumulation of such bioactive compounds in plants are enhanced through abiotic elicitation (Thakur et al., 2019). The stressful condition can also reduce the plant yield and quality. Therefore, the practical application of abiotic stress for bioactive compound accumulation requires an understanding of plant sensitivity and optimal conditions (Toscano et al., 2019). Ultraviolet (UV) radiation, especially UV-B (280-315 nm), has been reported to be an effective elicitor for enhancing their accumulation in various plants and can be easily applied to controlled environments (Singh et al., 2017).

UV region of the solar radiation is divided into UV-A (315-400 nm), UV-B, and UV-C (100-280 nm). UV-C and short-wavelength UV-B can trigger stress response in plants, damaging DNA and proteins due to the higher energy of UV quanta (Loconsole and Santamaria, 2021). However, UV-B radiation promotes

the phenolic accumulation more efficiently than UV-A with less energy or duration (Rechner et al., 2016; Moreira-Rodríguez et al., 2017). Short-term UV-B exposure near harvest is effective with minimal growth loss and energy cost (Dou et al., 2019; Toscano et al., 2019; Yoon et al., 2020). Although artificial light sources of UV-B radiation have not often been used in horticulture due to high prices and the uncontrollable energy and spectrum of traditional UV-B lamps, rapid technical advances of UV light-emitting diodes (LEDs) provide new opportunities for the precise manipulation of UV-B radiation with the desired wavelength and intensity for plants (Neugart and Schreiner, 2018; Kneissl et al., 2019). Efficient control methods for the artificial UV-B light sources should be identified for the commercial application of UV-B radiation for phenolic accumulation.

However, UV-B radiation utilization efficiency has not been sufficiently substantiated for the accumulation of bioactive compounds in plants. UV-B responses depend on its properties such as wavelength, fluence rate, and exposure time (Jenkins, 2009). The plant and leaf developmental stages are strong determinants of stress responses, resulting in different susceptibility at both organ and whole-plant levels (Rankenberg et al., 2021). The leaf developmental age and UV-B exposure co-determines the responses (Csepregi et al., 2017). However, the developmental age is not the only factor determining intraindividual heterogeneity of stress response. In general, plant structures are complex and three-dimensional (3D), with the non-uniform leaf distribution

and specific phyllotaxis. Under UV-B exposure, younger leaves located near the top of the plant can be more exposed than older leaves, which rely on light penetration in the plant's 3D structure. At the leaf level, optical properties such as absorption, reflection, and transmittance affect UV exposure to cells, tissues, and individual leaves (Robson et al., 2015, 2019). Even within a whole-plant, heterogenous UV-B exposure and sensitivity induce various responses in plants.

In plant factories, the harvest time for leafy vegetables is determined by minimizing the loss of light utilization efficiency as growth progresses and maximizing productivity per unit area. In South Korea, lettuce plants grown in plant factories are generally harvested when their leaf fresh mass reached about 120 g. In this study, kale plants were harvested 3-5 weeks after transplanting, when the fresh mass of the aerial part reached approximately 80-200 g. This study aimed to analyze the relationship between the UV-B-induced phenolic contents and UV-B radiation interception in plant structure through 3D models and optical simulations, to develop statistical model for estimating the distribution of phenolic contents, and to evaluate and optimize the lighting system with the simulation-based scenario analysis in controlled environments. This study is limited to the scope of pre-harvest UV-B exposure as triggers for the biosynthesis of phenolics in plants grown without UV-B radiation. The overall flow of this study is described in Fig. 1.
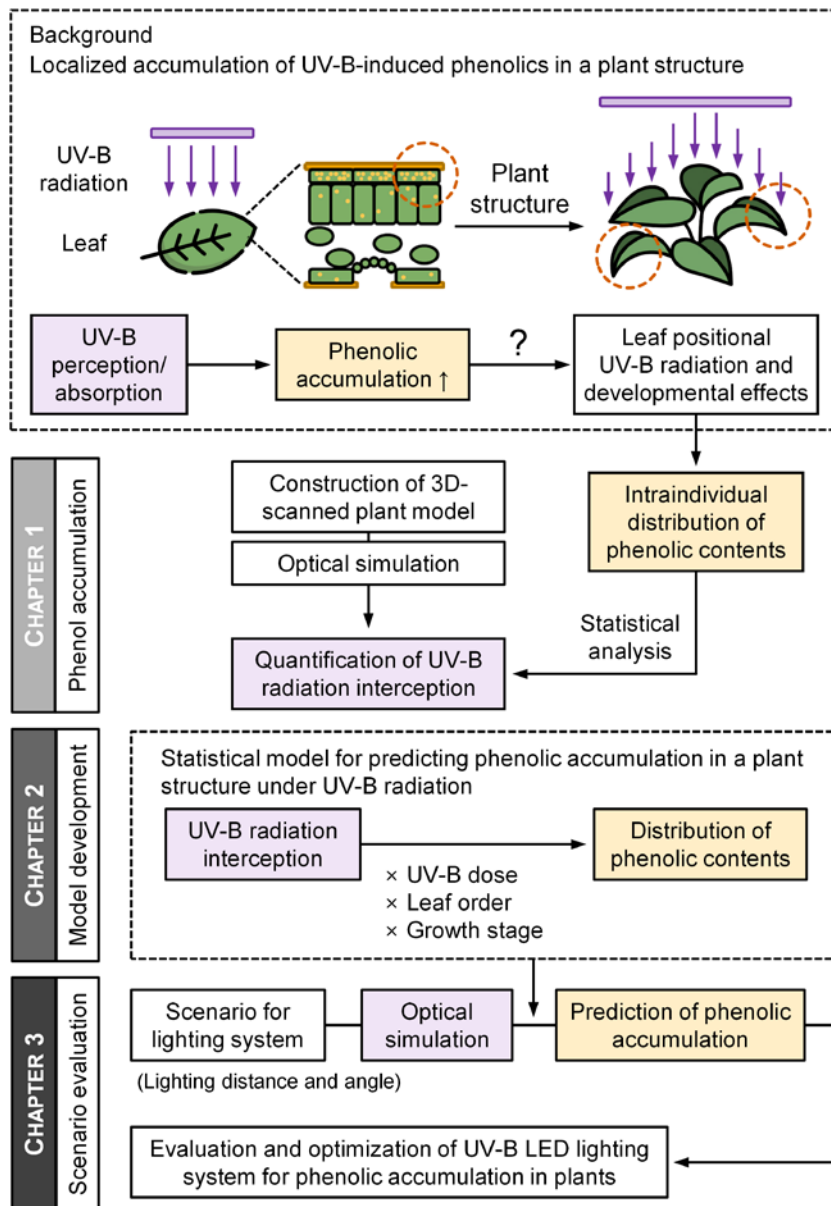
Fig. 1. The overall flow of this study. 3D, three-dimensional; LED, light-emitting diode.

LITERATURE REVIEW

Kale (*Brassica oleracea* L. var. *acephala*)

Antioxidant-rich vegetables and fruits have been reported to have health-promoting effects (Finley et al., 2011; Wang et al., 2011; Zhang et al., 2015; Adegbola et al., 2017). Kale has often been on the lists of commonly used term 'superfood' and has been considered as a source of nutraceuticals. Its main biological activities are antioxidant capacity, anticarcinogenic activity, and protection of cardiovascular and gastrointestinal tract (Cohen et al., 2000; Wang et al., 2004; Šamec et al., 2019). The high antioxidant capacities are attributed to its polyphenols, carotenoids, glucosinolates, and vitamin C and E (Galati and O'Brien, 2004; Lafarga et al., 2018). Phenolics, especially quercetin- and kaempferol-glycosides which are abundant in kale plants, have a wide range of beneficial properties for human health (Ortega-Hernández et al., 2021). These phenolics as secondary metabolites predominately accumulated in the vacuoles of epidermal and guard cells, are involved in plant defense mechanisms against to abiotic and biotic stressors (Singh et al., 2017). Kale belonging to the genus *Brassica* is characterized by the leaves which do not form a head. Kale leaves are commonly consumed fresh as salads or juice, and recently consumed as dried chips or freeze-dried powder. Kale-added apple juice (Biegańska-Marecik et al., 2017) and kale-added bread (Klopsch et al., 2019) have also been consumed. Such novel nutraceuticals have been developed to enhance their

economic value by improving the antioxidant capacities of kale plants.

Plant response to UV-B radiation

UV region of the solar spectrum is divided into UV-A, UV-B, and UV-C, of which only UV-A and UV-B at wavelengths greater than 290 nm reach the earth's surface. Plants perceive UV-B radiation through the UV-B specific UV RESISTANCE LOCUS 8 (UVR8) photoreceptor identified in *Arabidopsis* (Rizzini et al., 2011). The UV-B perception induces dissociation of the UVR8 homodimer, interacting with CONSTITUTIVE PHOTOMORPHOGENESIS1 (COP1) and initiating the UVR8-mediated UV-B signaling pathway (Wu et al., 2012). The signal transduction of UVR8-COP1 with the ELONGATED HYPOCOTYL5 (HY5) transcription factor plays a central role in the regulation of genes in photomorphogenic responses, including the biosynthesis of UV-protective phenolics and flavonoids (Heijde and Ulm, 2012; Robson et al., 2015). The UVR8 dimer can be re-associated by interaction of RUP2 (REPRESSOR OF UV-B PHOTOMORPHOGENESIS 2) protein (Heijde and Ulm, 2013). UVR8 signaling depends on the activity of the UVR8 monomer, but increased UV-B exposure in UV-B-acclimated plants results in UVR8 dimer/monomer cycle (Liao et al., 2020). UV-B responses are also mediated by nonspecific signaling pathway, which involve DNA damage and reactive oxygen species (ROS) accumulation (Jansen et al., 1998; Hideg et al., 2013).

UV-B radiation has been reported to have negative effects on photosynthetic

reactions, including chlorophyll fluorescence, CO_2 fixation, and stability of the

D1 and D2 proteins of photosystem II; however, at ambient or low UV-B levels,

the effects are less sensitive than expected (Jenkins, 2009; Hideg et al., 2013;

Wargent and Jordan, 2013; Martínez-Lüscher et al., 2013, 2015). The

accumulated phenolics act as UV-screen pigments in epidermal tissues and

increase their innate antioxidant potential for scavenging ROS generated under

UV-B exposure (Solovchenko and Merzlyak, 2008). UV-B radiation stimulates

both nonspecific and specific signaling pathway, depending on the UV-B

properties such as wavelength, fluence rate, and exposure duration (Jenkins,

2009).

Manipulation of UV-B radiation in horticulture

Two approaches to manipulate UV-B radiation in horticulture are UV-B

exclusion and supplementation (Schreiner et al., 2014). While the UV-B

exclusion is typically performed in greenhouse using specific filters such as

UV-absorbing covering materials, the UV-B supplementation is conducted in

greenhouse or growth chambers using artificial UV-B lamps. UV-B responses

depend on its properties related to the dose such as wavelength, fluence rate,

and exposure duration (Jenkins, 2009). In addition, various factors such as

sources (solar, broad-band, or narrow-band), exposure timing during a day, and

setup (greenhouses or growth chamber) also affect the both pathway and

determine UV-B response (Meyer et al., 2021). Traditional UV-B lamps were

prone to cause photosynthetic damage to plants due to the broad-band wavelength range including shorter wavelength close to UV-C as well as excessive and difficult-to-control energy (Mosadegh et al., 2019; Yoon et al., 2020). Recently, the performance of LED has been advanced to provide new opportunities for the precise manipulation of UV-B radiation with the desired wavelength and intensity for plants (Kneissl et al., 2019; Loi et al., 2020; Paradiso and Proietti, 2021).

Light interception with plant structure

Attenuation of photosynthetically active radiation (PAR, 400-700 nm) and UV radiation within plant canopies cannot be described easily due to the non-uniform spatial distribution of the leaves, non-random leaf angles, and their changes with the depth of the canopy or even with time (Aphalo et al., 2012). At the leaf level, optical properties such as absorption, reflection, and transmittance affect UV exposure to cells, tissues, and individual leaves (Robson et al., 2015, 2019). The decreases in UV irradiance with the canopy depth alter the UV/PAR ratio, which can determine the sensitivity to plant responses to UV (Deckmyn and Impens, 1997). Modeling the light environment perceived by plant organs have been studied in silico using Monte Carlo ray-tracing method and 3D plant model in the PAR range (Vos et al., 2010). Beyond simplified or virtual plant models, 3D-scanned plant models are sophisticated enough to be used for extracting morphological traits (Dornbusch et al., 2007;

Paulus et al., 2014) or estimating the canopy photosynthesis (Shin et al., 2021). In controlled environments, the optical simulations can be applied to analyze the light environment with artificial lighting (Hitz et al., 2019), and to analyze light interception of leafy vegetables along with 3D-scanned plant models (Kim et al., 2020; Saito et al., 2020).

LITERATURE CITED

Adegbola P, Aderibigbe I, Hammed W, Omotayo T (2017) Antioxidant and anti-inflammatory medicinal plants have potential role in the treatment of cardiovascular disease: A review. Am J Cardiovasc Dis 7:19–32.

Aphalo PJ, Albert A, Björn LO, McLeod AR, Robson TM, Rosenqvist E (Eds.) (2012) Beyond the visible: A handbook of best practice in plant UV photobiology. COST Action FA0906 UV4growth. Univ. of Helsinki, Finland.

Biegańska-Marecik R, Radziejewska-Kubzdela E, Marecik R (2017) Characterization of phenolics, glucosinolates, and antioxidant activity of beverages based on apple juice with addition of frozen and freeze-dried curly kale leaves (*Brassica oleracea* L. var. *acephala* L.). Food Chem 230:271–280.

Cohen JH, Kristal AR, Stanford JL (2000) Fruit and vegetable intakes and prostate cancer risk. J Natl Cancer Inst 92:61–68.

Csepregi K, Coffey A, Cunningham N, Prinsen E, Hideg É, Jansen MAK (2017) Developmental age and UV-B exposure co-determine antioxidant capacity and flavonol accumulation in *Arabidopsis* leaves. Environ Exp Bot 140:19–25.

Deckmyn G, Impens I (1997) The ratio UV-B/photosynthetically active radiation (PAR) determines the sensitivity of rye to increased UV-B

radiation. Environ Exp Bot 37:3–12.

Di Wu, Hu Q, Yan Z, Chen W, Yan C, Huang X, Zhang J, Yang P, Deng H, Wang J, Deng X, Shi Y (2012) Structural basis of ultraviolet-B perception by UVR8. Nature 484:214–219.

Dornbusch T, Wernecke P, Diepenbrock W (2007) A method to extract morphological traits of plant organs from 3D point clouds as a database for an architectural plant model. Ecol Model 200:119–129.

Dou H, Niu G, Gu M (2019) Pre-harvest UV-B radiation and photosynthetic photon flux density interactively affect plant photosynthesis, growth, and secondary metabolites accumulation in basil (*Ocimum Basilicum*) plants. Agronomy 9:434.

Finley JW, Kong AN, Hintze KJ, Jeffery EH, Ji LL, Lei XG (2011) Antioxidants in foods: State of the science important to the food industry. J Agric Food Chem 59:6837–6846.

Galati G, O'Brien PJ (2004) Potential toxicity of flavonoids and other dietary phenolics: Significance for their chemopreventive and anticancer properties. Free Radic Biol Med 37:287–303.

Heijde M, Ulm R (2012) UV-B photoreceptor-mediated signaling in plants. Trends Plant Sci 17:230–237.

Heijde M, Ulm R (2013) Reversion of the *Arabidopsis* UV-B photoreceptor UVR8 to the homodimeric ground state. Proc Natl Acad Sci USA 110:1113–1118.

Hideg É, Jansen MAK, Strid Å (2013) UV-B exposure, ROS, and stress: Inseparable companions or loosely linked associates? Trends Plant Sci 18:107–115.

Hitz T, Henke M, Graeff-Hönninger S, Munz S (2019) Three-dimensional simulation of light spectrum and intensity within an LED growth chamber. Comput Electron Agric 156:540–548.

Jansen MAK, Gaba V, Greenberg BM (1998) Higher plants and UV-B radiation: Balancing damage, repair, and acclimation. Trends Plant Sci 3:131–135.

Jenkins GI (2009) Signal transduction in responses to UV-B radiation. Annu Rev Plant Biol 60:407–431.

Kim J, Kang WH, Son JE (2020) Interpretation and evaluation of electrical lighting in plant factories with ray-tracing simulation and 3D plant modeling. Agronomy 10:1545.

Klopsch R, Baldermann S, Voss A, Rohn S, Schreiner M, Neugart S (2019) Narrow-banded UVB affects the stability of secondary plant metabolites in kale (*Brassica oleracea* var. *sabellica*) and pea (*Pisum sativum*) leaves being added to lentil flour fortified bread: A novel approach for producing functional foods. Foods 8:427.

Kneissl M, Seong T-Y, Han J, Amano H (2019) The emergence and prospects of deep-ultraviolet light-emitting diode technologies. Nat Photonics 13:233–244.

Kozai T (2018) Smart plant factory. Springer, Singapore.

Lafarga T, Viñas I, Bobo G, Simó J, Aguiló-Aguayo I (2018) Effect of steaming and sous vide processing on the total phenolic content, vitamin C, and antioxidant potential of the genus *Brassica*. Innov Food Sci Emerg Technol 47:412–420.

Liao X, Liu W, Yang H, Jenkins GI (2020) A dynamic model of UVR8 photoreceptor signaling in UV-B-acclimated *Arabidopsis*. New Phytol 227:857–866.

Loconsole D, Santamaria P (2021) UV lighting in horticulture: A sustainable tool for improving production quality and food safety. Horticulturae 7:9.

Loi M, Villani A, Paciolla F, Mulè G, Paciolla C (2020) Challenges and opportunities of light-emitting diode (LED) as key to modulate antioxidant compounds in plants: A review. Antioxidants 10:42.

Martínez-Lüscher J, Morales F, Delrot S, Sánchez-Díaz M, Gomés E, Aguirreolea J, Pascual I (2013) Short- and long-term physiological responses of grapevine leaves to UV-B radiation. Plant Sci 213:114–122.

Martínez-Lüscher J, Morales F, Delrot S, Sánchez-Díaz M, Gomès E, Aguirreolea J, Pascual I (2015) Characterization of the adaptive response of grapevine (cv. Tempranillo) to UV-B radiation under water deficit conditions. Plant Sci 232:13–22.

Meyer P, Van de Poel B, De Coninck B (2021) UV-B light and its application potential to reduce disease and pest incidence in crops. Hortic Res 8:194.

Moreira-Rodríguez M, Nair V, Benavides J, Cisneros-Zevallos L, Jacobo-

Velázquez DA (2017) UVA, UVB light doses and harvesting time differentially tailor glucosinolate and phenolic profiles in broccoli sprouts. Molecules 22:1065.

Mosadegh H, Trivellini A, Lucchesini M, Ferrante A, Maggini R, Vernieri P, Sodi AM (2019) UV-B physiological changes under conditions of distress and eustress in sweet basil. Plants 8:396.

Neugart S, Schreiner M (2018) UVB and UVA as eustressors in horticultural and agricultural crops. Sci Hortic 234:370–381.

Ortega-Hernández E, Antunes-Ricardo M, Jacobo-Velázquez DA (2021) Improving the health-benefits of kales (*Brassica oleracea* L. var. *acephala* DC) through the application of controlled abiotic stresses: A review. Plants 10:2629.

Paradiso R, Proietti S (2021) Light-quality manipulation to control plant growth and photomorphogenesis in greenhouse horticulture: The state of the art and the opportunities of modern LED systems. J Plant Growth Regul doi:10.1007/s00344-021-10337-y.

Paulus S, Schumann H, Kuhlmann H, Léon J (2014) High-precision laser scanning system for capturing 3D plant architecture and analyzing growth of cereal plants. Biosyst Eng 121:1–11.

Rankenberg T, Geldhof B, van Veen H, Holsteens K, Van de Poel B, Sasidharan R (2021) Age-dependent abiotic stress resilience in plants. Trends Plant Sci 26:692–705.

Rechner O, Neugart S, Schreiner M, Wu S, Poehling H-M (2016) Different narrow-band light ranges alter plant secondary metabolism and plant defense response to aphids. J Chem Ecol 42:989–1003.

Rizzini L, Favory J-J, Cloix C, Faggionato D, O'Hara A, Kaiserli E, Baumeister R, Schäfer E, Nagy F, Jenkins GI, Ulm R (2011) Perception of UV-B by the *Arabidopsis* UVR8 protein. Science 332:103–106.

Robson TM, Aphalo PJ, Banaś AK, Barnes PW, Brelsford CC, Jenkins GI, Kotilainen TK, Łabuz J, Martínez-Abaigar J, Morales LO, Neugart S, Pieristè M, Rai N, Vandenbussche F, Jansen MAK (2019) A perspective on ecologically relevant plant-UV research and its practical application. Photochem Photobiol Sci 18:970–988.

Robson TM, Klem K, Urban O, Jansen MAK (2015) Re-interpreting plant morphological responses to UV-B radiation. Plant Cell Environ 38:856–866.

Saito K, Ishigami Y, Goto E (2020) Evaluation of the light environment of a plant factory with artificial light by using an optical simulation. Agronomy 10:1663.

Šamec D, Urlić B, Salopek-Sondi B (2019) Kale (*Brassica oleracea* var. *acephala*) as a superfood: Review of the scientific evidence behind the statement. Crit Rev Food Sci Nutr 59:2411–2422.

Schreiner M, Martínez-Abaigar J, Glaab J, Jansen M (2014) UV-B induced secondary plant metabolites. Opt Photonik 9:34–37.

SharathKumar M, Heuvelink E, Marcelis LFM (2020) Vertical farming:

Moving from genetic to environmental modification. Trends Plant Sci 25:724–727.

Shin J, Hwang I, Kim D, Moon T, Kim J, Kang WH, Son JE (2021) Evaluation of the light profile and carbon assimilation of tomato plants in greenhouses with respect to film diffuseness and regional solar radiation using ray-tracing simulation. Agric For Meteorol 296:108219.

Singh VP, Singh S, Prasad SM, Parihar P (Eds.) (2017) UV-B radiation: From environmental stressor to regulator of plant growth. John Wiley & Sons, Ltd., Chichester, UK.

Solovchenko AE, Merzlyak MN (2008) Screening of visible and UV radiation as a photoprotective mechanism in plants. Russ J Plant Physiol 55:719–737.

Thakur M, Bhattacharya S, Khosla PK, Puri S (2019) Improving production of plant secondary metabolites through biotic and abiotic elicitation. J Appl Res Med Aromat Plants 12:1–12.

Toscano S, Trivellini A, Cocetta G, Bulgari R, Francini A, Romano D, Ferrante A (2019) Effect of preharvest abiotic stresses on the accumulation of bioactive compounds in horticultural produce. Front Plant Sci 10:1–17.

Vos J, Evers JB, Buck-Sorlin GH, Andrieu B, Chelle M, de Visser PHB (2010) Functional-structural plant modeling: A new versatile tool in crop science. J Exp Bot 61:2101–2115.

Wang LI, Giovannucci EL, Hunter D, Neuberg D, Su L, Christiani DC (2004) Dietary intake of Cruciferous vegetables, *Glutathione S-transferase* (GST)

polymorphisms and lung cancer risk in a Caucasian population. Cancer Causes Control 15:977–985.

Wang S, Melnyk JP, Tsao R, Marcone MF (2011) How natural dietary antioxidants in fruits, vegetables, and legumes promote vascular health. Food Res Int 44:14–22.

Wargent JJ, Jordan BR (2013) From ozone depletion to agriculture: Understanding the role of UV radiation in sustainable crop production. New Phytol 197:1058–1076.

Yoon HI, Kim D, Son JE (2020) Spatial and temporal bioactive compound contents and chlorophyll fluorescence of kale (*Brassica oleracea* L.) under UV-B exposure near harvest time in controlled environments. Photochem Photobiol 96:845–852.

Zhang Y-J, Gan R-Y, Li S, Zhou Y, Li A-N, Xu D-P, Li H-B (2015) Antioxidant phytochemicals for the prevention and treatment of chronic diseases. Molecules 20:21138–21156.

Quantitative Analysis of UV-B Radiation Interception in Three-Dimensional Structures of Kale Leaves and Intraindividual Distribution of Phenolic Contents

ABSTRACT

Ultraviolet-B (UV-B) acts as a regulatory stimulus, inducing the dose-dependent biosynthesis of phenolics including flavonoids at the leaf level. However, the heterogeneity of biosynthesis activation generated within a whole plant has not been fully understood until now and cannot be interpreted without quantification of UV-B radiation interception. In this study, spatial UV-B radiation interception of kale (*Brassica oleracea* L. var. *acephala*) plants was analyzed using ray-tracing simulation with three-dimensional-scanned models and leaf optical properties. The kale plants grown under a plant factory for 26 days after transplanting were subjected to UV-B radiation generated by light-emitting didoes with a peak at 310 nm for 12 h per day during 2 days right before harvest. The UV-B-induced phenolics accumulated more, with higher UV-B radiation interception and younger leaves. To distinguish the effects of UV-B energy and leaf developmental age, the contents were regressed

separately and simultaneously. The UV-B radiation interception contributed much more to determining total flavonoid content than leaf order, but relatively less to determining total phenolic content. This study confirmed the feasibility and relevance of UV-B radiation interception analysis and paves the way to explore the physical and physiological base determining the intraindividual distribution of phenolics under controlled environments.

INTRODUCTION

Ultraviolet (UV) radiation, especially UV-B (280-315 nm), has long been considered a potential stressor for plants, damaging DNA, proteins, and membranes caused by reactive oxygen species (ROS) generated due to the higher energy of UV-B quanta (Jansen et al., 1998). High doses of UV-B, such as a higher fluence rate, longer duration, and shorter wavelength, are likely to cause metabolic disorders, such as photosystem II (PSII) photodamage, and ultimately lead to death (Hu et al., 2013; Bashri et al., 2018; Khudyakova et al., 2019; Mosadegh et al., 2019). In contrast, low doses or ambient levels of UV-B, in which antioxidant capacity is sufficient to deal with the ROS level inflicted by UV-B, initiate numerous acclimation strategies, including changes in plant morphological, physiological, and biochemical traits (Jenkins, 2009; Hideg et al., 2013; Robson et al., 2015; Takshak and Agrawal, 2015; Schulze et al., 2019). One of the strategies is the accumulation of phenylpropanoids and flavonoids in the epidermis as a direct sun-screening strategy and their innate antioxidant potential to protect sensitive tissues from damage caused by UV-B exposure (Clé et al., 2008; Solovchenko and Merzlyak, 2008; Mewis et al., 2012; Si et al., 2015; Takshak and Agrawal, 2019). UV-B-induced phenolic accumulation increases linearly with UV-B dose and absorbance at the leaf level (Bilger et al., 2001; Hagen et al., 2009; Dou et al., 2019). The phenolic accumulation at the whole-plant level is determined by the leaf developmental

age (Majer and Hideg, 2012; Csepregi et al., 2017). A typical three-dimensional (3D) plant structure not only consists of leaves at different ages and positions, but also causes different UV-B intensities on the leaf surface, leading to the complexity of UV-B-induced responses within the whole plant.

UV exposure patterns in plants rely on both the radiation incident on the leaf surface and the absorption, reflection, and transmittance of the leaves, causing UV exposure to diverge into cells, tissues, and individual leaves (Robson et al., 2015, 2019). The penetration of UV radiation within a leaf depends on whether sun or shade leaves are present (Liakoura et al., 2003). Therefore, UV exposure patterns can be affected by plant architecture and leaf optical properties. However, the actual distribution of light harvest on the plant surface is difficult to be measured; thus, the patterns are still poorly understood at the whole-plant level. Recently, light interception analyses based on a 3D plant model have been conducted by ray-tracing simulation (Tang et al., 2015; Kim et al., 2016; Jung et al., 2018). Beyond simplified or virtual plant models, 3D-scanned plant models are sophisticated enough to be used for extracting morphological traits and plant architecture such as leaf width and plant height (Dornbusch et al., 2007; Paulus et al., 2014) and for estimating physiological responses of plants such as leaf or canopy photosynthesis (Kang et al., 2019; Kim et al., 2020a). In particular, 3D-scanned plant models and ray-tracing simulations can be applied to analyze the light environment and light interception of leafy vegetables grown under light-emitting diodes (LEDs) in

controlled environments (Hitz et al., 2019; Kim et al., 2020b). With the techniques, UV-B radiation absorbed by individual leaves can be quantified at the whole-plant level.

Even when exposed to the same stress level, the stress susceptibilities on individual leaves are determined by their developmental age. Many studies emphasize the importance of the plant's developmental stage for its antioxidant capacity and UV stress response (Heinze et al., 2018; Yoon et al., 2019). For phenolic accumulation within individual plants, the effects of leaf aging and positioning are non-separable (Wang and Lin, 2000; Vagiri et al., 2015). Thus, a few studies on the UV response according to leaf developmental age have been conducted in selected plants with a 2D structure, such as horizontal shoots of grapevines (Majer and Hideg, 2012) and rosettes of *Arabidopsis* (Csepregi et al., 2017). Uneven UV-B irradiation and leaf developmental age could result in spatial heterogeneity of plant stress levels and responses within a whole plant. The photochemical activity of PSII, which is sensitive to UV-B exposure, has been measured by chlorophyll fluorescence (ChlF) techniques and is considered to quantify the stress level on plants by various stressors, such as low temperature (Lee and Oh, 2015), drought (Yoon et al., 2020b), and UV-A (Lee et al., 2019) and UV-B radiation (Mosadegh et al., 2018; Dou et al., 2019; Khudyakova et al., 2019). Even within an individual plant, leaves more exposed to UV-B were found to have lower photochemical efficiency (F_v/F_m) values and higher contents of total flavonoids (Yoon et al., 2020a).

22

One of the hypotheses in this study is that the plant architecture and optical properties determine the spatial UV-B exposure pattern to a leaf surface within a whole plant. The other is that the leaf developmental age and UV-B level at individual leaves co-determine the plant's response to UV-B. This study aimed to reveal the interaction effect of UV-B radiation interception and leaf developmental age on total phenolic and flavonoid contents within a 3D plant structure in kale plants.

MATERIALS AND METHODS

Plant materials and growth conditions

Kale (*Brassica oleracea* L. var *acephala*) seeds were sown on sponge cubes in water culture under fluorescent lamps at a photosynthetic photon flux density (PPFD) of 150 μmol m^{-2} s^{-1} over the waveband 400-700 nm for 16-h light periods. The nutrient solution for *Brassica* was supplied with an electrical conductivity (EC) of 0.6 dS m^{-1} and pH of 6.9 after true leaves appeared. After the fourth true leaf appeared, the seedlings of uniform size were transplanted into plant factory modules with a deep flow technique system and were maintained at an air temperature of 20°C, a relative humidity of 70%, and a CO_2 concentration of 500 μmol mol^{-1}. The plants were irradiated with red, blue, and white (RBW) LEDs at a PPFD of 200 μmol m^{-2} s^{-1} for 16-h light periods. The spectrum of the RBW LED was measured using a spectroradiometer (Blue-Wave spectrometer, StellarNet Inc., Tampa, FL, USA) in the range of 380-900 nm (Fig. 1-1a). The nutrient solution was supplied with an EC of 1.2 dS m^{-1}. The plants were harvested at 26 days after transplanting (DAT).

UV treatments

Enhanced UV-B radiation was provided by UV-B LED with a spectrum peak at about 310 nm, which consisted of five bar module arrays containing twelve chips per bar (Ericsong Co., Ltd., Bucheon, Korea). The plants were exposed
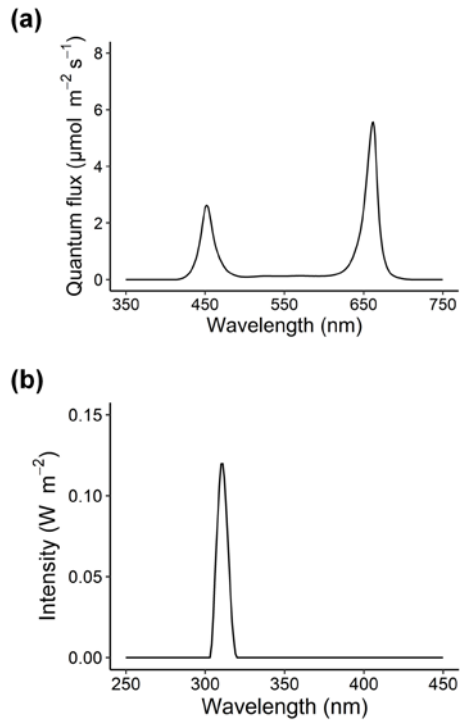
Fig. 1-1. Light spectra of red, blue, and white light-emitting diodes (RBW LEDs, a) and UV-B LED (b). RBW LED at a photosynthetically active radiation of 200 μmol m^{-2} s^{-1}; UV-B LED with a spectrum peak at 310 nm at a dose of 1.0 W m^{-2}.

to UV-B LEDs for 12 h per day for 2 days (+UV-B) with the RBW LEDs from the start of the light period and were harvested after recovery for 4 h. The UV-B dose was 1.0 W m^{-2} (43.2 kJ m^{-2} d^{-1}) at the bottom, which is equivalent to a biologically effective UV radiation (UV$_{BE}$) dose of 4.4 kJ m^{-2} d^{-1} (UV-B$_{BE}$ = 4.2, UV-C$_{BE}$ = 0.0, and UV-A$_{BE}$ = 0.2 per day). UV$_{BE}$ was calculated using a plant action spectrum in the UV range (Flint and Caldwell, 2003). Neugart et al. (2012) reported that UV-B radiation with 200% of ambient UV-B$_{BE}$/PPFD ratio (6.5×10^{-4}) was most effective to enhance the individual flavonols in kale plants among the ratios of 50-200%. Referring to the results, the UV-B$_{BE}$/PPFD ratio in the present study was set to 214% of the ambient ratio. The light intensity and spectrum of the UV-B LED were measured with a UV sensor (MU-200, Apogee Instruments, Inc., Logan, UT, USA) and the spectroradiometer in the range of 280-400 nm (Fig. 1-1b).

ChlF imaging

ChlF images of each leaf were obtained by quenching analysis using a closed chlorophyll fluorescence imaging system (FluorCam 800MF, Photon Systems Instruments, Brno, Czech Republic), and its software (FluorCam 7, Photon Systems Instruments) was used to control the image system and to process the images. All leaves were measured separately at harvest after the recovery time with three replicates. The fluorescence was detected by a high-sensitivity CCD camera, generating 1360×1024-pixel images with 16-bit resolution. The light

source included two red-orange LED panels (617 nm) for measuring light (a short flash of very weak intensity) and actinic light and another pair of cool white LED panels (6,500 K) for saturating pulses with an angle of 45°. The detailed ChlF quenching protocol is described in Fig. 1-2a. After 20 min of dark adaptation, the minimum fluorescence (F_o) was determined with a measuring light (5 s duration, < 0.5 µmol m^{-2} s^{-1}), followed by a saturating light pulse (800 ms duration, 1,200 µmol m^{-2} s^{-1}) so that the maximum fluorescence in the dark-adapted state (F_m) was recorded. After dark relaxation for 17 s, the leaves were exposed to actinic light (70 s duration, 600 µmol m^{-2} s^{-1}). The instantaneous fluorescence during light adaptation was measured before any of the saturating pulses and later declined to steady-state fluorescence in light (F'). The saturating pulses were applied 5 times, determining the maximum fluorescence during light adaptation and at the light-adapted steady state (F'_m).

All images of ChlF parameters for each leaf on the whole plant were individually obtained using imaging system software (Fig. 1-2b). Based on the basic ChlF signals, the maximum quantum yield of PSII (F_v/F_m), nonphotochemical quenching (NPQ), and PSII operating efficiency (Φ_{PSII}) can be derived as a set of equations (Cen et al., 2017; Yao et al., 2018):

$$F_v/F_m = (F_m - F_o)/F_m \qquad \qquad \text{Eq. 1-1}$$

$$NPQ = (F_m - F'_m)/F'_m \qquad \qquad \text{Eq. 1-2}$$

$$\Phi_{PSII} = (F'_m - F')/F'_m \qquad \qquad \text{Eq. 1-3}$$
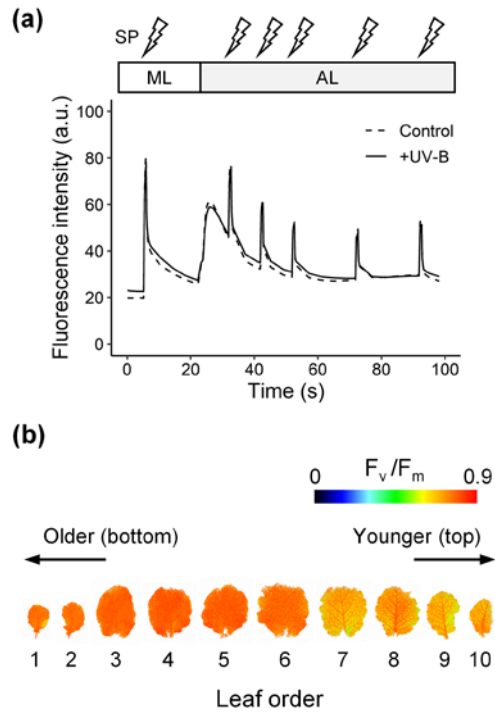
Fig. 1-2. Representative kinetic chlorophyll fluorescence curves (a) and the images according to the leaf order (b) of kale plants. ML, measuring light (a short flash of very weak intensity, 5 s duration, < 0.5 μmol m^{-2} s^{-1}); AL, actinic light; SP, saturating pulses (800 ms duration, 1,200 μmol m^{-2} s^{-1}); F_v/F_m, the maximum quantum yield of photosystem II (Eq. 1-1). The leaf order indicates the order from the oldest leaf at the bottom to the youngest leaf at the top in a whole plant.

A total of 250 ChlF images and kinetics were acquired. Data preprocessing and region-of-interest (ROI) selection were performed using the imaging system software, including segmentation for background exclusion and averaging within the ROI. The ROI was semi-automatically selected based on the same criteria, such as minimum size of selected pixels and selection range of signal level so that the entire leaf became one ROI. For statistical analysis, the mean and standard deviation of each parameter were obtained and analyzed.

Radiation interception on plants

3D-scanned plant model generation

Plant models were directly obtained by 3D scanning of three plants per treatment using a high-resolution portable 3D scanner (Go! SCAN50TM, Creaform Inc., Lévis, Quebec, Canada) with a resolution of 2 mm, and its scan software (Vxelement, Creaform Inc.) was used to record and export the scan data to mesh data. The 3D mesh data were corrected for holes and noise, and segmented into leaf mesh data. The segmented mesh data were then reconstructed into individual surface models for ray-tracing simulation using a reverse engineering software (Geomagic Design X, 3D Systems, Rock Hill, SC, USA). The constructed 3D plant models were transferred to a 3D computer-aided design (CAD) software (Solidworks, Dassault Systèmes, Vélizy-Villacoublay, France). The procedure from scan to simulation is described in Fig. 1-3.
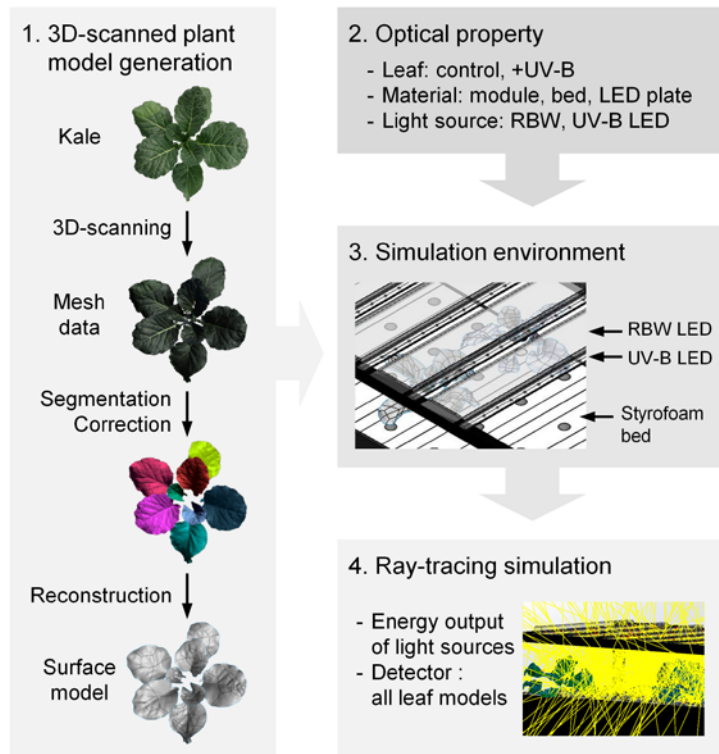
Fig. 1-3. Schematic diagram of radiation interception analysis from three-dimensional (3D) scanning to simulation in kale plants (modified from Kim et al., 2020a). RBW LED, red, blue, and white light-emitting diodes.

Optical properties and simulation environment

The spectral transmittance (Tr) and reflectance (Ref) of leaves were measured using the spectroradiometer at 1-nm resolution with a 50-mm integrating sphere (IC-2, StellarNet Inc.), and the optical properties of their 3D models were determined. The measurements were made on three leaves from three plants each per treatment, according to the leaf positions sampled at the top, middle, and bottom (Fig. 1-4). In the same way, the optical properties of the materials within the cultivation environment, such as the plant factory module, styrofoam bed, RBW LED plate, and UV-B LED bar, were measured.

For simulation, the materials of the cultivation environment were implemented as a 3D virtual environment using the 3D CAD software with the same size and layout as the actual environment. Spectral power distributions of RBW and UV-B LEDs were set with the measured spectra, and the physical light distribution was set as a Lambertian distribution with a half angle of 60°. All 3D models were placed in the same position and orientation as the actual materials and plants.

Ray-tracing simulation

The ray-tracing simulation was performed using a ray-tracing software (Optisworks, Optis Inc., La Farlède, France) with a total of 500 mega-rays. To match the light intensity in the virtual environment with the actual light intensity, a cylinder-shaped detector was modeled and placed based on the
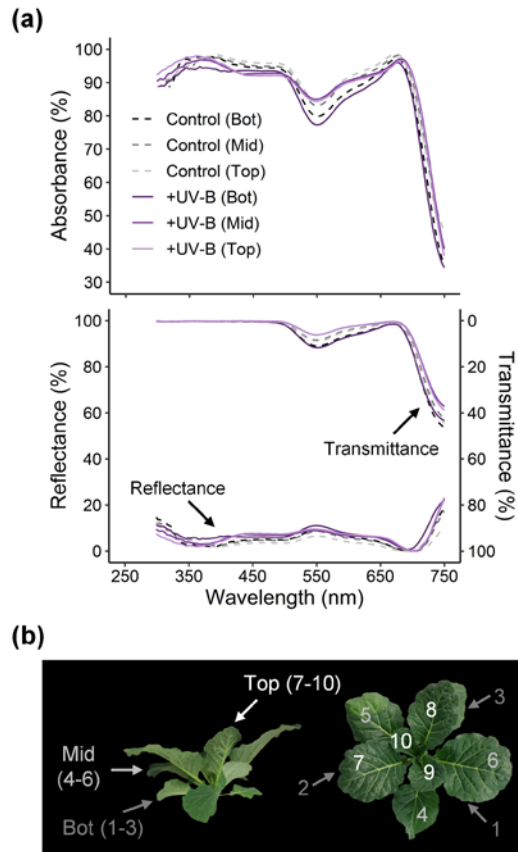
Fig. 1-4. Optical properties of leaves (a) at different positions (b) in kale plants. The transmittance, reflectance, and absorbance of kale leaves measured individually at the top (7-10th leaves), middle (4-6th leaves, Mid), and bottom (1st-3rd leaves, Bot) of the plant (b) in control and UV-B treatment (+UV-B) with three replicates.

quantum sensor. The energy outputs of light sources were set to 7.1017 W for RBW LED plates and 0.0176 W for UV-B LED chips, representing a PPFD of 200 μmol $m^{-2}\,s^{-1}$ and a UV intensity of 1.0 W m^{-2}, respectively. All leaf surface models were set up as separate detectors, and all simulations of the treatments were performed under the same conditions. The simulation results are represented as photosynthetically active radiation (PAR) interception in the range of 400-700 nm and UV radiation interception in the range of 280-400 nm.

Phenolics and antioxidant capacity (AOC)

Sample preparation

All leaves of three plants per treatment were sampled at 26 DAT and lyophilized using a freeze dryer (FD8512, Ilshin Biobase Co., Yangju, Korea) at −80°C under a vacuum of 0.007 mmHg for 120 h. The 50-mg freeze-dried samples were ground and extracted with 1 mL of 70% (v/v) methanol and 2.8-mm ceramic beads using a bead mill homogenizer (Beadruptor 4, Omni International, Kennesaw, GA, USA).

Total phenolic content (TPC)

TPC was measured by the Folin-Ciocalteu colorimetric method (Ainsworth and Gillespie, 2007). The extract was incubated in the dark at room temperature for 48 h and then centrifuged at 1×10^4 g for 10 min. The supernatant of 50 μL was collected in a 2-mL tube, and 750 μL of 10% Folin-Cioalteu solution (Junsei

Chemical Co., Ltd., Tokyo, Japan) and 135 μL of distilled water were added. After vortex mixing, 600 μL of 700 mM Na_2CO_3 was added, followed by incubation at room temperature for 2 h. The absorbance of the samples was read at 765 nm using a spectrophotometer (Photolab 6100vis, WTW, Weilheim, Germany), and the standard unit was expressed as milligrams of gallic acid (Sigma–Aldrich Chemical Corp., St. Louis, MO, USA) equivalent per gram of dry weight (mg GAE g^{-1} DW).

Total flavonoid content (TFC)

TFC was measured by the aluminum chloride colorimetric method (Dewanto et al., 2002). The extract was incubated in the dark at 4°C for 12 h and then centrifuged at 1×10^4 g for 10 min. The supernatant of 150 μL was collected in a 2-mL tube, and 135 μL of distilled water and 45 μL of 5% $NaNO_2$ were added. After 5 min, 90 μL of 10% $AlCl_3$ was added. After an additional 5 min, 300 μL of 1 M NaOH and 165 μL of distilled water were added, and all reactants were thoroughly mixed. After incubating for 6 min, the absorbance of the samples was read at 510 nm using the spectrophotometer, and the standard unit was expressed as milligrams of catechin acid (Supelco, Bellefonte, PA, USA) equivalent per gram of dry weight (mg CE g^{-1} DW).

AOC

AOC was measured using the 2,2-diphenyl-1-picrylhydrazyl (DPPH) assay

(Andarwulan et al., 2010). The DPPH was purchased from Alfa Aesar (Ward Hill, MA, USA). The extract was incubated in the dark at room temperature for 48 h and then centrifuged at 1×10^4 g for 10 min. The supernatant of 100 μL was collected in a 2-mL microtube, and 1.25 mL of 6 μM DPPH methanol solution was added. After reaction for 30 min, the absorbance values of the samples and blank were read at 517 nm (A_{sample} and A_{blank}, respectively). The AOC_{DPPH} was expressed as a percentage of DPPH radical scavenging activity as follows:

$$AOC_{DPPH}\ (\%) = (A_{blank} - A_{sample})/A_{blank} \times 100 \qquad \text{Eq. 1-4}$$

Plant growth characteristics

Leaf fresh weight was measured at harvest, and its dry weight was measured after drying in an oven at 70°C for 72 h. Leaf developmental age was numbered in order from the oldest leaf at the bottom to the youngest leaf at the top, ranging from 1 to 10 in all samples (Fig. 1-2b). The areas of individual leaves were obtained from the mesh data of the 3D plant model using the reverse engineering software.

Statistical analysis

All visualization and statistical analyses were performed using R software (R 3.6.2, R Foundation, Vienna, Austria) and SAS software (SAS institute Inc.,

Cary, NC, USA). Comparisons of the mean trait values between the treatments were performed with two-way ANOVA and Tukey's honestly significant difference (HSD) test to assess the effects of the UV-B treatment, leaf order, and their interactions. Pearson's correlation and multiple regression were also conducted. The regression result was evaluated by the coefficient of determination (R^2) and P-value, and the contribution of independent variables was evaluated by standard regression coefficient and squared semi-partial correlation.

RESULTS

Distributions of PAR and UV-B radiation interceptions on kale plants

The spatial distributions of PAR and UV radiation interceptions on the 3D kale models were visually depicted along with the actual plant structure, including leaf height, angle, and surface curvature (Fig. 1-5a, b). The PAR and UV radiation interceptions increased with height within the plants regardless of the treatments (Fig. 1-5c, d). On average, the PAR interception was similar in control and UV-B-treated plants (135.9 ± 6.17 and 129.2 ± 4.31 μmol m^{-2} s^{-1}, respectively). In the UV-B-treated plants, the average UV radiation interception was 0.70 ± 0.14 W m^{-2}, which is equivalent to 30.3 ± 5.83 kJ m^{-2} d^{-1}. The vertical distributions of PAR and UV radiation interceptions showed high linearity ($R^2 = 0.983$, $P < 0.001$, data not shown).

The distributions of PAR and UV radiation interceptions at different leaf orders were described with violin plots based on kernel density estimation and box plots (Fig. 1-6). Overall, the median radiation interception was lower in the bottom parts around the 1st-4th leaves and similar in the middle and upper parts. In particular, the distribution in the middle parts could not be characterized. For example, although the median values of PAR interception were similar in the 5th-8th leaves in the control, the bimodal density and longer box (interquartile range) indicated that the intercepted light intensity was extremely dispersed at the same leaf order.

37
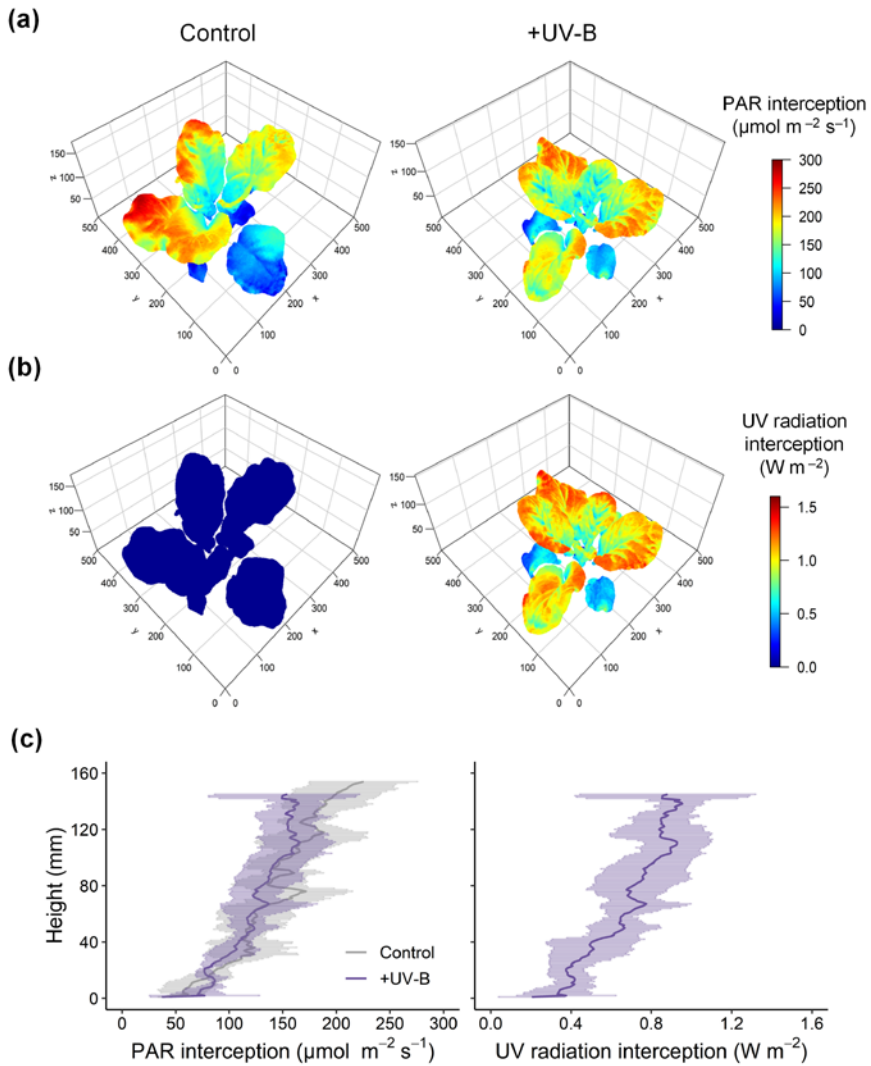
Fig. 1-5. Representative simulated photosynthetically active radiation (PAR, a) and biologically effective UV radiation (b) interceptions and vertical distributions (c) on control and UV-B-treated kale plants. The three axes (x, y, z) represent the actual size in mm. The centerline and area are represented as the mean ± SD ($n = 3$) at each height of the plant model.
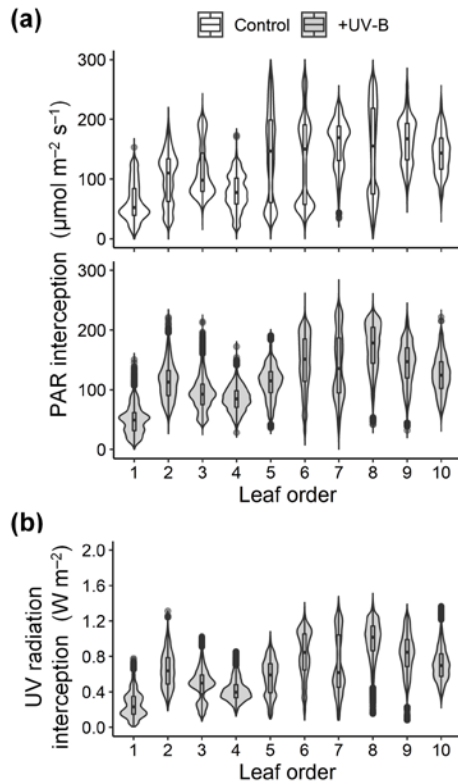
Fig. 1-6. Distributions of photosynthetically active radiation (PAR, a) and biologically effective UV radiation (b) interceptions on individual leaves of control and UV-B-treated kale plants. Leaf order indicates the order from the oldest leaf at the bottom to the youngest leaf at the top in a whole plant. Based on kernel density estimation, the shape of the violin represents the frequencies of values. The boxes, horizontal lines, whiskers, and points indicate interquartile ranges, medians, 95% confidence intervals, and outliers, respectively.

Growth characteristics according to UV-B radiation and leaf order

Both UV-B treatment and leaf order significantly affected the fresh weight and leaf area of individual kale leaves, but not dry weight (Table 1-1). When compared at the same leaf order, however, the three growth parameters at all orders were not significantly different between the control and UV-B-treated plants. Total growth parameters also decreased in the UV-B-treated plants, but were not significantly different from those in the control plants. Similarly, the total PAR interception per plant did not differ significantly between the control and the UV-B-treated plants (Table 1-2).

Leaf photochemistry and NPQ according to UV-B radiation and leaf order

Leaf photochemical efficiency was significantly affected by UV-B treatment or leaf order indicating leaf developmental age (Table 1-3). Both F_v/F_m and Φ_{PSII} decreased with younger leaves and were lower on average in the UV-B-treated plants than in the control. However, the F_v/F_m and Φ_{PSII} were not significantly different between the treatments at the same leaf order, and the interactions between UV-B treatment and leaf order could not be demonstrated. In contrast, NPQ was significantly affected by the UV-B treatment, leaf order, and their interaction. Across all data, Pearson's correlation coefficient between NPQ and leaf order was 0.54 at $P < 0.001$ (data not shown), indicating that the NPQ increased with younger leaves. The NPQ was higher in the UV-B treatment than in the control (0.64 and 0.49 on average, respectively). Compared to the control,

Table 1-1. Leaf growth of kale plants grown under the control and UV-B exposure conditions for 2 days before harvest.

Leaf order	Leaf fresh weight (g)		Leaf dry weight (g)		Leaf area (cm²)	
	Control	+UV-B	Control	+UV-B	Control	+UV-B
2	2.36 ± 1.54	2.66 ± 0.40	0.18 ± 0.11	0.21 ± 0.01	32.3 ± 9.7	45.2 ± 4.2
3	5.15 ± 2.84	4.87 ± 1.39	0.41 ± 0.26	0.38 ± 0.08	84.5 ± 49.4	87.2 ± 28.2
4	8.31 ± 1.55	8.57 ± 0.99	0.70 ± 0.20	0.82 ± 0.19	168.3 ± 34.4	155.0 ± 13.8
5	8.97 ± 1.33	8.44 ± 1.25	0.88 ± 0.14	0.86 ± 0.15	179.4 ± 17.0	186.9 ± 14.1
6	10.2 ± 2.56	8.62 ± 0.69	0.93 ± 0.33	0.89 ± 0.17	200.1 ± 36.4	178.1 ± 13.4
7	10.1 ± 1.09	7.06 ± 1.97	0.96 ± 0.21	0.79 ± 0.29	182.7 ± 20.0	147.1 ± 28.9
8	7.40 ± 1.76	5.80 ± 1.54	0.77 ± 0.21	0.66 ± 0.18	139.5 ± 17.9	115.1 ± 33.5
9	5.38 ± 0.86	4.18 ± 1.05	0.57 ± 0.09	0.50 ± 0.12	91.2 ± 1.8	64.2 ± 19.4
10	3.59 ± 0.53	2.82 ± 0.50	0.43 ± 0.08	0.37 ± 0.06	49.9 ± 6.4	37.7 ± 14.8
Total	79.5 ± 14.0	67.8 ± 6.3	7.39 ± 1.83	6.91 ± 0.94	1,142.5 ± 184.8	1,006.0 ± 67.6
Significance						
UV-B	*		ns		**	
Leaf order	***		***		***	
UV-B × leaf order	ns		ns		ns	

Leaf order indicates the leaf developmental age in order from the oldest leaf at the bottom to the youngest leaf at the top in a whole plant.

Data represent mean ± SD ($n = 3$).

Asterisks indicate significant differences by two-way ANOVA.

*, $P < 0.05$; **, $P < 0.01$; ***, $P < 0.001$; ns, not significant.

Table 1-2. Total radiation interception of kale plants grown under the control and UV-B exposure conditions for 2 days before harvest.

Treatment	Total radiation interception per plant	
	PAR (mmol d^{-1} per plant)	UV$_{BE}$ (MJ d^{-1} per plant)
Control	914.3 ± 209.50	-
+UV-B	739.5 ± 102.24	2.91 ± 0.47

Data represent mean $\pm$ SD ($n = 3$).

The means between the treatments were not significantly different.

PAR, photosynthetically active radiation in the range of 400-700 nm; UV$_{BE}$, biologically effective UV radiation in the range of 280-400 nm.

Table 1-3. Chlorophyll fluorescence parameters in individual leaves of kale plants grown under the control and UV-B exposure conditions for 2 days before harvest.

Leaf order	F_v/F_m		Φ_{PSII}		NPQ	
	Control	+UV-B	Control	+UV-B	Control	+UV-B
2	0.76 ± 0.01	0.77 ± 0.01	0.57 ± 0.01	0.61 ± 0.01	0.49 ± 0.15	0.40 ± 0.03
3	0.78 ± 0.01	0.78 ± 0.00	0.62 ± 0.02	0.58 ± 0.04	0.39 ± 0.05	0.45 ± 0.11
4	0.78 ± 0.02	0.78 ± 0.01	0.56 ± 0.04	0.52 ± 0.01	0.65 ± 0.39	0.47 ± 0.03
5	0.78 ± 0.00	0.77 ± 0.01	0.50 ± 0.03	0.47 ± 0.01	0.45 ± 0.03	0.47 ± 0.04
6	0.78 ± 0.02	0.76 ± 0.03	0.46 ± 0.03	0.43 ± 0.03	0.43 ± 0.03	0.55 ± 0.10
7	0.74 ± 0.04	0.71 ± 0.06	0.44 ± 0.03	0.42 ± 0.04	0.45 ± 0.04	0.71 ± 0.39
8	0.74 ± 0.02	0.68 ± 0.01	0.44 ± 0.03	0.42 ± 0.05	0.49 ± 0.04	0.57 ± 0.18
9	0.71 ± 0.03	0.67 ± 0.04	0.45 ± 0.03	0.41 ± 0.03	0.49 ± 0.13	0.85 ± 0.27
10	0.72 ± 0.01	0.66 ± 0.02	0.48 ± 0.04	0.41 ± 0.01	0.57 ± 0.01	1.27 ± 0.13*
Significance						
UV-B	**		*		**	
Leaf order	***		***		**	
UV-B × leaf order	ns		ns		**	

Leaf order indicates the leaf developmental age in order from the oldest leaf at the bottom to the youngest leaf at the top in a whole plant.

F_v/F_m, maximum quantum yield of photosystem II (PSII); Φ_{PSII}, PSII operating efficiency; NPQ, nonphotochemical quenching.

Data represent mean ± SD ($n = 3$).

Asterisks indicate significant differences for each parameter by two-way ANOVA and Tukey's HSD test.

*, $P < 0.05$; **, $P < 0.01$; ***, $P < 0.001$; ns, not significant.

the NPQ increased more greatly with younger leaves of the UV-B treated plants, especially 2.2-fold in the youngest leaves.

Phenolics and AOC according to UV-B radiation and leaf order

Effects of UV-B treatment and leaf order on both TPC and TFC were significant (Fig. 1-7a, b). TPC in the UV-B-treated plants did not increase in 2nd leaf, but increased by 68.4% in 7th leaf compared to the control. Compared to the control, TFC in the UV-B-treated plants increased by 37.6% in 3rd leaf and 98.2% in 7th leaf. Across all data, TPC was positively correlated with TFC, and their Pearson's correlation coefficient was 0.73 at $P < 0.001$ (Fig. 1-8a). Similarly, both TPC and TFC were positively correlated with UV radiation interception on individual leaves, and their correlation coefficients were 0.83 and 0.58 at $P < 0.001$, respectively (Fig. 1-8b, c). The AOC_{DPPH} was significantly affected by UV-B treatment, leaf order indicating leaf developmental age, and their interaction (Fig. 1-7c). The AOC_{DPPH} was higher in the UV-B-treated plants than in the control (82.4 and 66.7% on average, respectively). Compared to the control, the AOC_{DPPH} increased more greatly with older leaves of the UV-B-treated plants, up to 1.6-fold.

Multiple regression models for TPC, TFC, and AOC_{DPPH} with leaf order and UV radiation interception were developed and showed high explanatory power (Fig. 1-9). Although the standardized regression coefficients of leaf order (LO) and UV_{BE} interception (UVi) for TPC were 0.54 and 0.53, respectively, and

44
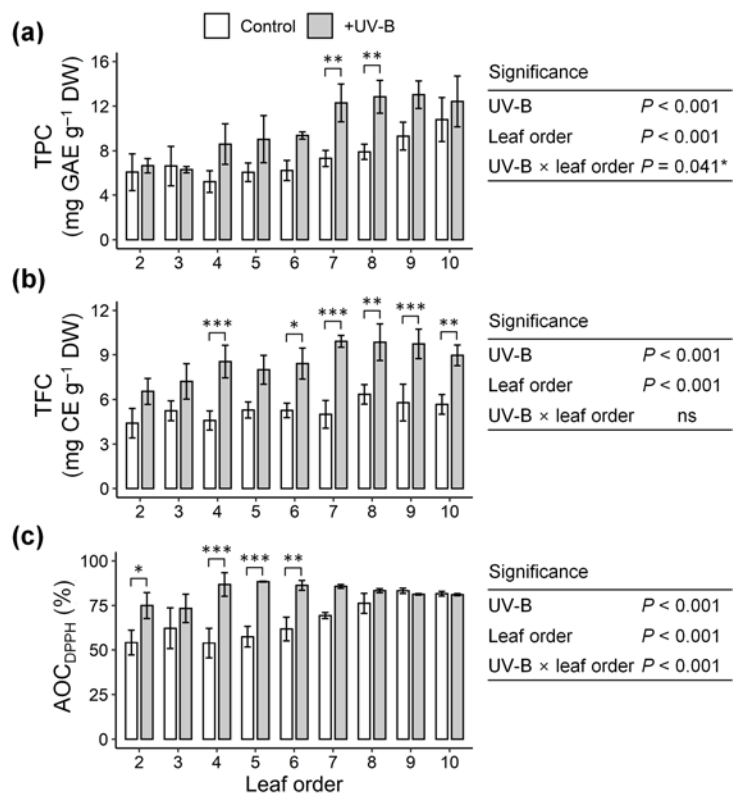
Fig. 1-7. Total phenolic content (TPC, a), total flavonoid content (TFC, b), and antioxidant capacity represented as DPPH radical scavenging activity (AOC$_{DPPH}$, c) in individual leaves of control and UV-B-treated kale plants. Leaf order indicates the leaf developmental age in order from the oldest leaf at the bottom to the youngest leaf at the top in a whole plant. Asterisks indicate significant differences for each parameter ($n = 3$, mean ± SD) by two-way ANOVA and Tukey's HSD test. *, $P < 0.05$; **, $P < 0.01$; ***, $P < 0.001$; ns, not significant.
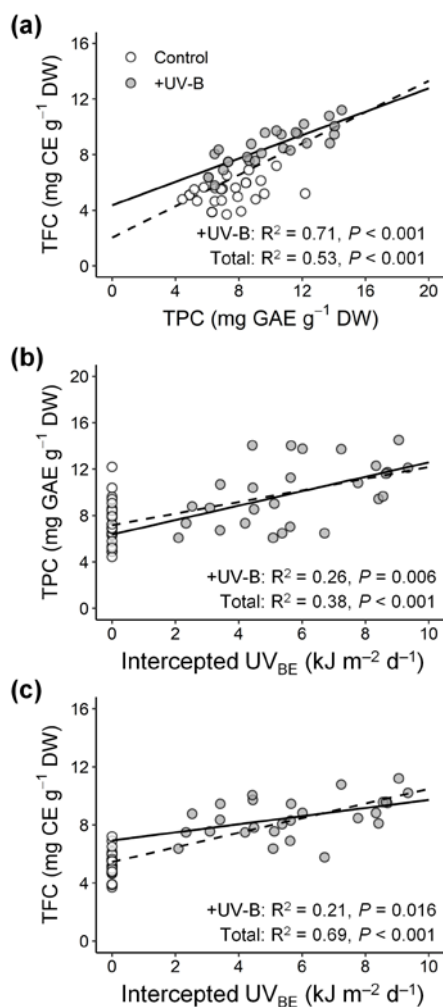
Fig. 1-8. Relationships of total phenolic content (TPC), total flavonoid content (TFC), and biologically effective UV radiation (UV_{BE}) interception in individual leaves of control and UV-B-treated kale plants. TPC versus TFC (a); UV radiation interception versus TPC (b) or TFC (c). The solid and dashed lines show linear fits of the +UV-B data set ($n = 27$) and the entire data set ($n = 56$), respectively. The linear regression in the control data set was not significant ($P = 0.062$, $n = 29$). The coefficient of determination (R^2) and P-value for each regression are shown within the panels.
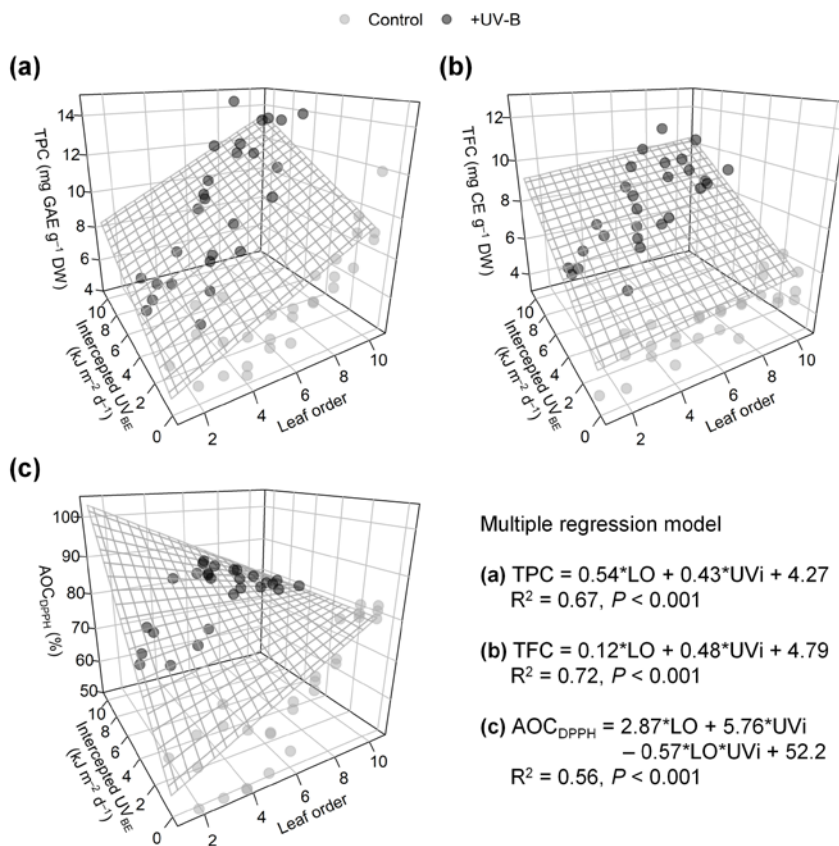
Fig. 1-9. Multiple regression models for total phenolic content (TPC, a), total flavonoid content (TFC, b), and antioxidant capacity represented as DPPH radical scavenging activity (AOC_{DPPH}, c) with leaf order (LO) and biologically effective UV radiation (UV_{BE}) interception (UVi). The points indicate the measured TPC, TFC, and AOC_{DPPH} in individual leaves of control and UV-B-treated kale plants. The plane or surface indicated linear or nonlinear regression model of the entire data set ($n = 56$), respectively, and the regression equation, R^2, and *P*-value are shown in the bottom right.

semi-partial correlations were 0.40 and 0.27, respectively, indicating that leaf order contributed more to determining TPC than UV-B radiation interception. The standardized regression coefficients of LO and UVi for TFC were 0.16 and 0.80, respectively, and the squared semi-partial correlations were 0.09 and 0.63, respectively, indicating that UV-B radiation interception contributed much more to determining TFC than leaf order. Similar to the results with and without UV-B treatment, the regression model for AOC_{DPPH} regressed well with the interaction between LO and UVi (Figs. 1-7c, 1-9c). All estimated coefficients were significant for the regression models.

DISCUSSION

Effects of supplemental UV-B radiation on 3D plant structure and its physiological interaction could help to understand how this spatial relationship can affect the antioxidant phenolic contents in plants. As hypothesized in this study, the plant structure and optical properties of the leaves determined the spatial UV-B absorbed by the leaf surface within the whole plant. The developmental age and intercepted UV-B level of individual leaves were confirmed to co-determine the UV-B-induced accumulation of phenolics, and statistical analyses of each factor were possibly conducted with the quantification of UV-B radiation interception. The short-term pre-harvest UV-B exposure improved phenolic accumulation without negative effects on growth and photosynthesis in kale plants, which is consistent with the previous research in basil (dos S. Nascimento et al., 2020).

Leaf morphology, optical property, and UV-B radiation interception

UV-B radiation induces changes in whole leaf morphology, such as shorter petioles, shorter stems, and thicker or smaller leaves, which can affect radiation interception in canopy structure (Barnes et al., 1996; Robson et al., 2015). In this study, the UV-B treatment also induced smaller leaves than the control (Table 1-1), which is consistent with the previous studies (Cen and Bornman, 1993; Yin et al., 2012; Yang et al., 2018). However, the low and short-term UV-

B doses did not cause noticeable changes in total leaf area or PAR interception (Tables 1-1, 1-2, Figs. 1-5a, c, 1-6a). UV-screening pigments accumulate in the epidermis to absorb UV radiation and avoid UV-induced damage (Cen and Bornman, 1993; Solovchenko and Merzlyak, 2008; Agati et al., 2011; Schulze et al., 2019). Similarly, the absorbance in the range of 280-350 nm was higher in the upper leaves of the UV-B-treated plants than in those of the control (Fig. 1-4).

Effects of UV-B radiation on leaf morphology and optical properties could be comprehensively considered through a 3D-scanned plant model and simulation parameters in the radiation interception analysis (Figs. 1-3, 1-4). In this study, both the PAR and UV radiation interceptions increased with height but varied with leaf order (Figs. 1-5c, d, 1-6). The phyllotaxis of the kale is a spiral pattern, which is a common pattern, and most often, the divergence angle is close to the golden angle of about 137.5°. The distribution of radiation interception depending on leaf order (Fig. 1-6) was consistent with the patterns of simulated light capture efficiency in digitized *Arabidopsis* leaves placed at a divergence angle of 137.5° (Strauss et al., 2020). In addition, this arrangement could minimize the overlapping leaf area to maximize light capture, which may cause the linear distribution of radiation interception with height in the kale plants (Strauss et al., 2020). The leaf height and arrangement due to divergence angle, i.e., plant structure, caused within-individual heterogeneity of PAR and UV-B radiation interceptions regardless of leaf order.

The PAR and UV-B radiation interceptions were not greater at the upper leaf without shade than at the bottom in this experimental condition (Fig. 1-6), due to the physical light distribution (PLD) of the LEDs, lighting distance from the light sources, and leaf angles. The LEDs used in this study, placed about 15 cm above the plant, had a wider PLD with a beam angle of 120°, which caused the overlap of light between multiple LED modules. In empty growth chambers, the light intensity was lower at a distance of 15 cm from the LED modules than at the longer distance (> 30 cm) (Hitz et al., 2019). With lettuce plants in the LED growth chamber, the total PAR interception increased as the lighting distance increased up to 30 cm, i.e., about 20 cm above the plant (Kim et al., 2020b). That is, when an artificial light source for plant cultivation such as LED is closely irradiated, the plant can receive less light. Even if the PLD and lighting distance are the same, more light is received when the light is incident perpendicular to the leaf surface. In leaves with high curvature, the difference in light interception according to the incident light angle is more noticeable (Kim et al., 2020a). Therefore, the upper leaves with high curvature and leaf inclination angle may receive much less light than expected.

Effects of UV-B on photosynthetic characteristics

Many early studies on UV-B radiation have reported negative effects on photosynthetic reactions, including ChlF, CO_2 fixation, and stability of the D1 and D2 proteins of PSII; however, at ambient or low UV-B levels, the effects

are less sensitive than expected (Jenkins, 2009; Hideg et al., 2013; Wargent and Jordan, 2013; Martínez-Lüscher et al., 2013, 2015). Such low UV-B effects are at least partially mediated by the UV-B specific UV RESISTANCE LOCUS 8 (UVR8) photoreceptor and signaling pathway with CONSTITUTIVE PHOTOMORPHOGENESIS1 (COP1) (Jenkins, 2009; Tilbrook et al., 2013; Singh et al., 2014). In this study, the low and short-term UV-B doses did not cause noticeable damage to the PSII photochemistry of kale leaves but affected NPQ (Table 1-3). NPQ, also called energy-dependent quenching, qE, is the major mechanism of photoprotection, which allows thermal dissipation of excess energy (Schulze et al., 2019). After UV-B exposure, qE is regulated by UVR8-mediated signaling together with COP1 (Allorent et al., 2016). In the present results, although there was no significant difference in UV radiation interception between the upper leaves (younger leaves), the significant increase in NPQ in the youngest leaves was presumed to be due to age-dependent susceptibility to UV-B exposure.

Effects of UV-B radiation on phenolic and flavonoid contents

UV-B-induced phenolic and flavonoid contents were analyzed with the UV radiation interception and leaf order of kale leaves at the whole-plant level (Figs. 1-7, 1-8, 1-9). As a response to UV-B, the enhanced biosynthesis of flavonoids and related phenolics has well been documented in various plants, including blueberry (Inostroza-Blancheteau et al., 2014), broccoli (Mewis et al., 2012),

lettuce (Lee et al., 2014), sweet basil (Mosadegh et al., 2018), and wheat (Chen et al., 2019), which are regarded as protective mechanisms against enhanced UV-B exposure. The accumulated phenolics act as UV-screen pigments in epidermal tissues and increase their innate antioxidative potential for scavenging ROS generated under UV-B exposure (Solovchenko and Merzlyak, 2008; Agati et al., 2011; Takshak and Agrawal, 2019). The signal transduction of UVR8-COP1 with the ELONGATED HYPOCOTYL5 (HY5) transcription factor plays a central role in the regulation of genes involved in controlling the biosynthesis of UV-protective phenolics (Jenkins, 2009; Matsuura et al., 2013; Singh et al., 2014). In this study, the UV-B$_{BE}$ dose of 4.2 kJ m^{-2} d^{-1} was sufficient to increase TPC and TFC, and the contents increased with the amount of intercepted UV-B radiation in the range of 2-10 kJ m^{-2} d^{-1} (Fig. 1-8b, c). Similarly, Takshak and Agrawal (2015) reported that supplemental UV-B (ambient + 3.6 kJ m^{-2} d^{-1} of UV-B$_{BE}$) increased the contents of flavonoids and phenolics and enhanced the activities of phenylpropanoid pathway enzymes in the medicinal plant *Coleus forskohlii*. UV-B-induced phenolic biosynthesis also depends on background light, i.e., PAR intensity (Vidović et al., 2015). In this study, the TPC was positively correlated with PAR interception ($r = 0.33$ at $P < 0.05$), but the TFC was not (data not shown). The ratio of TFC to TPC was higher in the UV-B-treated plants than in the control (Fig. 1-8a), implying that flavonoids were more highly biosynthesized among the related phenolics induced by UV-B exposure.

Leaf age as a physiological determinant of UV-B-induced phenolic content

Leaf order indicating leaf developmental age had a significant impact, such as higher TPC and AOC_{DPPH} in younger leaves, but did not affect the TFC in kale leaves without UV-B exposure (Fig. 1-7). The relationship between leaf developmental age and phenolic content was not straightforward, as the content may increase, decrease, or not change with leaf age (Csepregi et al., 2017). However, the increases in TPC and TFC were higher with younger leaves in this study. Similarly, the quercetin contents were increased more greatly by UV-B exposure in young leaves than in older leaves of two Brassicaceae, *Sinapis alba* and *Nasturtium officinale* (Reifenrath and Müller, 2007). In gingko, younger leaves showed distinct increases in quercetin and kaempferol contents and were more sensitive to UV-B radiation than old leaves (Sun et al., 2010). In grapevines, UV-B-exposed younger leaves showed higher UV-absorbing pigments, phenolics, and AOC than the older leaves (Majer and Hideg, 2012). Particularly in primary leaves of barley, flavonoids are needed for efficient UV-B protection without changes in variable chlorophyll fluorescence (Reuber et al., 1996). These previous studies showed that UV-B-induced antioxidant responses are dependent on leaf developmental age. In contrast, the AOC_{DPPH} was increased in older leaves from 2nd to 6th leaf (Fig. 1-7c). The increases in TPC and TFC in young leaves led to an increase in AOC_{DPPH}. However, the measured value at the upper younger leaves was saturated, and no further increase was observed.

Potential for estimating UV-B-induced phenolic content in 3D plant structure

Multiple regression analyses for TPC, TFC, and AOC_{DPPH} with leaf order and UV-B radiation interception were conducted to assess their relationships considering the effect of leaf positioning (Fig. 1-9). Although the experimental UV-B dose was the same, the heterogeneous UV-B doses depending on leaf position were reflected as UV-B radiation interception. UV-B radiation interception and leaf order were separately linearly involved in UV-B-induced phenolic contents, and their determinant power was dependent on the type of the compounds. Dose- and structure-dependent responses of phenolic accumulation were reported in kale plants exposed to short-term and moderate UV-B radiation (Neugart et al., 2012). In long-term adaptation, the sensitivity of plants to the overall UV-B response is also determined by growth attributes, such as growth rate, epidermal cell surface, and accumulated UV-B-absorbing phenolics (Hofmann et al., 2001). The data presented here suggest that the intraindividual distribution of antioxidant phenolic contents under low and short-term UV-B radiation can be estimated by UV-B radiation interception with leaf order indicating leaf developmental age. UV-B exposure further enhanced the intraindividual heterogeneity of TPC and TFC within the 3D plant structure when compared with those without UV-B radiation (Fig. 1-10). As a further study, the determinants for the distribution of UV-B-induced metabolites should be analyzed at various growth stages and canopy levels.
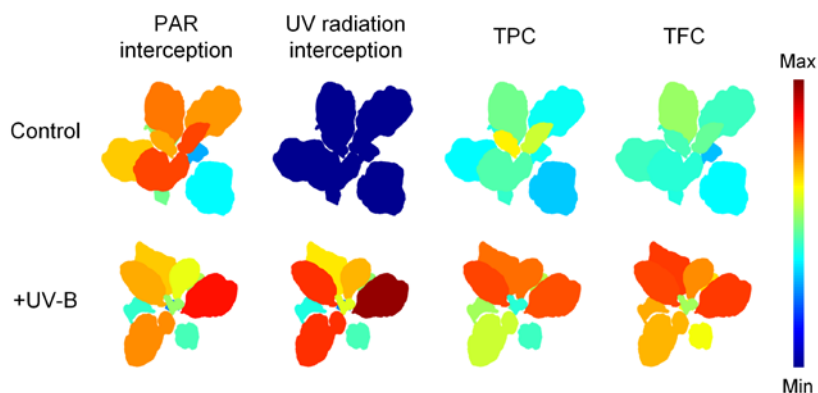
Fig. 1-10. Representative distributions of average radiation interception and phenolic contents in the leaves of control and UV-B-treated kale plants (n = 3). PAR, photosynthetically active radiation in the range of 400-700 nm; UV, biologically effective UV radiation in the range of 280-400 nm; TPC, total phenolic content; TFC, total flavonoid content. The color bar indicates each range of 0-200 μmol m^{-2} s^{-1} for PAR interception, 0-10 kJ m^{-2} d^{-1} for UV radiation interception, 0-16 mg gallic acid equivalent g^{-1} dry weight for TPC, and 0-12 mg catechin acid equivalent g^{-1} dry weight for TFC.

Overall, short-term UV-B radiation did not cause noticeable changes in growth and photochemical activity in PSII, but promoted TPC and TFC and enhanced the AOC of kale. UV radiation interception was determined by plant architecture and leaf optical properties and was quantified with a 3D plant model and ray-tracing simulation. The spatial distributions of phenolics were more heterogeneous within the whole plant under UV-B exposure. The intraindividual distributions of phenolics could be determined by UV-B radiation interception and leaf order, and their determinant power was dependent on the type of the compounds. These quantitative approaches could contribute to finding optimal UV-B dose levels and estimating the bioactive compound contents without harm to even whole plants from a practical point of view. In addition to the accumulation of secondary metabolites, the various plant responses to UV-B radiation will be better understood in 3D plant structures through light interception analysis.

LITERATURE CITED

Agati G, Biricolti S, Guidi L, Ferrini F, Fini A, Tattini M (2011) The biosynthesis of flavonoids is enhanced similarly by UV radiation and root zone salinity in *Ligustrum vulgare* leaves. J Plant Physiol 168:204–212.

Ainsworth EA, Gillespie KM (2007) Estimation of total phenolic content and other oxidation substrates in plant tissues using Folin-Ciocalteu reagent. Nat Protoc 2:875–877.

Allorent G, Lefebvre-Legendre L, Chappuis R, Kuntz M, Truong TB, Niyogi KK, Ulm R, Goldschmidt-Clermont M (2016) UV-B photoreceptor-mediated protection of the photosynthetic machinery in *Chlamydomonas reinhardtii*. Proc Natl Acad Sci USA 113:14864–14869.

Andarwulan N, Batari R, Sandrasari DA, Bolling B, Wijaya H (2010) Flavonoid content and antioxidant activity of vegetables from Indonesia. Food Chem 121:1231–1235.

Barnes PW, Ballaré CL, Caldwell MM (1996) Photomorphogenic effects of UV-B radiation on plants: Consequences for light competition. J Plant Physiol 148:15–20.

Bashri G, Singh M, Mishra RK, Kumar J, Singh VP, Prasad SM (2018) Kinetin regulates UV-B-induced damage to growth, photosystem II photochemistry, and nitrogen metabolism in tomato seedlings. J Plant Growth Regul 37:233–245.

Bilger W, Johnsen T, Schreiber U (2001) UV-excited chlorophyll fluorescence as a tool for the assessment of UV-protection by the epidermis of plants. J Exp Bot 52:2007–2014.

Cen H, Weng H, Yao J, He M, Lv J, Hua S, Li H, He Y (2017) Chlorophyll fluorescence imaging uncovers photosynthetic fingerprint of citrus Huanglongbing. Front Plant Sci 8:1–11.

Cen Y-P, Bornman JF (1993) The effect of exposure to enhanced UV-B radiation on the penetration of monochromatic and polychromatic UV-B radiation in leaves of *Brassica napus*. Physiol Plant 87:249–255.

Chen Z, Ma Y, Weng Y, Yang R, Gu Z, Wang P (2019) Effects of UV-B radiation on phenolic accumulation, antioxidant activity, and physiological changes in wheat (*Triticum aestivum* L.) seedlings. Food Biosci 30:100409.

Clé C, Hill LM, Niggeweg R, Martin CR, Guisez Y, Prinsen E, Jansen MAK (2008) Modulation of chlorogenic acid biosynthesis in *Solanum lycopersicum*: Consequences for phenolic accumulation and UV-tolerance. Phytochemistry 69:2149–2156.

Csepregi K, Coffey A, Cunningham N, Prinsen E, Hideg É, Jansen MAK (2017) Developmental age and UV-B exposure co-determine antioxidant capacity and flavonol accumulation in *Arabidopsis* leaves. Environ Exp Bot 140:19–25.

Dewanto V, Xianzhong W, Adom KK, Liu RH (2002) Thermal processing enhances the nutritional value of tomatoes by increasing total antioxidant

activity. J Agric Food Chem 50:3010–3014.

Dornbusch T, Wernecke P, Diepenbrock W (2007) A method to extract morphological traits of plant organs from 3D point clouds as a database for an architectural plant model. Ecol Model 200:119–129.

dos S. Nascimento LB, Brunetti C, Agati G, Lo Iacono C, Detti C, Giordani E, Ferrini F, Gori A (2020) Short-term pre-harvest UV-B supplement enhances the polyphenol content and antioxidant capacity of *Ocimum basilicum* leaves during storage. Plants 9:797.

Dou H, Niu G, Gu M (2019) Pre-harvest UV-B radiation and photosynthetic photon flux density interactively affect plant photosynthesis, growth, and secondary metabolites accumulation in basil (*Ocimum basilicum*) plants. Agronomy 9:434.

Flint SD, Caldwell MM (2003) A biological spectral weighting function for ozone depletion research with higher plants. Physiol Plant 117:137–144.

Hagen SF, Borge GIA, Solhaug KA, Bengtsson GB (2009) Effect of cold storage and harvest date on bioactive compounds in curly kale (*Brassica oleracea* L. var. *acephala*). Postharvest Biol Technol 51:36–42.

Heinze M, Hanschen FS, Wiesner-Reinhold M, Baldermann S, Gräfe J, Schreiner M, Neugart S (2018) Effects of developmental stages and reduced UVB and low UV conditions on plant secondary metabolite profiles in pak choi (*Brassica rapa* subsp. *chinensis*). J Agric Food Chem 66:1678–1692.

Hideg É, Jansen MAK, Strid Å (2013) UV-B exposure, ROS, and stress:

Inseparable companions or loosely linked associates? Trends Plant Sci 18:107–115.

Hitz T, Henke M, Graeff-Hönninger S, Munz S (2019) Three-dimensional simulation of light spectrum and intensity within an LED growth chamber. Comput Electron Agric 156:540–548.

Hofmann RW, Campbell BD, Fountain DW, Jordan BR, Greer DH, Hunt DY, Hunt CL (2001) Multivariate analysis of intraspecific responses to UV-B radiation in white clover (*Trifolium repens* L.). Plant Cell Environ 24:917–927.

Hu Z, Li H, Chen S, Yang Y (2013) Chlorophyll content and photosystem II efficiency in soybean exposed to supplemental ultraviolet-B radiation. Photosynthetica 51:151–157.

Inostroza-Blancheteau C, Reyes-Díaz M, Arellano A, Latsague M, Acevedo P, Loyola R, Arce-Johnson P, Alberdi M (2014) Effects of UV-B radiation on anatomical characteristics, phenolic compounds, and gene expression of the phenylpropanoid pathway in highbush blueberry leaves. Plant Physiol Biochem 85:85–95.

Jansen MAK, Gaba V, Greenberg BM (1998) Higher plants and UV-B radiation: Balancing damage, repair, and acclimation. Trends Plant Sci 3:131–135.

Jenkins GI (2009) Signal transduction in responses to UV-B radiation. Annu Rev Plant Biol 60:407–431.

Jung DH, Lee JW, Kang WH, Hwang IH, Son JE (2018) Estimation of whole

plant photosynthetic rate of Irwin mango under artificial and natural lights using a three-dimensional plant model and ray-tracing. Int J Mol Sci 19:1–14.

Kang WH, Hwang I, Jung DH, Kim D, Kim J, Kim JH, Park KS, Son JE (2019) Time change in spatial distributions of light interception and photosynthetic rate of paprika estimated by ray-tracing simulation. Prot Hortic Plant Fact 28:279–285.

Khudyakova AY, Kreslavski VD, Shmarev AN, Lyubimov VY, Shirshikova GN, Pashkovskiy PP, Kuznetsov VV, Allakhverdiev SI (2019) Impact of UV-B radiation on the photosystem II activity, pro-/antioxidant balance and expression of light-activated genes in *Arabidopsis thaliana hy4* mutants grown under light of different spectral composition. J Photochem Photobiol B Biol 194:14–20.

Kim D, Kang WH, Hwang I, Kim J, Kim JH, Park KS, Son JE (2020a) Use of structurally-accurate 3D plant models for estimating light interception and photosynthesis of sweet pepper (*Capsicum annuum*) plants. Comput Electron Agric 177:105689.

Kim J, Kang WH, Son JE (2020b) Interpretation and evaluation of electrical lighting in plant factories with ray-tracing simulation and 3D plant modeling. Agronomy 10:1545.

Kim JH, Lee JW, Ahn TI, Shin JH, Park KS, Son JE (2016) Sweet pepper (*Capsicum annuum* L.) canopy photosynthesis modeling using 3D plant

architecture and light ray-tracing. Front Plant Sci 7:1–10.

Lee JH, Oh MM (2015) Short-term low temperature increases phenolic antioxidant levels in kale. Hortic Environ Biotechnol 56:588–596.

Lee JH, Oh MM, Son KH (2019) Short-term ultraviolet (UV)-A light-emitting diode (LED) radiation improves biomass and bioactive compounds of kale. Front Plant Sci 10:1–13.

Lee MJ, Son JE, Oh MM (2014) Growth and phenolic compounds of *Lactuca sativa* L. grown in a closed-type plant production system with UV-A, -B, or -C lamp. J Sci Food Agric 94:197–204.

Liakoura V, Bornman JF, Karabourniotis G (2003) The ability of abaxial and adaxial epidermis of sun and shade leaves to attenuate UV-A and UV-B radiation in relation to the UV absorbing capacity of the whole leaf methanolic extracts. Physiol Plant 117:33–43.

Majer P, Hideg É (2012) Developmental stage is an important factor that determines the antioxidant responses of young and old grapevine leaves under UV irradiation in a greenhouse. Plant Physiol Biochem 50:15–23.

Martínez-Lüscher J, Morales F, Delrot S, Sánchez-Díaz M, Gomés E, Aguirreolea J, Pascual I (2013) Short- and long-term physiological responses of grapevine leaves to UV-B radiation. Plant Sci 213:114–122.

Martínez-Lüscher J, Morales F, Delrot S, Sánchez-Díaz M, Gomès E, Aguirreolea J, Pascual I (2015) Characterization of the adaptive response of grapevine (cv. Tempranillo) to UV-B radiation under water deficit

conditions. Plant Sci 232:13–22.

Matsuura HN, de Costa F, Yendo ACA, Fett-Neto AG (2013) Photoelicitation of bioactive secondary metabolites by ultraviolet radiation: Mechanisms, strategies, and applications. In: Chandra S, Lata H, Varma A (Eds.) Biotechnology for medicinal plants. Springer, Berlin, pp 171–190.

Mewis I, Schreiner M, Nguyen CN, Krumbein A, Ulrichs C, Lohse M, Zrenner R (2012) UV-B irradiation changes specifically the secondary metabolite profile in broccoli sprouts: Induced signaling overlaps with defense response to biotic stressors. Plant Cell Physiol 53:1546–1560.

Mosadegh H, Trivellini A, Ferrante A, Lucchesini M, Vernieri P, Mensuali A (2018) Applications of UV-B lighting to enhance phenolic accumulation of sweet basil. Sci Hortic 229:107–116.

Mosadegh H, Trivellini A, Lucchesini M, Ferrante A, Maggini R, Vernieri P, Sodi AM (2019) UV-B physiological changes under conditions of distress and eustress in sweet basil. Plants 8:396.

Neugart S, Zietz M, Schreiner M, Rohn S, Kroh LW, Krumbein A (2012) Structurally different flavonol glycosides and hydroxycinnamic acid derivatives respond differently to moderate UV-B radiation exposure. Physiol Plant 145:582–593.

Paulus S, Schumann H, Kuhlmann H, Léon J (2014) High-precision laser scanning system for capturing 3D plant architecture and analyzing growth of cereal plants. Biosyst Eng 121:1–11.

Reifenrath K, Müller C (2007) Species-specific and leaf-age dependent effects of ultraviolet radiation on two Brassicaceae. Phytochemistry 68:875–885.

Reuber S, Bornman JF, Weissenbock G (1996) A flavonoid mutant of barley (*Hordeum vulgare* L.) exhibits increased sensitivity to UV-B radiation in the primary leaf. Plant Cell Environ 19:593–601.

Robson TM, Aphalo PJ, Banaś AK, Barnes PW, Brelsford CC, Jenkins GI, Kotilainen TK, Łabuz J, Martínez-Abaigar J, Morales LO, Neugart S, Pieristè M, Rai N, Vandenbussche F, Jansen MAK (2019) A perspective on ecologically relevant plant-UV research and its practical application. Photochem Photobiol Sci 18:970–988.

Robson TM, Klem K, Urban O, Jansen MAK (2015) Re-interpreting plant morphological responses to UV-B radiation. Plant Cell Environ 38:856–866.

Schulze E-D, Beck E, Buchmann N, Clemens S, Müller-Hohenstein K, Scherer-Lorenzen M (2019) Light. In: Schulze E-D, Beck E, Buchmann N, Clemens S, Müller-Hohenstein K, Scherer-Lorenzen M (Eds.) Plant ecology. Springer, Berlin, pp 57–90.

Si C, Yao XQ, He XL, Chu JZ, Ma CH, Shi XF (2015) Effects of enhanced UV-B radiation on biochemical traits in postharvest flowers of medicinal chrysanthemum. Photochem Photobiol 91:845–850.

Singh S, Agrawal SB, Agrawal M (2014) UVR8 mediated plant protective responses under low UV-B radiation leading to photosynthetic acclimation. J Photochem Photobiol B Biol 137:67–76.

Solovchenko AE, Merzlyak MN (2008) Screening of visible and UV radiation as a photoprotective mechanism in plants. Russ J Plant Physiol 55:719–737.

Strauss S, Lempe J, Prusinkiewicz P, Tsiantis M, Smith RS (2020) Phyllotaxis: Is the golden angle optimal for light capture? New Phytol 225:499–510.

Sun M, Gu X, Fu H, Zhang L, Chen R, Cui L, Zheng L, Zhang D, Tian J (2010) Change of secondary metabolites in leaves of *Ginkgo biloba* L. in response to UV-B induction. Innov Food Sci Emerg Technol 11:672–676.

Takshak S, Agrawal SB (2015) Defense strategies adopted by the medicinal plant *Coleus forskohlii* against supplemental ultraviolet-B radiation: Augmentation of secondary metabolites and antioxidants. Plant Physiol Biochem 97:124–138.

Takshak S, Agrawal SB (2019) Defense potential of secondary metabolites in medicinal plants under UV-B stress. J Photochem Photobiol B Biol 193:51–88.

Tang L, Hou C, Huang H, Chen C, Zou J, Lin D (2015) Light interception efficiency analysis based on three-dimensional peach canopy models. Ecol Inform 30:60–67.

Tilbrook K, Arongaus AB, Binkert M, Heijde M, Yin R, Ulm R (2013) The UVR8 UV-B photoreceptor: Perception, signaling, and response. Arabidopsis Book 11. doi:10.1199/tab.0164

Vagiri M, Conner S, Stewart D, Andersson SC, Verrall S, Johansson E, Rumpunen K (2015) Phenolic compounds in blackcurrant (*Ribes nigrum* L.)

leaves relative to leaf position and harvest date. Food Chem 172:135–142.

Vidović M, Morina F, Milić S, Zechmann B, Albert A, Winkler, JB, Veljović Jovanović S (2015) Ultraviolet-B component of sunlight stimulates photosynthesis and flavonoid accumulation in variegated *Plectranthus coleoides* leaves depending on background light. Plant Cell Environ 38:968–979.

Wang SY, Lin H-S (2000) Antioxidant activity in fruits and leaves of blackberry, raspberry, and strawberry varies with cultivar and developmental stage. J Agric Food Chem 48:140–146.

Wargent JJ, Jordan BR (2013) From ozone depletion to agriculture: Understanding the role of UV radiation in sustainable crop production. New Phytol 197:1058–1076.

Yang Y, Niu K, Hu Z, Niklas KJ, Sun S (2018) Linking species performance to community structure as affected by UV-B radiation: An attenuation experiment. J Plant Ecol 11:286–296.

Yao J, Sun D, Cen H, Xu H, Weng H, Yuan F, He Y (2018) Phenotyping of *Arabidopsis* drought stress response using kinetic chlorophyll fluorescence and multicolor fluorescence imaging. Front Plant Sci 9:1–15.

Yin L, Zhang M, Li Z, Duan L, Wang S (2012) Enhanced UV-B radiation increases glyphosate resistance in velvetleaf (*Abutilon theophrasti*). Photochem Photobiol 88:1428–1432.

Yoon HI, Kim D, Son JE (2020a) Spatial and temporal bioactive compound

contents and chlorophyll fluorescence of kale (*Brassica oleracea* L.) under UV-B exposure near harvest time in controlled environments. Photochem Photobiol 96:845–852.

Yoon HI, Kim JS, Kim D, Kim CY, Son JE (2019) Harvest strategies to maximize the annual production of bioactive compounds, glucosinolates, and total antioxidant activities of kale in plant factories. Hortic Environ Biotechnol 60:883–894.

Yoon HI, Zhang W, Son JE (2020b) Optimal duration of drought stress near harvest for promoting bioactive compounds and antioxidant capacity in kale with or without UV-B radiation in plant factories. Plants 9:295.

Prediction of Total Phenolic Contents in Three-Dimensional Structure of Kale Leaves According to UV-B Radiation Interception and Developmental Age

ABSTRACT

Ultraviolet-B (UV-B, 280-315 nm) radiation has been used as an elicitor to enhance secondary metabolites in plants. Local accumulation of phenolics due to uneven UV-B exposure with leaf position and age-dependent sensitivity to UV-B radiation is unpredictable in plant structure. The purpose of this study was to develop a model for predicting phenolic accumulation according to UV-B radiation interception and growth stage using ray-tracing simulation and three-dimensional-scanned models. For this purpose, the phenolic accumulation in kale (*Brassica oleracea* L. var. *acephala*) grown under a controlled environment for 23, 30, and 38 days after transplanting was evaluated according to pre-harvest narrow-band UV-B radiation and leaf age. The 6 or 12 h UV-B radiation from UV-B light-emitting diodes with a peak at 310 nm significantly increased the total phenolic content (TPC), total flavonoid content (TFC), total anthocyanin content (TAC), UV-B absorbing pigment

content (UAPC), and the antioxidant capacity in kale leaves. Multiple regression models for the TPC, TFC, TAC, and UAPC were developed based on daily UV-B energy absorbed by leaves and developmental age using a second-order multi-polynomial equation. The developed models accurately predicted the TPC, TFC, TAC, and UAPC in plant structures with R^2 values > 0.78 and normalized root mean squared errors of about 30% in test data, across the three growth stages. The UV-B energy yields for TPC, TFC, and TAC were highest in the intermediate leaves, while those for UAPC were highest in young leaves at the last stage. To our knowledge, this study proposed the first statistical models for estimating UV-B-induced phenolic contents. As a further step, simulations based on the statistical models will help to predict phenolic accumulation with effective UV-B energy input, saving experimental time and cost.

Additional keywords: antioxidants, flavonoids, light interception, secondary metabolites

INTRODUCTION

Food systems considering improved nutrition have been one of the major challenges facing the world and are being emphasized by the Food and Agriculture Organization of the United Nations. Nutrition-dense foods that may decrease the risk of some diseases or/and be used for curing some illnesses are known by the name 'functional food' or the more commonly used term 'superfood'. Among these foods, *Brassica* species are vegetables containing high levels of nutrients and health-promoting phytochemicals (Francisco et al., 2017). Kale (*B. oleracea* var. *acephala*) is a functional food that benefits human health, supported by many scientific evidences, and is a rich source of bioactive compounds such as polyphenols and carotenoids with antioxidant capacity (Šamec et al., 2018). Biosynthesis of such bioactive compounds is improved through biotic and abiotic elicitation (Thakur et al., 2019).

Ultraviolet (UV) radiation, especially UV-B (280-315 nm), has been reported as an effective elicitor (Loconsole and Santamaria, 2021). Contrary to the long-held opinion that UV-B radiation is predominantly harmful to plants, recent studies have highlighted that a low fluence rate of UV-B radiation triggers distinct changes in the secondary metabolism, resulting in bioactive compound accumulation such as phenolics and flavonoids (Schreiner et al., 2012). The accumulation of phenolics in epidermal tissues plays as sunscreens and their innate antioxidant potential protects underlying sensitive tissues from

UV-B-induced damage (Takshak and Agrawal, 2019). However, the localized accumulation may complicate the distribution of phenolics depending on developmental age and uneven UV-B exposure with leaf position (Csepregi et al., 2017; Yoon et al., 2021a).

UV-B-induced metabolic changes are multifaceted in terms of optical, morphological, and physiological factors; therefore, the use of UV-B radiation requires more precise manipulation to enhance the phenolic content (Schreiner et al., 2012). The actual dose perceived by the plant tissue depends not only on UV-B intensity from the light source, but also on various optical factors and the morphological structure of the plant (Schreiner et al., 2012). Even under natural light, the attenuation of UV radiation in the plant canopy is affected by the spatial distribution and angle of the leaves, which are difficult to be mathematically described (Aphalo et al., 2012). Even without plants, lighting conditions with various optical factors, such as lighting distance, physical light distribution, and spectral power distribution of light sources, affect the spatial light distribution simulated in a growth chamber (Hitz et al., 2019). In addition, the simulated light absorbed by leaves depends on planting density and lighting arrangement as well as the three-dimensional (3D) structure of the plant in a controlled environment (Kim et al., 2020).

The developmental stage of plants is a strong determinant of the stress response and susceptibility to various environmental stresses (Rankenberg et al., 2021). In some cases, physiologically young leaves showed higher

72

sensitivity to UV-B radiation, resulting in higher amounts of phenolics, higher antioxidant capacity, or higher expression of phenylpropanoid pathway genes (Majer and Hideg, 2012; Rizi et al., 2021). Furthermore, phenolic changes were more affected by developmental stage than by UV-B levels in pak choi plants (Heinze et al., 2018). However, young leaves, typically located near the top of the plant, are exposed to targeted lighting conditions, while older leaves rely on light penetration in the 3D structure of plants. The effect of developmental stage cannot be separated from positional light-exposure effect. For experimental purposes, positional UV-exposure effects can be avoided by selecting plants with a 2D structure (Majer and Hideg, 2012; Csepregi et al., 2017). UV dose absorbed by the leaves in 3D structure has been attempted to be quantified through simulation with a 3D-scanned plant model, and the UV-exposure and developmental effects could be separately analyzed (Yoon et al., 2021a, b).

For the application of UV-B radiation to phenolic production, a common strategy is to find a combination of UV-B-related factors, such as UV-B dose (fluence rate and duration), timing (plant developmental stage at which UV-B exposure is initiated), or wavelength/type of UV-B (Schreiner et al., 2009; Rechner et al., 2016; Dou et al., 2019). Traditional UV-B lamps are prone to cause photosynthetic damage to plants due to their broad-band wavelength range including shorter wavelengths close to UV-C (< 280 nm) and excessive and difficult-to-control energy (Mosadegh et al., 2019; Yoon et al., 2020). Recently, the performance of light-emitting diodes (LEDs) has advanced

enough to provide light of the desired wavelength and intensity for plants (Kneissl et al., 2019; Loi et al., 2020; Paradiso and Proietti, 2021). Narrow-band UV-B LEDs have also been applied at low doses to enhance health-promoting compound accumulation without damaging plants (Wiesner-Reinhold et al., 2021). Since the application of UV-B radiation incurs additional energy costs, either UV-B energy efficiency or maximum phenolic production should be pursued in controlled environmental agriculture. Prediction of UV-B-induced phenolic content will allow us to find the optimal UV-B conditions for maximizing phenolic production.

Statistical modeling has widely been applied because the modeling is simple but powerful for predicting and quantifying the relationship between variables (Kim et al., 2016). Plant developmental stage affects plant structures as well as their sensitivity to UV-B radiation (Yoon et al., 2021b). Thus, the phenolic production could be quantified with the modeling based on developmental age and UV-B radiation on the plant structure. The present study focused on pre-harvest UV-B exposure as an elicitor for the biosynthesis of phenolics in non-acclimated plants to rule out possible UV-B acclimation effects (Liao et al., 2020). This study aimed to analyze UV-B-induced phenolic accumulation with pre-harvest UV-B exposure based on UV-B radiation interception and developmental stage of plants, and ultimately aimed to develop statistical models and investigate the UV-B energy yield for the phenolic accumulation. For this purpose, the contents of phenolics, flavonoids,

anthocyanin, UV-absorbing pigments, and chlorophylls were evaluated in individual leaves with UV-B radiation interception simulated with 3D-scanned plant models according to growth stage.

MATERIALS AND METHODS

Plant materials and experimental conditions

Kale (*B. oleracea* L. var. *acephala*) seeds were sown on sponge cubes in water culture under florescent lamps at a photosynthetic photon flux density (PPFD) of 150 μmol m^{-2} s^{-1} over the waveband 400-700 nm for 16-h light period. After true leaves appeared, seedlings were supplied with a nutrient solution for *Brassica*: N 137.8, P 30.9, K 140.9, Ca 104.6, Mg 54.8, Fe 2.76, Cu 0.02, Zn 0.05, Mn 0.68, B 0.50, and Mo 0.01 mg L^{-1}, at an electrical conductivity (EC) of 0.6 dS m^{-1}. After the fourth true leaf appeared, the seedlings of uniform size were transplanted into plant factory modules with a deep flow technique system. The modules were maintained at an air temperature of 20°C, relative humidity of 70%, CO_2 concentration of 500 μmol mol^{-1}, EC of 1.2 dS m^{-1}, and pH of 6.9. The plants were irradiated with red, blue, and white LEDs at a PPFD of 255 μmol m^{-2} s^{-1} (at 7 cm from the center of the ground) for a 16-h light period. The four plants per treatment were harvested separately at 23, 30, and 38 days after transplanting (DAT).

For UV treatment, UV-B LEDs with a spectral peak at about 310 nm were used, and the irradiance on 7 cm above the center of bottom was 3.0 W m^{-2}. The spectrum and intensity of photosynthetically active radiation (PAR) and UV-B LEDs were measured using a spectroradiometer (Blue-Wave spectrometer, StellarNet Inc., Tampa, FL, USA) in the range of 250-900 nm

(Fig. 2-1a). The plants at 23, 30, and 38 DAT were irradiated with UV-B LEDs for 6 or 12 h (UV6h or UV12h), and then harvested after recovery for 4 h. The UV6h and UV12h treatments corresponded to 15.6 and 31.3 kJ m^{-2} d^{-1} biologically effective UV-B radiation (UV-B$_{BE}$), respectively, calculated using a biological spectral weighting function for plants (Flint and Caldwell, 2003). The arrangements of PAR and UV-B LEDs are shown in Fig. 2-1b.

3D-Scanning to optical simulation for radiation interception analysis

UV radiation interception analysis with a 3D-scanned plant model and ray-tracing simulation were performed as previously described (Kim et al., 2020; Yoon et al., 2021a) (Fig. 2-2). In brief, plant models were directly obtained using a high-resolution portable 3D scanner (Go! SCAN50TM, Creaform Inc., Lévis, Quebec, Canada) and its software (Vxelement, Creaform Inc.). Four plants per treatment were 3D-scanned after the UV treatment at 23, 30, and 38 DAT. After repair for holes and noise, the 3D mesh data were segmented into leaf mesh data and reconstructed to individual surface models using a reverse engineering software (Geomagic Design X, 3D Systems, Rock Hill, SC, USA). The virtual plant factory modules based on the dimensions measured were constructed using a 3D computer-aided design software (Solidworks, Dassault Systèmes, Vélizy-Villacoublay, France). The 3D model arrangement and simulation parameters, including the optical properties of materials and plants and the setting of light sources and detectors, are described in Fig. 2-2. All 3D
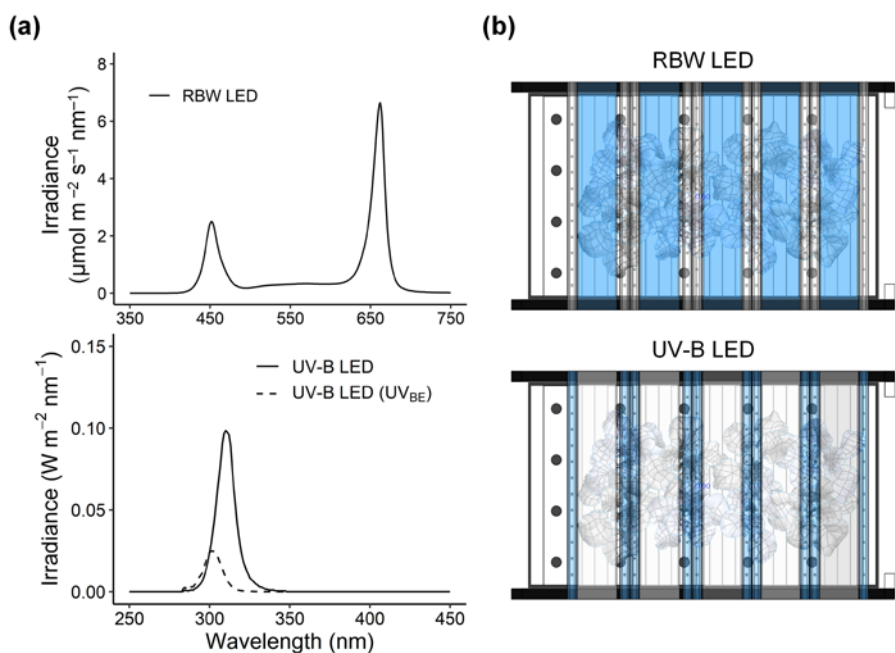
Fig. 2-1. Spectra (a) and arrangement (b) of red, blue, and white light-emitting diodes (RBW LED) and UV-B LED used in the plant factory. Irradiance of UV-B LEDs with a spectral peak at about 310 nm was 3.0 W m^{-2} in 280-400 nm. UV-B$_{BE}$ indicates biologically effective UV-B calculated using a biological spectral weighting function for plants (Flint and Caldwell, 2003), and thereby its spectral peak was at about 302 nm. The RBW LEDs irradiated at a photosynthetic photon flux density of 255 μmol m^{-2} s^{-1}.

(a) Construction of 3D-scanned plant model

23 DAT   30 DAT   38 DAT

Cultivated kale

GO!Ω SCAN   VXelements

- 3D scan (*n* = 4 per treatment and growth stage)
- Export as mesh data

3D mesh data

Dx Geomagic® Design X™

- Holes and noise correction
- Segmentation into individual leaves

Segmented mesh

- Fitting segmented mesh to leaf surface model

Surface model
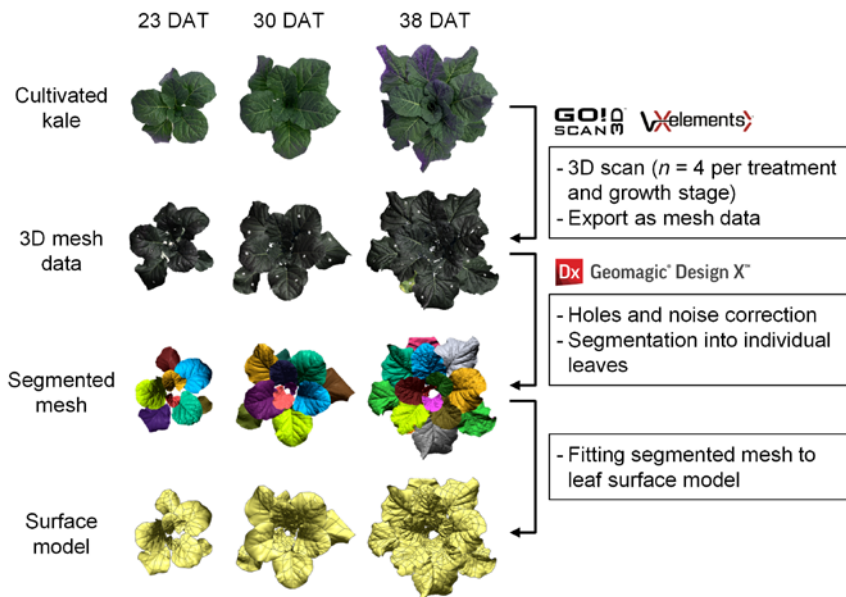
(b) Construction of virtual environment

DS SOLIDWORKS   OPTISWORKS

Plant (leaf) surface model   RBW LED plate

- Optical properties of module materials, plants, and light sources

UV-B LED bar

Growth module model (styrofoam/acrylic bed, aluminum frame)

Optical properties of kale leaves

Transmittance (TR)
Reflectance (REF)

TR or REF (%)

Wavelength (nm)
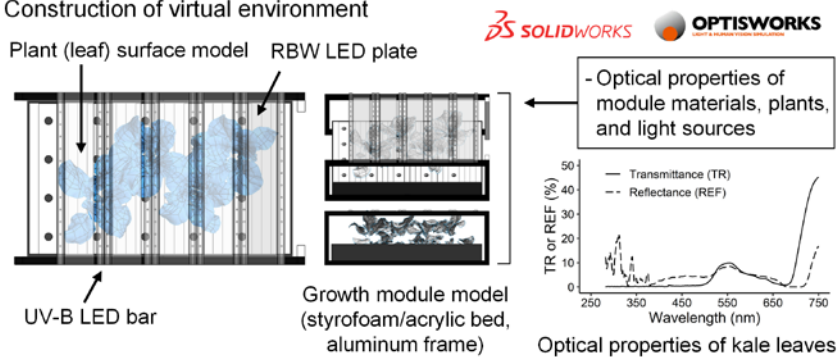
(c) Ray-tracing simulation

Light sources	UV-B LED bar (12 chips) × 10 bars
Spectral power distribution	Spectrum in Fig. 2-1
Physical light distribution	Lambertian distribution with a half angle of 60°
Energy output	0.02139 W for each chip
Number of rays	1 Giga-rays
Detector	All leaf surface model

Fig. 2-2. Schematic diagram of 3D-scanning to optical simulation for radiation interception analyzed in kale plants. After construction of 3D-scanned plant

model (a), virtual environment for simulation (b) consisted of 3D model of growth module, light sources, and plants with actual dimensions and arrangement. Ray-tracing simulation (c) was conducted with these parameters. TR, transmittance; REF, reflectance.

models were placed in the same position and orientation as the actual materials and plants. The ray-tracing simulation was performed using a ray-tracing software (Optisworks, Optis Inc., La Farlède, France). The daily UV-B radiation interception on individual leaves was calculated from the simulation results with UV-exposure durations.

Growth characteristics

Fresh masses of individual leaves were measured separately at harvest with four plants per treatment (Fig. A2-1). After photographing all leaves, the areas of individual leaves were calculated with an image analysis software (ImageJ 1.53, National Institutes of Health, Bethesda, MD, USA). Leaf order was determined as an absolute order of emergence (the first true leaf was set as 1) and was numbered from the oldest leaf at the bottom to the youngest at the top in the plant. Leaf groups at each growth stage were determined based on relative growth rate of individual leaf, which are shown in Fig. A2-2 and Table A2-1 (Behn et al., 2011; Pontarin et al., 2020). Leaf groups 1, 2, and 3 were corresponded to leaf orders 1-3, 4-7, and 8-11, respectively, at 23 DAT, leaf orders 3-6, 7-9, and 10-14, respectively, at 30 DAT, and leaf orders 4-8, 9-12, and 13-18, respectively, at 38 DAT. Growth parameters including fresh mass, leaf area, and root dry mass were measured as shown in Fig. A2-3.

Phenolic content, antioxidant capacity (AOC), and photosynthetic pigment

Sample preparation

The whole leaves were sampled separately at harvest and frozen at −80°C. After lyophilization with a freeze dryer (FD8512, Ilshin Biobase Co., Yangju, Korea) at −80°C under a vacuum of 0.007 mm Hg for 120 h, the leaf dry mass was determined. The lyophilized sample was pulverized in liquid nitrogen using a cryogenic grinder (SPEX 6875D Freezer/Mill, SPEX SamplePrep, Metuchen, NJ, USA), and then stored in the dark at 4°C until needed for analysis. The freeze-milled samples used for the analysis were corresponded to leaf orders 5-9, 5-13, and 5-17 at 23, 30, and 38 DAT, respectively.

Total phenolic content (TPC) and total flavonoid content (TFC)

For determining TPC and TFC, aliquots of the powdered sample (50 mg) were mixed with 1 mL of 80% (v/v) methanol, incubated in the dark at 4°C for 18 h, and then centrifuged at 11,000 × g at 4°C for 10 min. TPC was determined according to the Folin-Ciocalteu colorimetric method (Ainsworth and Gillespie, 2007). The supernatant of 100 μL was collected in a 2-mL tube and mixed with 200 μL of 10% (v/v) Folin–Ciocalteu solution (Junsei Chemical Co., Ltd., Tokyo, Japan) and 400 μL of distilled water. After vortex mixing, 800 μL of 700 mM Na_2CO_3 was added. The mixture was shaken for 10 s and incubated in a water bath at 45°C for 15 min. The absorbance was read at 765 nm using a spectrophotometer (Photolab 6100vis, WTW, Weilheim, Germany), and the TPC was expressed as milligrams of gallic acid (Sigma–Aldrich Chemical

Corp., St. Louis, MO, USA) equivalent per gram of dry mass (mg GAE g^{-1} DM).

TFC was determined according to the aluminum chloride colorimetric method (Dewanto et al., 2002). The supernatant of 100 μL was collected in a 2-mL tube, and mixed with 500 μL of distilled water and 30 μL of 5% (w/v) $NaNO_2$. After 6 min, 60 μL of 10% (w/v) $AlCl_3$ was added. After 5 min, 200 μL of 1 M NaOH and 110 μL of distilled water were added, and all reactants were thoroughly mixed. After incubating for 5 min, the absorbance was read at 510 nm, and the TFC was expressed as milligrams of catechin acid (Supelco, Bellefonte, PA, USA) equivalent per gram of dry mass (mg CE g^{-1} DM).

Total anthocyanin content (TAC) and UV-absorbing pigment content (UAPC)

For determining TAC and UAPC, the aliquots of the powdered sample (20 mg) were mixed with 1 mL of 1% acidified methanol, incubated in the dark at 4°C for 48 h, and then centrifuged at 11,000 × g at 4°C for 15 min. The supernatant of the extract was diluted 2-fold, and the absorbance was read at 530 and 657 nm (A_{530} and A_{657}, respectively). TAC was determined with the corrected absorbance as $A_{530} - 0.25A_{657}$ (Sytar et al., 2018) and expressed as milligrams of cyanidin 3-glucoside (Sigma–Aldrich Chemical Corp.) equivalent per gram of dry mass (mg C3GE g^{-1} DM). The supernatant of the extract was diluted 20-fold, and the absorbance was read at 285 and 330 nm (Si et al., 2015; Khudyakova et al., 2019). UAPC was determined as the average of two

absorbances, and expressed as absorbance per gram of dry mass (OD g^{-1} DM).

AOC

AOC can be determined depending on the choice of assay, and analyzing phenol-rich samples by a single assay is recommended to be avoided (Csepregi et al., 2016). Thus, both the 2, 2'-azino-bis (3-ethylbenzothiazoline-6-sulfonic acid)-diammonium salt (ABTS) assay and the 2, 2-diphenyl-1-picrylhydrazyl (DPPH) assay were performed. The powdered sample (50 mg) were mixed with 1 mL of 80% (v/v) methanol, and the mixture was incubated in the dark at 4°C for 42 h and then centrifuged at $11,000 \times g$ at 4°C for 10 min. The ABTS radical scavenging activity was determined as described by Re et al. (1999). Briefly, the ABTS radical cation (ABTS$^{\bullet+}$) reagent was produced by reacting 7 mM ABTS solution (Sigma–Aldrich Chemical Corp.) with 2.45 mM $K_2S_2O_8$ (1:1, v/v), and stored in the dark at 4°C for 18 h before use. The ABTS$^{\bullet+}$ solution was diluted with 80% methanol to obtain appropriate absorbance. The supernatant of 50 μL was added to 1.8 mL of diluted ABTS$^{\bullet+}$ solution. After 6 min of incubation in the dark at room temperature, the absorbance was read at 734 nm. The DPPH radical scavenging activity was determined as described by Brand-Williams et al. (1995). DPPH was purchased from Alfa Aesar (Ward Hill, MA, USA), and DPPH solution was freshly made in methanol before use. The supernatant of 100 μL was added to 1.8 mL of 0.12 mM DPPH methanol solution. After incubation in the dark at room temperature for 30 min, the

absorbance was read at 517 nm. A calibration curve for ABTS and DPPH assays was constructed using L-ascorbic acid (Samchun Pure Chemical Co., Ltd., Pyeongtaek, Korea). The AOC_{ABTS} and AOC_{DPPH} were expressed as milligrams of ascorbic acid equivalent per gram of dry mass (mg AAE g^{-1} DM).

Photosynthetic pigment content

For determining photosynthetic pigment, the aliquots of the powdered sample (50 mg) were mixed with 1 mL of 80% (v/v) acetone, incubated in the dark at room temperature for 24 h, and then centrifuged at 11,000 $\times$ g for 10 min. Chlorophyll a and b, and carotenoid contents were calculated based on absorbance at 663, 647, and 470 nm according to the method of Lichtenthaler and Buschmann (2001), and expressed as milligrams of chlorophyll or carotenoid per gram of dry mass (mg g^{-1} DM).

Multiple regression model and UV-B yield

TPC, TFC, TAC, UAPC, and AOC per leaf were calculated by multiplying their concentrations (mg eq. g^{-1} DM) by the leaf dry mass (g DM). Multiple linear regressions were used to develop statistical models for predicting the phenolic accumulation. The model was obtained by stepwise regression using backward elimination method based on a second-order multi-polynomial (quadratic) model, including the single effect of leaf order and UV radiation interception and the interaction effect:

$$M(L,U) = \beta_0 + \beta_1 L + \beta_2 L^2 + \beta_3 U + (\beta_4 L + \beta_5 L^2) U \qquad \text{Eq. 2-1}$$

where M is phenolic content per leaf (mg eq. per leaf), L is leaf order numbered as an absolute order of leaf emergence, U is daily UV radiation interception per leaf (kJ d^{-1} per leaf), and β_0-β_5 are regression coefficients obtained by the regression analysis at each growth stage. The UV-B energy yield for phenolic accumulation per leaf was determined as the change in phenolic content per absorbed UV-B energy and calculated as the slope of multiple regression surface against UV interception as follows:

$$Y(L,U) = [M(L, U) - M(L, 0)] / U = \beta_3 + \beta_4 L + \beta_5 L^2 \qquad \text{Eq. 2-2}$$

where Y is UV-B energy yield for phenolic accumulation per leaf (mg eq. kJ^{-1} d) at each L and U.

Statistical analysis

For all data, the homogeneity of variance was evaluated by Levene's test and the normality was evaluated by Shapiro–Wilk test. Comparisons of the mean values were performed with one-way or two-way ANOVA and Tukey's honestly significant difference (HSD) test to assess the effects of the UV-B treatment (control, UV6h, and UV12h), leaf group 1-3, or growth stage (23, 30, and 28 DAT). For data that failed the normality test, the Kruskal-Wallis test and

Dunn's test were used, and for data that failed the homogeneity of variance, Welch's ANOVA and Games-Howell test were used.

For model development, nine plants per growth stage were used to data set, which corresponded to a total of 250 data points, including 66, 74, and 110 data points at 23, 30, and 38 DAT, respectively, after removing outliers with the interquartile range. For accuracy of the multiple regression model, a data set (not used to develop the model) including nine plants and 76 data points was used for validation. The coefficient of determination (R^2), root mean squared error (RMSE), and normalized RMSE (NRMSE) were selected. All visualization and statistical analyses were performed using R software (R 4.0.2, R Foundation, Vienna, Austria).

RESULTS

Age-dependent changes in phenolic content according to UV-B radiation

TPC, TFC, TAC, UAPC, AOC_{ABTS}, and AOC_{DPPH} were significantly affected by UV-B radiation, growth stage, and leaf groups (Table 2-1). Across all data, the contents of all the compounds were significantly higher in the UV12h treatment than in the control. The TPC, TFC, TAC, AOC_{ABTS}, and AOC_{DPPH} were significantly different depending on the growth stage, except for UAPC. The TPC, TFC, and AOC_{DPPH} were significantly higher in the order of 30, 38, and 23 DAT. Whereas the AOC_{ABTS} were significantly higher in the order of 23, 30, and 38 DAT, the TAC was significantly higher in the reverse order. Whereas the TPC and TFC were not significantly different depending on the leaf group, the UAPC, AOC_{ABTS}, and AOC_{DPPH} were significantly higher in the order of leaf groups 3, 2, and 1, and the TAC was significantly higher in the reverse order. The TPC and TFC were highest in leaf groups 2 and 3 at 30 DAT, respectively, in UV12h treatment (13.2% and 31.6% higher, respectively, than in the control at each metabolite and stage). The TAC was highest in leaf group 1 at 38 DAT in the UV12h treatment (35.2% higher than in the control). The increase rates of TPC, TFC, TAC, UAPC, and AOC_{ABTS} in the UV12h treatment relative to the control were highest in leaf group 3 at 23 DAT. The TPC, TFC, TAC, UAPC, AOC_{ABTS}, and AOC_{DPPH} in individual leaves were significantly higher in the order of 38, 30, and 23 DAT, with the values affected by the leaf

Table 2-1. Phenolic content and antioxidant capacity in individual leaves of kale plants according to UV-B radiation and leaf group at 23, 30, and 38 days after transplanting (DAT).

DAT	Leaf group	UV-B radiation	TPC	TFC	TAC	UAPC	AOC$_{ABTS}$	AOC$_{DPPH}$
23	2	Control	8.03 b	3.99	0.81	1.02 b	4.85 b	3.70 c
		UV6h	8.03 b	3.99	0.88	1.22 a	5.67 b	4.64 b
		UV12h	8.98 a	4.14	1.08	1.33 a	6.10 a	5.57 a
	3	Control	7.97	3.06 b	0.66 b	1.16 b	4.49 b	3.87 b
		UV6h	8.78	4.30 ab	0.77 ab	1.41 ab	5.78 ab	5.31 ab
		UV12h	9.44	5.65 a	1.28 a	1.57 a	6.10 a	5.73 a
30	1	Control	9.37 ab	4.97 b	0.85	0.98	4.10	4.30
		UV6h	9.20 b	5.26 ab	1.01	1.11	3.71	3.90
		UV12h	10.3 a	6.17 a	0.92	1.06	4.10	5.40
	2	Control	9.96 b	5.04 b	0.68	1.00 b	4.43 b	4.98 b
		UV6h	10.4 b	6.55 a	0.80	1.13 ab	4.77 b	5.32 ab
		UV12h	11.3 a	6.76 a	0.80	1.27 a	5.57 a	5.75 a
	3	Control	10.6	5.49 b	0.64	1.23 b	5.19 b	5.40 b
		UV6h	10.5	6.22 b	0.71	1.42 ab	5.65 ab	5.49 a
		UV12h	10.8	7.23 a	0.78	1.66 a	6.07 a	5.70 a
38	1	Control	9.11 b	4.74 b	1.21 b	1.02	3.74	3.80
		UV6h	10.2 a	5.56 a	1.38 ab	1.02	4.00	4.00
		UV12h	10.7 a	6.01 a	1.63 a	1.20	4.02	4.26
	2	Control	9.83 b	4.82 b	1.06 ab	1.14	4.40 b	4.87 b
		UV6h	10.4 a	5.86 a	0.91 b	1.14	5.09 a	5.32 a
		UV12h	10.0 ab	5.42 ab	1.31 a	1.26	4.50 b	5.21 ab
	3	Control	10.2	4.98 b	0.71	1.34 b	5.56 b	5.66 b
		UV6h	9.90	5.58 a	0.68	1.41 ab	5.92 a	5.67 a
		UV12h	10.1	5.38 ab	0.79	1.52 a	5.74 b	5.68 ab

		TPC	TFC	TAC	UAPC	AOC$_{ABTS}$	AOC$_{DPPH}$
UV-B	Control	9.38 B	4.64 B	0.83 B	1.11 C	4.60 B	4.57 C
	UV6h	9.66 B	5.41 A	0.90 B	1.23 B	5.07 A	4.96 B
	UV12h	10.2 A	5.85 A	1.07 A	1.35 A	5.25 A	5.40 A
DAT	23	8.50 C	4.12 C	0.92 A	1.27	5.47 A	4.76 B
	30	10.3 A	5.97 A	0.80 B	1.21	4.84 B	5.12 A
	38	10.0 B	5.37 B	1.08 A	1.23	4.78 B	4.94 B
Leaf group	1	9.78	5.45	1.17 A	1.07 C	3.95 C	4.17 C
	2	9.66	5.17	0.93 B	1.17 B	5.04 B	5.04 B
	3	9.82	5.31	0.77 C	1.42 A	5.60 A	5.38 A
Significance							
DAT		***	***	***	ns	***	***
Leaf group		ns	ns	***	***	***	***
DAT × leaf group		*	***	***	***	***	***

TPC, total phenolic content (mg GAE g^{-1} DM); TFC, total flavonoid content (mg CE g^{-1} DM); TAC, total anthocyanin content (mg C3GE g^{-1} DM); UAPC, UV-absorbing pigment content (OD g^{-1} DM); AOC$_{ABTS}$ or AOC$_{DPPH}$, antioxidant capacity using ABTS or DPPH assay, respectively (mg AAE g^{-1} DM).

Different letters indicate significant differences by post-hoc test at $P < 0.05$ for each parameter referring to the Materials and Methods: lowercase, among UV-B radiation ($n = 4$); uppercase, among UV-B radiation ($n = 31$-32), DAT ($n = 24$ for 23 DAT or $n = 36$ for the others) or leaf group ($n = 24$ for group 1 or $n = 36$ for the others).

Asterisks indicate significant differences by two-way ANOVA with DAT and leaf group.

*, $P < 0.05$; ***, $P < 0.001$; ns, not significant.

UV-B radiation interception according to leaf group and growth stage

UV-B radiation interception with a 3D-scanned plant model was simulated along with the actual plant structure at each growth stage (Fig. 2-3a). The UV radiation interception (UVR_{int}) was significantly higher in the order of leaf groups 3, 2, and 1 (Fig. 2-3b). Across all stages, the UVR_{int} was significantly lower by 51.7% in leaf group 1 and significantly higher by 31.4% in the group 3 than in the group 2. The means of UVR_{int} at 23, 30, and 38 DAT were 1.20,

Table 2-2. Chlorophyll and carotenoid contents in individual leaves of kale plants according to UV-B radiation and leaf group at 23, 30, and 38 days after transplanting (DAT).

DAT	Leaf group	UV-B radiation	Chlorophyll a (mg g⁻¹ DM)	Chlorophyll b (mg g⁻¹ DM)	Chlorophyll a/b ratio	Total chlorophyll (mg g⁻¹ DM)	Carotenoid (mg g⁻¹ DM)
23	2	Control	6.24 b	2.69 b	2.32 b	8.93	1.59
		UV6h	7.24 ab	3.04 a	2.38 b	10.3	1.73
		UV12h	7.65 a	3.00 ab	2.55 a	10.7	1.73
	3	Control	7.62	2.87	2.66	10.5	1.92
		UV6h	8.54	3.27	2.62	11.8	2.18
		UV12h	7.87	2.99	2.63	10.9	2.16
30	1	Control	7.97	3.36 ab	2.38	11.3 ab	1.95 ab
		UV6h	9.12	3.98 a	2.28	13.1 a	2.22 a
		UV12h	7.61	3.31 b	2.30	10.9 b	1.94 b
	2	Control	8.98	3.49 ab	2.58 b	12.5	2.24
		UV6h	9.58	3.81 a	2.52 b	13.4	2.33
		UV12h	8.44	3.18 b	2.65 a	11.6	2.16
	3	Control	8.58	3.34 a	2.57	11.9 ab	2.34 ab
		UV6h	9.21	3.57 a	2.58	12.8 a	2.56 a
		UV12h	7.72	2.91 b	2.65	10.6 b	2.21 b
38	1	Control	7.51	3.26	2.32	10.8	2.08
		UV6h	8.43	3.50	2.40	11.9	2.16
		UV12h	7.77	3.31	2.34	11.1	2.19
	2	Control	8.63 a	3.33 a	2.62	12.0 ab	2.18 ab
		UV6h	8.56 a	3.24 ab	2.65	11.8 a	2.30 a
		UV12h	7.01 b	2.66 b	2.65	9.67 b	1.96 b
	3	Control	7.92 a	3.07 a	2.58	11.0 b	2.24 b
		UV6h	8.45 a	3.26 a	2.59	11.7 a	2.47 a
		UV12h	6.53 b	2.55 b	2.57	9.08 c	1.94 c

UV-B	Control	7.94 B	3.19 B	2.50	11.1 B	2.07 B
	UV6h	8.64 A	3.46 A	2.50	12.1 A	2.24 A
	UV12h	7.56 C	2.99 C	2.54	10.6 C	2.03 B
DAT	23	7.51 B	2.98 B	2.51	10.5 B	1.87 B
	30	8.58 A	3.44 A	2.50	12.0 A	2.22 A
	38	7.87 B	3.13 B	2.52	11.0 B	2.17 A
Leaf group	1	8.07	3.46 A	2.34 B	11.5	2.09 B
	2	8.04	3.16 B	2.55 A	11.2	2.03 B
	3	8.07	3.10 B	2.60 A	11.2	2.23 A
Significance						
DAT		***	***	ns	***	***
Leaf group		ns	**	***	ns	***
DAT × leaf group		**	ns	***	*	**

Different letters indicate significant differences (by post-hoc test at $P < 0.05$) for each parameter referring to Materials and Methods: lowercase, among UV-B radiation ($n = 4$); uppercase, among UV-B radiation ($n = 31$-32), DAT ($n = 24$ for 23 DAT or $n = 36$ for the others) or leaf group ($n = 24$ for group 1 or $n = 36$ for the others).

Asterisks indicate significant differences by two-way ANOVA with DAT and leaf group.

*, $P < 0.05$; **, $P < 0.01$; ***, $P < 0.001$; ns, not significant.
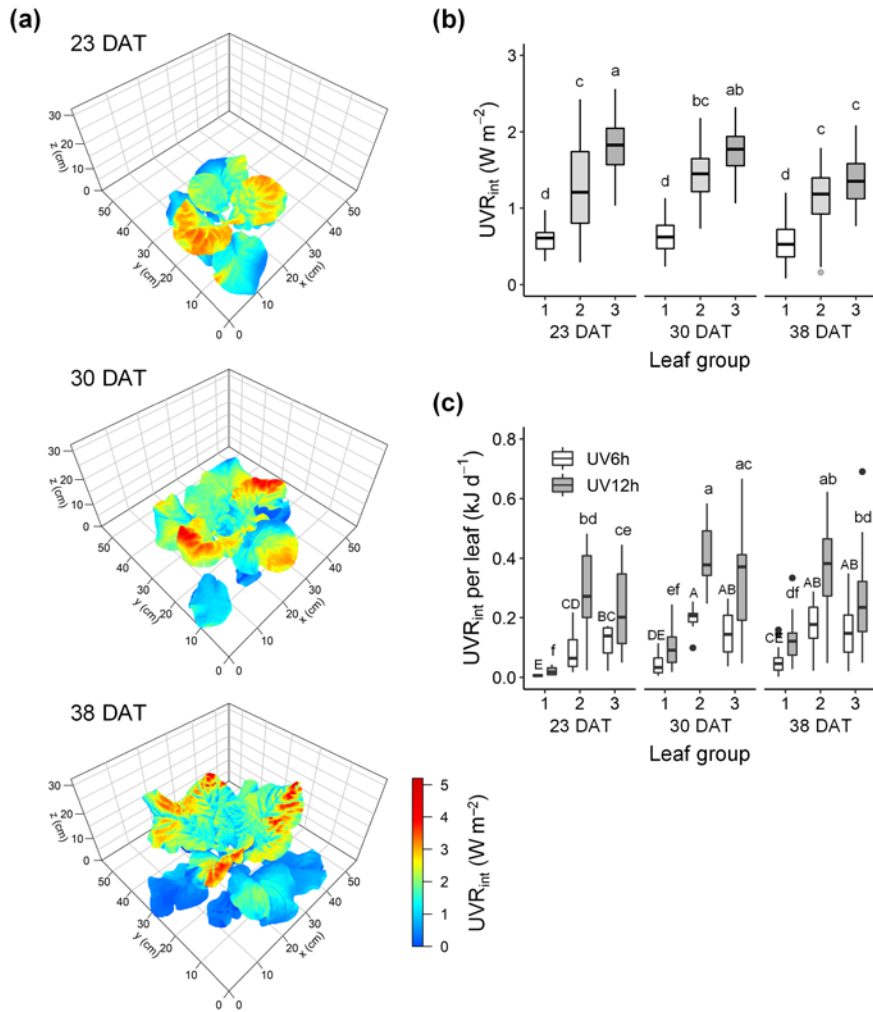
Fig. 2-3. Representative simulated UV-B radiation interception (UVR$_{int}$) on 3D-scanned models (a), mean UVR$_{int}$ (b), and daily UVR$_{int}$ per leaf (c) of kale plants according to UV-B radiation and leaf group at 23, 30, and 38 days after transplanting (DAT). Different letters indicate significant differences at $P < 0.05$ for UVR$_{int}$ value ($n = 26$-47) and for daily UVR$_{int}$ per leaf ($n = 11$-25) with growth stage and leaf group by two-way ANOVA and Tukey's HSD test.

1.28, and 1.05 W m^{-2}, respectively. The daily UVR_{int} per leaf did not significantly differ between the leaf groups 2 and 3 and was affected by individual leaf area (Fig. 2-3c). Across all data, the daily UVR_{int} per plant was significantly higher with growth stage (1.7 ± 0.5, 2.2 ± 0.3, and 2.6 ± 0.4 kJ d^{-1} per plant at 23, 30, and 38 DAT, respectively).

Prediction models of phenolic content based on UV-B radiation interception and leaf order according to growth stage

Multiple regression models for the phenolic contents per leaf based on daily UVR_{int} per leaf and leaf order were developed according to growth stage, and all models were significant at $P < 0.001$ (Fig. 2-4, Table 2-3). The models for the TPC, TFC, and UAPC in individual leaves at each growth stage showed high explanatory power, with $R^2 = 0.62\text{-}0.79$. However, the models for the TAC per leaf showed a low explanatory power, with $R^2 < 0.51$. All estimated coefficients were significant for the regression models. From the models, spatial and intraindividual distributions of TPC and TFC on the 3D-scanned plant model were estimated (Fig. 2-5). The R^2 values for the four models were higher in the data set integrated from the models across whole growth stage than in the models at each growth stage (Table 2-3, Fig. A2-5).

The accuracies of the models for TPC, TFC, TAC, and UAPC per leaf were validated with test data sets (Fig. 2-6). All models performed well for the whole growth stage, with $R^2 = 0.78\text{-}0.79$. The TPC, TFC, and UAPC models showed
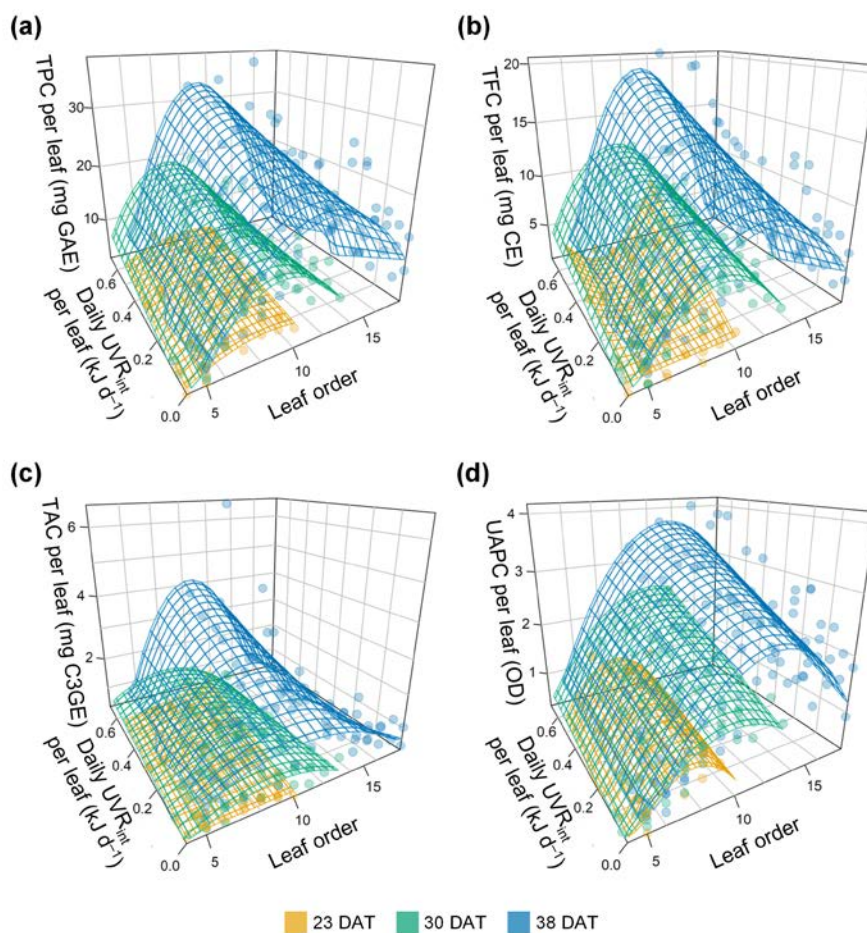
Fig. 2-4. Multiple linear regression for phenolic content per leaf of kale plants with daily UV-B radiation interception (UVR$_{int}$) per leaf and leaf order at 23, 30, and 38 days after transplanting (DAT): TPC, total phenolic content (a); TFC, total flavonoid content (b); TAC, total anthocyanin content (c); UAPC, UV-absorbing pigment content (d). The surfaces were obtained by stepwise multiple regression models referring to Eq. 2-1 and Table 2-3.

Table 2-3. Multiple regression results and models to predict phenolic content per leaf of kale plants at 23, 30, and 38 days after transplanting (DAT) based on leaf order (L) and daily UV-B radiation interception per leaf (U) referring to Eq. 2-1.

Model	DAT	R^2	Adj R^2	RMSE	NRMSE	P-value	Model equation
TPC	23	0.63	0.61	1.23	17.3	<0.001	$M(L, U) = -5.01 + 2.72L - 0.16L^2 + 6.54U$
	30	0.77	0.76	2.17	18.4	<0.001	$M(L, U) = -25.29 + 8.30L - 0.44L^2 + (4.54L - 0.38L^2)U$
	38	0.72	0.70	3.90	22.3	<0.001	$M(L, U) = -26.03 + 7.62L - 0.31L^2 + (-73.52 + 17.18L - 0.80L^2)U$
	Integ	0.83	0.83	2.91	22.2		
TFC	23	0.62	0.60	0.73	21.4	<0.001	$M(L, U) = 2.42 + (39.67 - 12.02L + 0.96L^2)U$
	30	0.78	0.77	1.35	19.6	<0.001	$M(L, U) = -13.38 + 4.52L - 0.25L^2 + (2.34L - 0.15L^2)U$
	38	0.74	0.73	2.16	23.3	<0.001	$M(L, U) = -12.23 + 3.80L - 0.16L^2 + (-47.53 + 10.88L - 0.49L^2)U$
	Integ	0.83		1.65	23.5		
TAC	23	0.39	0.38	0.25	34.4	<0.001	$M(L, U) = 0.48 + 0.18LU$
	30	0.46	0.43	0.24	26.0	<0.001	$M(L, U) = -1.21 + 0.48L - 0.03L^2 + (0.30L - 0.03L^2)U$
	38	0.51	0.48	0.65	36.9	<0.001	$M(L, U) = -0.44 + 0.41L - 0.02L^2 + (-17.19 + 3.92L - 0.19L^2)U$
	Integ	0.66		0.47	37.9		
UAPC	23	0.63	0.59	0.20	17.9	<0.001	$M(L, U) = -3.18 + 1.13L - 0.08L^2 + 1.05U$
	30	0.79	0.78	0.25	17.7	<0.001	$M(L, U) = -1.78 + 0.64L - 0.03L^2 + 0.17LU$
	38	0.72	0.71	0.48	23.1	<0.001	$M(L, U) = -3.67 + 0.99L - 0.04L^2 + 0.14LU$
	Integ	0.79		0.38	22.6		

TPC, total phenolic content per leaf (mg GAE per leaf); TFC, total flavonoid content per leaf (mg CE per leaf); TAC, total anthocyanin content per leaf (mg C3GE per leaf); UAPC, UV-absorbing pigment content per leaf (OD per leaf). R^2, the coefficient of determination; Adj R^2, adjusted R^2; RMSE, root mean squared error; NRMSE, normalized RMSE (%). Integ, integration results in the data set across all growth stages integrated from the models at each growth stage.
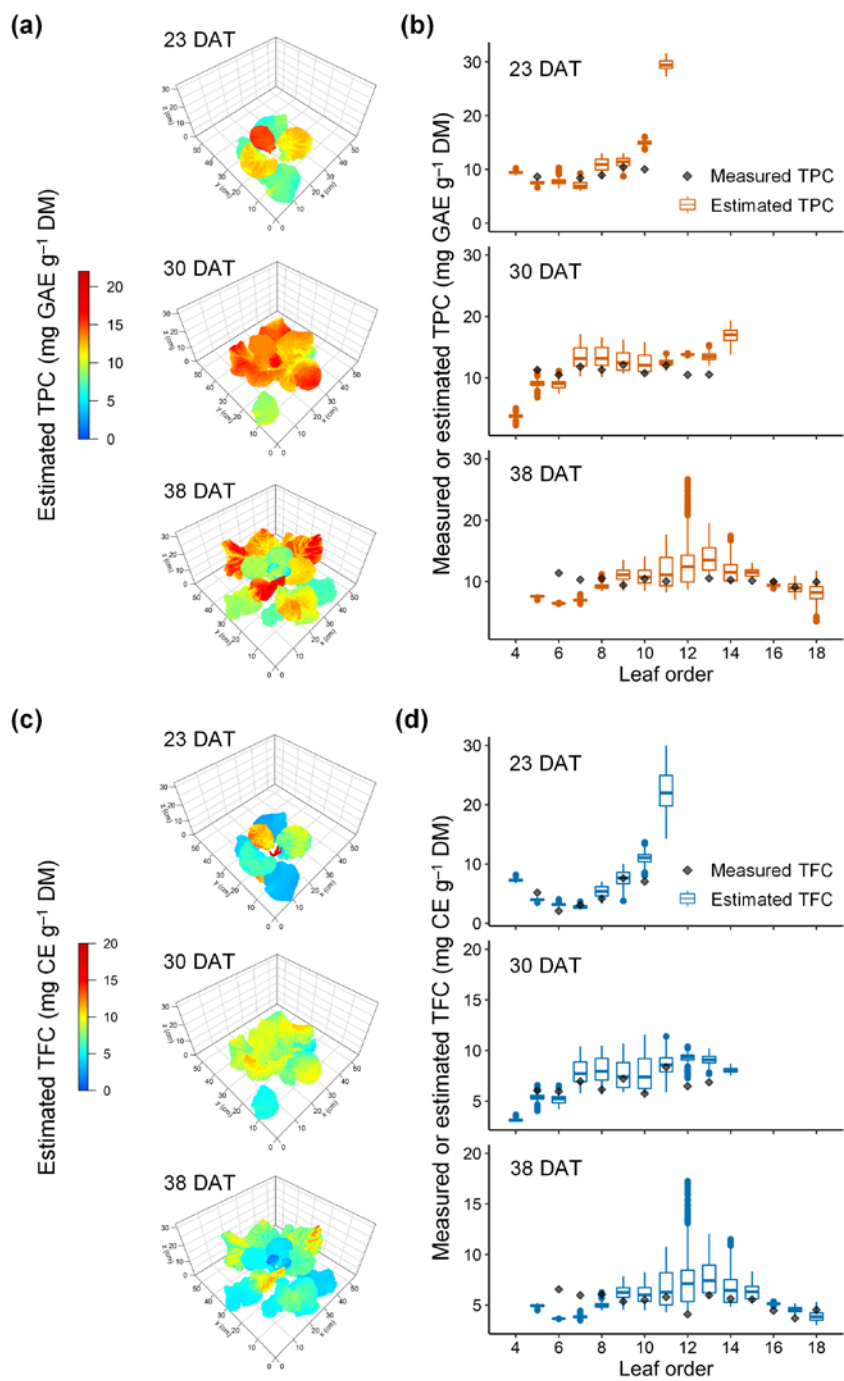
Fig. 2-5. Representative estimated distribution of total phenolic content (TPC,

a, b) and total flavonoid content (TFC, c, d) in the leaves of kale plants under 12-h UV-B exposure at 23, 30, and 38 days after transplanting (DAT). The multiple regression models refer to Fig. 2-4 and Table 2-3, and the 3D-scanned plant model refers to Fig. 2-3.
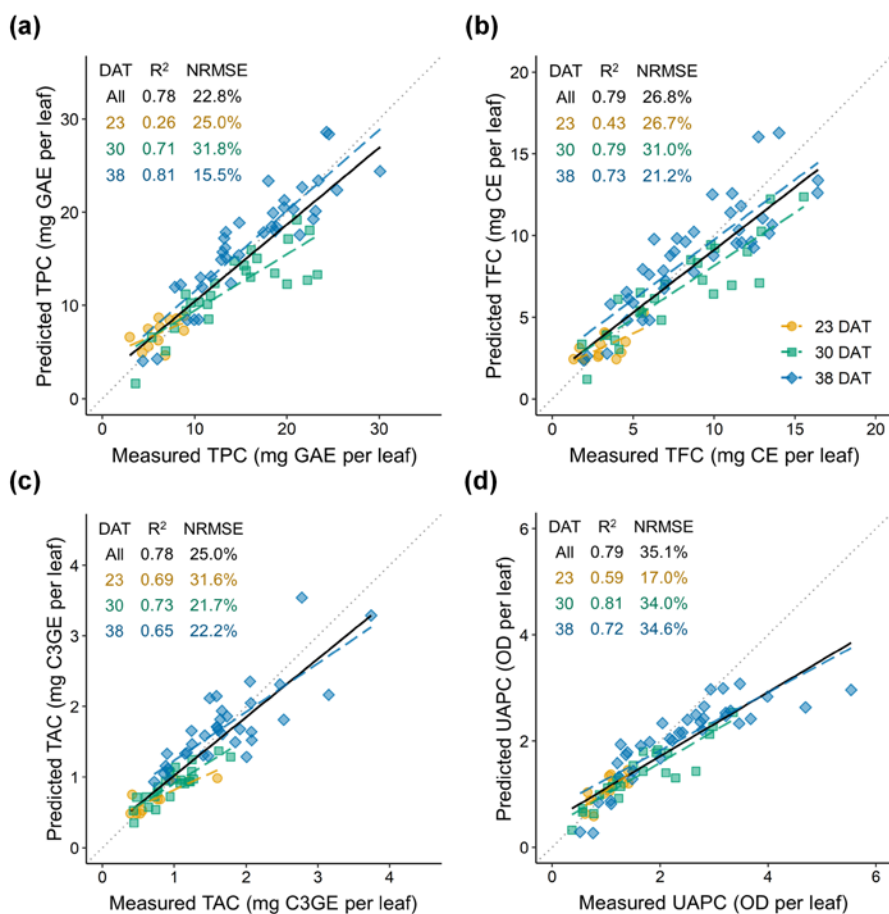
Fig. 2-6. Model accuracy for predicting phenolic content per leaf of kale plants using test data set: TPC, total phenolic content per leaf (a); TFC, total flavonoid content per leaf (b); TAC, total anthocyanin content per leaf (c); UAPC, UV-absorbing pigment content per leaf (d). The coefficient of determination (R^2) and the normalized root mean squared error (NRMSE) are presented inside each panel. The multiple regression models at 23, 30, and 38 days after transplanting (DAT) are shown in Fig. 2-4 and Table 2-3. All in DAT indicate the results in the data set across all growth stages integrated from the models at each growth stage.

high performance with $R^2 > 0.7$, except for those at 23 DAT. The TAC model showed high performance with $R^2 > 0.6$ at all growth stages. The TPC model for the whole growth stage showed approximately 22.8% relative error, meaning that the model could predict the TPC per leaf with 77.2% accuracy during 23-38 DAT. Likewise, the models could predict TFC, TAC, and UAPC per leaf with 73.2, 75.0, and 64.9% accuracy, respectively, during 23-38 DAT.

UV-B energy yield for phenolic content with growth stage

The UV-B energy yields for the TPC, TFC, TAC, and UAPC based on absorbed UV energy were significantly different depending on the growth stage, leaf group, and their interaction (Table 2-4). The UV-B energy yields for the TPC, TFC, and TAC were highest in leaf group 2 at 38 DAT, which were 1.5-, 1.4-, and 3-fold higher, respectively, than those at 30 DAT. The yield for the UAPC was highest in leaf group 3 at 38 DAT, which was 1.2-fold higher than at 30 DAT. Across the three growth stages, the UV-B energy yields for the TPC, TFC, and UAPC significantly increased as growth progressed but that for TAC decreased. The yields for the TPC, TFC, and UAPC were 1.3-, 1.6-, and 1.3-fold higher, respectively, at 30 DAT than at 23 DAT. Across leaf groups, the energy yields for the TPC, TFC, and TAC were significantly higher in leaf group 2 than in the other leaves (2.5-, 1.6-, and 5.6-fold increases on average, respectively), whereas that for the UAPC was higher in leaf group 3 (1.7-fold increase on average, than in the other leaves). In leaf group 2, those for the TPC

Table 2-4. UV-B energy yields for phenolic content per leaf of kale plants with leaf group at 23, 30, and 38 days after transplanting (DAT) referring to Eq. 2-2 and Table 2-3.

DAT	Leaf group	UV-B energy yield			
		TPC	TFC	TAC	UAPC
23	2	6.54 c	3.14 d	1.05 bc	1.05 e
	3	6.54 c	7.68 b	1.53 b	1.05 e
30	1	13.1 b	7.91 b	0.89 bc	0.87 f
	2	11.6 b	8.70 b	0.81 bc	1.33 d
	3	2.47 c	6.63 bc	0.23 cd	1.86 b
38	1	3.80 c	2.16 d	0.32 cd	0.95 ef
	2	17.9 a	12.2 a	3.31 a	1.53 c
	3	3.65 c	5.05 cd	-0.28 d	2.15 a
DAT	23	6.54 B	4.91 B	1.22 A	1.05 C
	30	8.47 A	7.67 A	0.61 B	1.40 B
	38	8.02 A	6.31 A	1.00 A	1.58 A
Leaf group	1	7.40 B	4.39 C	0.54 B	0.91 C
	2	12.2 A	8.11 A	1.81 A	1.30 B
	3	3.69 C	6.06 B	0.23 B	1.83 A
Significance					
DAT		*	***	*	***
Leaf group		***	***	***	***
DAT × leaf group		***	***	***	***

TPC, yield for total phenolic content (mg GAE kJ^{-1} d); TFC, yield for total flavonoid content (mg CE kJ^{-1} d); TAC, yield for total anthocyanin content (mg C3GE kJ^{-1} d); UAPC, yield for UV-absorbing pigment content (OD kJ^{-1} d).
Different letters indicate significant differences by two-way or one-way ANOVA and post-hoc test at $P < 0.05$ for each parameter referring to Materials and Methods.
*, $P < 0.05$; ***, $P < 0.001$.

and TFC increased significantly as growth progressed but decreased or were similar in the group 3. The UV-B yields for the UAPC in both leaf groups 2 and 3 increased significantly as growth progressed.

DISCUSSION

Narrow-band UV-B radiation on plants

Variables affecting the perception of UV-B radiation by plants, such as dose (fluence rate and duration), timing during a day or growth stages, light sources (solar, broad-band, or narrow-band UV lamp), and setup (greenhouse or chamber), make it hard to define the intensity or dose thresholds of UV-B radiation (Meyer et al., 2021). This confusion without coherence hampers understanding of plant physiology as well as commercial use to bioactive compound production. High doses of UV-B (high fluence rate, long duration, or shorter wavelength) cause metabolic disorders, such as chlorophyll degradation and generation of reactive oxygen species (ROS), supporting the long-held opinion that UV-B radiation is harmful for plants (Jordan, 2002). Recent studies have highlighted the regulatory properties of moderate UV-B radiation (low and ecologically-relevant level or longer wavelength) as an eustressor and numerous acclimation strategies, including changes in secondary metabolism (Hideg et al., 2013; Neugart and Schreiner, 2018). In general, plants perceive UV-B radiation by the specific receptor UV RESISTANCE LOCUS 8 (UVR8), leading to signal transduction of UVR8-COP1 (CONSTITUTIVE PHOTOMORPHOGENESIS1) with ELONGATED HYPOCOTYL5 (HY5) and HY5 HOMOLOG (HYH) transcription factors (Liang et al., 2019). O'Hara et al. (2019) reported that the expression of a gene encoding the transcription

factor ARABIDOPSIS NAC DOMAIN PROTEIN 13 (ANAC13) was induced over a range of UV-B wavelengths at low doses, with a maximum response at 310 nm. Rácz and Hideg (2021) reported that the antioxidant enzyme activities under narrow-band 311 nm UV-B radiation evoked opposite responses from broad-band UV radiation. These suggestions may support the results in the present study, that the contents of bioactive compounds increased in kale plants exposed to UV-B radiation generated by the narrow-band 310 nm UV-B LED despite the high fluence rate without distinct damage to growth or chlorophyll content (Tables 2-1, 2-2, Fig. A2-3).

Effect of UV-B radiation on phenolic content in plants

UV-B radiation has been reported to be effective in increasing phenolic contents and AOC. In this study, the TPC, TFC, TAC, UAPC, and AOC per DM and per leaf were significantly higher with longer UV-B exposure (Table 2-1, Fig. A2-4). As a response to UV-B radiation, the enhanced biosynthesis of phenylpropanoids has well been documented in *Brassica* species including kale (Neugart and Bumke-Vogt, 2021; Castillejo et al., 2021). Under UV-B exposure, phenolics and flavonoids accumulate in epidermal tissues and act as direct UV-screens, i.e., main components of UAP (Neugart and Schreiner, 2018). The innate antioxidant potential of the compounds increases ROS scavenging activity and protects sensitive tissues from the high UV-B energy (Hideg et al., 2013). Dou et al. (2019) reported that AOC was positively correlated with UV-

B dose, resulting from linear increases in the TPC and TFC in basil.

Plant and leaf developmental stages determine the UV-B-induced accumulation of bioactive compounds, but the relationships are not straightforward. In this study, the leaf groups 1, 2, and 3 correspond to relatively old, intermediate, and young leaves at each growth stage, respectively, as determined by the order of leaf emergence and the relative growth state (Fig. A2-2). The increase rates of phenolic accumulation with UV-B radiation were highest in young leaves at 23 DAT, but those were not always higher in younger leaves than the other leaves at 30 and 38 DAT (Table 2-1). Rizi et al. (2021) reported that UV-B-exposed young leaves of *Salvia verticillata* showed higher phenylpropanoid production than old leaves as higher gene expression of the key enzymes in their synthesis. However, young leaves are typically located near the top of the plant, and are more exposed to UV-B radiation than the other leaves. At the plant canopy levels, higher canopy porosity was positively correlated with the contents of flavonoids, such as kaempferol and quercetin in red wine grapes (Martínez-Lüscher et al., 2019). Therefore, at least locally accumulated UV-B-induced phenolics are determined by structural factors such as leaf position, area, and curvature as well as by developmental age.

UV-B radiation interception on plant structures

The plant structure varies depending on its phyllotaxis and changes as the plant grows, but the plants are exposed to UV-B sources in a one-size-fits-all manner.

The UV-B energy absorbed and its physiological interaction at individual leaves inevitably lead to a heterogeneous response in the plant. In this study, UV radiation interception was simulated well along with structural properties, including leaf height, angle, and surface curvature using ray-tracing simulation and a 3D-scanned plant model (Fig. 2-3). Previous studies on light interception in plant structure have focused on the spatial distribution of PAR interception and photosynthesis using simulations (Sarlikioti et al., 2011; Shin et al., 2021). In controlled environments, the PAR interception was determined by the physical structures and arrangements of plants and artificial lighting (Kim et al., 2020; Saito et al., 2020). As growth progressed, plant height increased, but the UVR_{int} value of the leaf group 3 decreased (Fig. 2-3b). Reduced overlap of radiation at the position close to the UV-B LEDs with a narrow radiation area and the mutual shading by neighboring plants decreased the UVR_{int} despite growth progress (Yoon et al., 2021b).

Predicting models of phenolic content in 3D plant structures

In general, major environmental factors are controlled to optimize crop photosynthesis and growth in controlled environments (Carotti et al., 2021). Secondary metabolite production has been attempted to be maximized beyond biomass controlling environmental factors including temperature, relative humidity, photoperiod, and light spectrum (Shim et al., 2018; Johnson et al., 2019; Appolloni et al., 2021). Unlike other environmental factors,

supplementation with UV-B radiation near harvest could be more effective

without growth loss or additional energy input (dos S. Nascimento et al., 2020;

Yoon et al., 2020). Since UV-B exposure is a potent abiotic elicitor for the

biosynthesis of secondary metabolites, its energy inputs should be optimized

(Thakur et al., 2019; Toscano et al., 2019). Optimization of various elicitors

have mostly been reported in the studies of in vitro plant tissue culture

(Ghorbani et al., 2015; Farjaminezhad and Garoosi, 2021).

The present study developed statistical models to assess how UV-B

radiation as an elicitor enhances the phenolic accumulation in kale plants. For

this purpose, the daily absorbed UV-B energy and the phenolic contents were

analyzed as each value per leaf (Figs. 2-3c, A2-4). The developed models

suitably explained the TPC, TFC, and UAPC as functions of UV-B radiation

interception and leaf order according to growth stage (Table 2-3, Figs. 2-4, 2-

5). These models showed high accuracies for predicting the TPC, TFC, TAC,

and UAPC (Fig. 2-6). The relatively low R^2 of the models at 23 DAT might be

due to the small number of measured samples, which was less than half of the

total (Figs. 2-6c, d, A2-1).

Statistical modeling is an effective tool for quantifying the relationship

between dependent and independent variables by the statistical significance of

their correlations (Kim et al., 2016). Kim et al. (2018) developed a statistical

model for glucosinolate content in Chinese cabbage using a second-order multi-

polynomial equation with growth duration and temperature as independent

variables. In the present study, the model structure was determined according to the linear pattern of phenolic accumulation with UV-B dose as shown in the results from previous studies (Dou et al., 2019; Yoon et al., 2021a) or quadratic pattern with leaf group as shown in Fig. A2-4 and the results from a previous study (Yoon et al., 2021b). However, the developed models were limited to kale plants between 23 and 38 DAT in the UVR_{int} range below 2.5 W m^{-2} (Fig. 2-3). Within the 3D plant structure, UV-B radiation further enhanced the intraindividual heterogeneity of phenolic contents (Yoon et al., 2021a). Using UV-B radiation interception on a 3D-scanned plant model, the developed models could extend the prediction of phenolic accumulation from intraindividual distribution level to the spatial distribution level (Fig. 2-4). This approach to the distribution of metabolites in 3D plant structure could provide the groundwork for plant metabolism and plant-environment interaction studies (Floros et al., 2017).

Application to phenolic production in controlled environment agriculture
The main goal of controlled environment agriculture is to maximize plant productivity and minimize practical production costs, including energy cost (Kozai, 2018). The utilization efficiency of lighting systems on plant structures could be calculated using ray-tracing simulations and 3D-scanned plant models (Kim et al., 2020; Saito et al., 2020). The simulation results along with the photosynthesis model could be used to find out the optimal lighting system with

maximal light use efficiency for photosynthesis (Kim et al., 2020). In the present study, the UV-B energy yield for phenolic content was calculated (Table 2-4). The annual production of bioactive compounds was simply estimated based on plant density (plant m^{-2}) and cultivation cycle per year according to harvest time (Yoon et al., 2019). In this study, the optimal harvest time was 30 DAT with the highest annual production of TFC due to greater plant density and number of cycles per year, despite of smaller plants and lower UV-B yield at 30 DAT than at 38 DAT. Further steps in the modeling procedure for agriculture and food systems were model simulation and model-based analysis (Kim et al., 2016). These steps allow us to investigate numerous scenarios and predict the system responses with cost and input in an effective way (Kreutz and Timmer, 2009). Therefore, the developed model in this study could be used to predict the phenolic accumulation with effective UV-B energy input through model-based simulation in various environments.

In conclusion, this is the first study on the prediction of phenolic content with UV-B radiation interception and developmental age. Multiple regression models for the TPC, TFC, TAC, and UAPC were developed and validated with high accuracy. Pre-harvest UV-B radiation was also identified as a suitable strategy for commercial production of secondary metabolites in controlled environments. Ultimately the model-based simulation will be used to find out the optimal conditions for the production of secondary metabolites, saving production time and cost.

LITERATURE CITED

Ainsworth EA, Gillespie KM (2007) Estimation of total phenolic content and other oxidation substrates in plant tissues using Folin-Ciocalteu reagent. Nat Protoc 2:875–877.

Aphalo PJ, Albert A, Björn LO, McLeod AR, Robson TM, Rosenqvist E (Eds.) (2012) Beyond the visible: A handbook of best practice in plant UV photobiology. COST Action FA0906 UV4growth. Univ. of Helsinki, Finland.

Appolloni E, Pennisi G, Zauli I, Carotti L, Paucek I, Quaini S, Orsini F, Gianquinto G (2021) Beyond vegetables: Effects of indoor LED light on specialized metabolite biosynthesis in medicinal and aromatic plants, edible flowers, and microgreens. J Sci Food Agric doi: 10.1002/jsfa.11513.

Behn H, Schurr U, Ulbrich A, Noga G (2011) Development-dependent UV-B responses in red oak leaf lettuce (*Lactuca sativa* L.): Physiological mechanisms and significance for hardening. Eur J Hortic Sci 76:33–40.

Brand-Williams W, Cuvelier ME, Berset C (1995) Use of a free radical method to evaluate antioxidant activity. LWT Food Sci Technol 28:25–30.

Carotti L, Graamans L, Puksic F, Butturini M, Meinen E, Heuvelink E, Stanghellini C (2021) Plant factories are heating up: Hunting for the best combination of light intensity, air temperature, and root-zone temperature in lettuce production. Front Plant Sci 11:909.

Castillejo N, Martínez-Zamora L, Artés-Hernández F (2021) Periodical UV-B radiation hormesis in biosynthesis of kale sprouts nutraceuticals. Plant Physiol Biochem 165:274–285.

Csepregi K, Coffey A, Cunningham N, Prinsen E, Hideg É, Jansen MAK (2017) Developmental age and UV-B exposure co-determine antioxidant capacity and flavonol accumulation in *Arabidopsis* leaves. Environ Exp Bot 140:19–25.

Csepregi K, Neugart S, Schreiner M, Hideg É (2016) Comparative evaluation of total antioxidant capacities of plant polyphenols. Molecules 21:208.

Dewanto V, Xianzhong W, Adom KK, Liu RH (2002) Thermal processing enhances the nutritional value of tomatoes by increasing total antioxidant activity. J Agric Food Chem 50:3010–3014.

dos S. Nascimento LB, Brunetti C, Agati G, Lo Iacono C, Detti C, Giordani E, Ferrini F, Gori A (2020) Short-term pre-harvest UV-B supplement enhances the polyphenol content and antioxidant capacity of *Ocimum basilicum* leaves during storage. Plants 9:797.

Dou H, Niu G, Gu M (2019) Pre-harvest UV-B radiation and photosynthetic photon flux density interactively affect plant photosynthesis, growth, and secondary metabolites accumulation in basil (*Ocimum Basilicum*) plants. Agronomy 9:434.

Farjaminezhad R, Garoosi G (2021) Improvement and prediction of secondary metabolites production under yeast extract elicitation of *Azadirachta indica*

cell suspension culture using response surface methodology. AMB Express 11:43.

Flint SD, Caldwell MM (2003) A biological spectral weighting function for ozone depletion research with higher plants. Physiol Plant 117:137–144.

Floros DJ, Petras D, Kapono CA, Melnik AV, Ling TJ, Knight R, Dorrestein PC (2017) Mass spectrometry based molecular 3D-cartography of plant metabolites. Front Plant Sci 8:1–9.

Francisco M, Tortosa M, Martínez-Ballesta M, Velasco P, García-Viguera C, Moreno DA (2017) Nutritional and phytochemical value of *Brassica* crops from the agri-food perspective. Ann Appl Biol 170:273–285.

Ghorbani M, Ghorbani A, Omidi M, Hashemi SM (2015) Response surface modeling of noradrenaline production in hairy root culture of purslane (*Portulaca oleracea* L.). Turkish J Agric Food Sci Technol 3:349.

Heinze M, Hanschen FS, Wiesner-Reinhold M, Baldermann S, Gräfe J, Schreiner M, Neugart S (2018) Effects of developmental stages and reduced UVB and low UV conditions on plant secondary metabolite profiles in pak choi (*Brassica rapa* subsp. *chinensis*). J Agric Food Chem 66:1678–1692.

Hideg É, Jansen MAK, Strid Å (2013) UV-B exposure, ROS, and stress: Inseparable companions or loosely linked associates? Trends Plant Sci 18:107–115.

Hitz T, Henke M, Graeff-Hönninger S, Munz S (2019) Three-dimensional simulation of light spectrum and intensity within an LED growth chamber.

Comput Electron Agric 156:540–548.

Johnson AJ, Meyerson E, de la Parra J, Savas TL, Miikkulainen R, Harper CB (2019) Flavor-cyber-agriculture: Optimization of plant metabolites in an open-source control environment through surrogate modeling. PLoS One 14:e0213918.

Jordan BR (2002) Review: Molecular response of plant cells to UV-B stress. Funct Plant Biol 29:909.

Khudyakova AY, Kreslavski VD, Shmarev AN, Lyubimov VY, Shirshikova GN, Pashkovskiy PP, Kuznetsov VV, Allakhverdiev SI (2019) Impact of UV-B radiation on the photosystem II activity, pro-/antioxidant balance, and expression of light-activated genes in *Arabidopsis thaliana hy4* mutants grown under light of different spectral composition. J Photochem Photobiol B Biol 194:14–20.

Kim D-G, Cho B-K, Lee W-H (2016) A novel approach in analyzing agriculture and food systems: Review of modeling and its applications. Kor J Agric Sci 43:163–175.

Kim D-G, Shim J-Y, Ko M-J, Chung S-O, Chowdhury M, Lee W-H (2018) Statistical modeling for estimating glucosinolate content in Chinese cabbage by growth conditions. J Sci Food Agric 98:3580–3587.

Kim J, Kang WH, Son JE (2020) Interpretation and evaluation of electrical lighting in plant factories with ray-tracing simulation and 3D plant modeling. Agronomy 10:1545.

Kneissl M, Seong T-Y, Han J, Amano H (2019) The emergence and prospects of deep-ultraviolet light-emitting diode technologies. Nat Photonics 13:233–244.

Kozai T (2018) Smart plant factory. Springer, Singapore.

Kreutz C, Timmer J (2009) Systems biology: Experimental design. FEBS J 276:923–942.

Liang T, Yang Y, Liu H (2019) Signal transduction mediated by the plant UV-B photoreceptor UVR8. New Phytol 221:1247–1252.

Liao X, Liu W, Yang H, Jenkins GI (2020) A dynamic model of UVR8 photoreceptor signaling in UV-B-acclimated *Arabidopsis*. New Phytol 227:857–866.

Lichtenthaler HK, Buschmann C (2001) Chlorophylls and carotenoids: Measurement and characterization by UV-VIS spectroscopy. Curr Protoc Food Anal Chem 1:F4.3.1-F4.3.8.

Loconsole D, Santamaria P (2021) UV lighting in horticulture: A sustainable tool for improving production quality and food safety. Horticulturae 7:9.

Loi M, Villani A, Paciolla F, Mulè G, Paciolla C (2020) Challenges and opportunities of light-emitting diode (LED) as key to modulate antioxidant compounds in plants: A review. Antioxidants 10:42.

Majer P, Hideg É (2012) Developmental stage is an important factor that determines the antioxidant responses of young and old grapevine leaves under UV irradiation in a greenhouse. Plant Physiol Biochem 50:15–23.

Martínez-Lüscher J, Brillante L, Kurtural SK (2019) Flavonol profile is a reliable indicator to assess canopy architecture and the exposure of red wine grapes to solar radiation. Front Plant Sci 10:32–42.

Meyer P, Van de Poel B, De Coninck B (2021) UV-B light and its application potential to reduce disease and pest incidence in crops. Hortic Res 8:194.

Mosadegh H, Trivellini A, Lucchesini M, Ferrante A, Maggini R, Vernieri P, Sodi AM (2019) UV-B physiological changes under conditions of distress and eustress in sweet basil. Plants 8:396.

Neugart S, Bumke-Vogt C (2021) Flavonoid glycosides in *Brassica* species respond to UV-B depending on exposure time and adaptation time. Molecules 26:494.

Neugart S, Schreiner M (2018) UVB and UVA as eustressors in horticultural and agricultural crops. Sci Hortic 234:370–381.

O'Hara A, Headland LR, Díaz-Ramos LA, Morales LO, Strid Å, Jenkins GI (2019) Regulation of *Arabidopsis* gene expression by low fluence rate UV-B independently of UVR8 and stress signaling. Photochem Photobiol Sci 18:1675–1684.

Paradiso R, Proietti S (2021) Light-quality manipulation to control plant growth and photomorphogenesis in greenhouse horticulture: The state of the art and the opportunities of modern LED systems. J Plant Growth Regul doi:10.1007/s00344-021-10337-y.

Pontarin N, Molinié R, Mathiron D, Tchoumtchoua J, Bassard S, Gagneul D,

Thiombiano B, Demailly H, Fontaine J-X, Guillot X, Sarazin V, Quéro A, Mesnard F (2020) Age-dependent metabolic profiles unravel the metabolic relationships within and between flax leaves (*Linum usitatissimum*). Metabolites 10:218.

Rácz A, Hideg É (2021) Narrow-band 311 nm ultraviolet-B radiation evokes different antioxidant responses from broad-band ultraviolet. Plants 10:1570.

Rankenberg T, Geldhof B, van Veen H, Holsteens K, Van de Poel B, Sasidharan R (2021) Age-dependent abiotic stress resilience in plants. Trends Plant Sci 26:692–705.

Re R, Pellegrini N, Proteggente A, Pannala A, Yang M, Rice-Evans C (1999) Antioxidant activity applying an improved ABTS radical cation decolorization assay. Free Radic Biol Med 26:1231–1237.

Rechner O, Neugart S, Schreiner M, Wu S, Poehling H-M (2016) Different narrow-band light ranges alter plant secondary metabolism and plant defense response to aphids. J Chem Ecol 42:989–1003.

Rizi MR, Azizi A, Sayyari M, Mirzaie-Asl A, Conti L (2021) Increased phenylpropanoids production in UV-B irradiated *Salvia verticillata* as a consequence of altered genes expression in young leaves. Plant Physiol Biochem 167:174–184.

Saito K, Ishigami Y, Goto E (2020) Evaluation of the light environment of a plant factory with artificial light by using an optical simulation. Agronomy 10:1663.

Šamec D, Urlić B, Salopek-Sondi B (2019) Kale (*Brassica oleracea* var. *acephala*) as a superfood: Review of the scientific evidence behind the statement. Crit Rev Food Sci Nutr 59:2411–2422.

Sarlikioti V, de Visser PHB, Marcelis LFM (2011) Exploring the spatial distribution of light interception and photosynthesis of canopies by means of a functional-structural plant model. Ann Bot 107:875–883.

Schreiner M, Krumbein A, Mewis I, Ulrichs C, Huyskens-Keil S (2009) Short-term and moderate UV-B radiation effects on secondary plant metabolism in different organs of nasturtium (*Tropaeolum majus* L.). Innov Food Sci Emerg Technol 10:93–96.

Schreiner M, Mewis I, Huyskens-Keil S, Jansen MAK, Zrenner R, Winkler JB, O'Brien N, Krumbein A (2012) UV-B-induced secondary plant metabolites: Potential benefits for plant and human health. CRC Crit Rev Plant Sci 31:229–240.

Shim J-Y, Kim H-Y, Kim D-G, Lee Y-S, Chung S-O, Lee W-H (2018) Optimizing growth conditions for glucosinolate production in Chinese cabbage. Hortic Environ Biotechnol 59:649–657.

Shin J, Hwang I, Kim D, Moon T, Kim J, Kang WH, Son JE (2021) Evaluation of the light profile and carbon assimilation of tomato plants in greenhouses with respect to film diffuseness and regional solar radiation using ray-tracing simulation. Agric For Meteorol 296:108219.

Si C, Yao XQ, He XL, Chu JZ, Ma CH, Shi XF (2015) Effects of enhanced UV-

B radiation on biochemical traits in postharvest flowers of medicinal chrysanthemum. Photochem Photobiol 91:845–850.

Sytar O, Bośko P, Živčák M, Brestic M, Smetanska I (2018) Bioactive phytochemicals and antioxidant properties of the grains and sprouts of colored wheat genotypes. Molecules 23:2282.

Takshak S, Agrawal SB (2019) Defense potential of secondary metabolites in medicinal plants under UV-B stress. J Photochem Photobiol B Biol 193:51–88.

Thakur M, Bhattacharya S, Khosla PK, Puri S (2019) Improving production of plant secondary metabolites through biotic and abiotic elicitation. J Appl Res Med Aromat Plants 12:1–12.

Toscano S, Trivellini A, Cocetta G, Bulgari R, Francini A, Romano D, Ferrante A (2019) Effect of preharvest abiotic stresses on the accumulation of bioactive compounds in horticultural produce. Front Plant Sci 10:1–17.

Wiesner-Reinhold M, Gomes JVD, Herz C, Tran HTT, Baldermann S, Neugart S, Filler T, Glaab J, Einfeldt S, Schreiner M, Lamy E (2021) Subsequent treatment of leafy vegetables with low doses of UVB-radiation does not provoke cytotoxicity, genotoxicity, or oxidative stress in a human liver cell model. Food Biosci 43:101327.

Yoon HI, Kim D, Son JE (2020) Spatial and temporal bioactive compound contents and chlorophyll fluorescence of kale (*Brassica olerace*a L.) under UV-B exposure near harvest time in controlled environments. Photochem

Photobiol 96:845–852.

Yoon HI, Kim HY, Kim J, Oh MM, Son JE (2021a) Quantitative analysis of UV-B radiation interception in 3D plant structures and intraindividual distribution of phenolic contents. Int J Mol Sci 22:2701.

Yoon HI, Kim HY, Kim J, Son JE (2021b) Quantitative analysis of UV-B radiation interception and bioactive compound contents in kale by leaf position according to growth progress. Front Plant Sci 12:667456.

Yoon HI, Kim JS, Kim D, Kim CY, Son JE (2019) Harvest strategies to maximize the annual production of bioactive compounds, glucosinolates, and total antioxidant activities of kale in plant factories. Hortic Environ Biotechnol 60:883–894.

CHAPTER 3

Evaluation of UV-B Lighting Design for Phenolic Production in Kale Leaves Using Optical Simulation with Three-Dimensional Plant Models in Plant Factories

ABSTRACT

Ultraviolet-B (UV-B, 280-315 nm) radiation has been reported to be an effective elicitor for improving bioactive compound contents in plants. This study aimed to predict phenolic contents in kale (*Brassica oleracea* L. var. *acephala*) plants exposed to pre-harvest UV-B with UV-B radiation interception on individual leaves using optical simulation, and evaluate the simulation-based scenarios of UV-B light-emitting diode (LED) arrangements in plant factories. For estimating model parameters, three treatments were employed without or with pre-harvest UV-B radiation generated by UV-B LEDs with a peak at 310 nm arranged between the plant rows and above the rows. Scenario analysis was performed with variables of lighting system, such as vertical or horizontal lighting distance and lighting angle of UV-B LED, and evaluated through simulated UV-B radiation interception (UVR_{int}), and phenol and flavonoid accumulations. UV-B radiation significantly enhanced the total

phenolic content (TPC), total flavonoid contents (TFC), UV-B absorbing pigment content, and antioxidant capacity in kale plants. Between the two UV-B LED arrangements, the UVR_{int}, TPC, and TFC differed by 30.7, 12.0, and 15.0%, respectively. In the scenario analysis, the optimal lighting system for UV-B radiation use efficiency was determined depending on the TPC and TFC. Although the uniformity and efficiency were opposite in most scenarios, both values for phenolic production increased with changes in horizontal position. These evaluation and optimization methods using model-based simulations will help to design custom UV-B lighting systems for the production of bioactive compounds in commercial plant factories.

Additional keywords: antioxidants, flavonoids, light interception, ray-tracing simulation, secondary metabolites, vertical farming

INTRODUCTION

Plant factories with artificial lighting, known as vertical farms, are plant production systems that control the environment independently from the external environment and address the demands of consumers (SharathKumar et al., 2020). The plant factories are appropriate for the safe and stable production of highly functional/high-value-added plants, such as medicinal plants and functional vegetables (Kozai, 2018; Kozai et al., 2019). Kale (*Brassica oleracea* var. *acephala*) is a functional vegetable and is a rich source of health-promoting phytochemicals with antioxidant capacity (Šamec et al., 2019). The productions of such bioactive compounds are improved through abiotic stress/elicitation (Isah, 2019; Thakur et al., 2019). However, most environmental factors affecting plant quality, such as health-promoting phytochemicals, are still controlled by trial-and-error based on cultivation experiences.

Ultraviolet (UV) radiation, especially UV-B (280-315 nm), has been reported to be an effective elicitor that can be easily applied to enhance bioactive compound contents (Loconsole and Santamaria, 2021). One substantial response to UV-B radiation involves the induction and biosynthesis of phenolics including flavonoids, which act as UV-screening components and have antioxidant potential (Neugart and Schreiner, 2018). The UV-B light-emitting diode (LED) has been developed and can be precisely manipulated

with an intensity and spectrum suitable for plants (Robson et al., 2019). Although advances are being made, the performance of UV LEDs to date is low due to their low power efficiency and high operation voltages (Kneissl et al., 2019). Therefore, short-term UV-B exposure near harvest is effective in enhancing the phenolic accumulation in vegetables without growth reduction or with minimal energy input (Dou et al., 2019; Toscano et al., 2019; Yoon et al., 2020). The short-term UV-B exposure could be controlled and optimized as it can be considered a photo-elicitor for the phenolic production (Matsuura et al., 2013; Thakur et al., 2019).

Light environments in plant factories are determined not only by the optical characteristics of light sources, but also by those of the structures and cultivation space (Kozai et al., 2016). The light distribution on the growing space greatly varies in the presence of plants (Saito et al., 2020). The light distribution absorbed on the leaf surface in plant structures could be analyzed through three-dimensional (3D)-scanned plant model and optical simulations (Kim et al., 2020b). UV-B radiation also reaches individual leaf surface differently within the 3D plant structure (Yoon et al., 2021a). The phenolics were heterogeneously distributed due to uneven UV-B exposure on individual leaves. The plant structure that changed according to growth stages also influenced the enhancement of phenolic contents (Yoon et al., 2021b). Therefore, factors related to UV-B radiation for phenolic production should be estimated and optimized with UV-B radiation interception on plant structures.

In plant factories with high energy use, lighting factors should be optimized based on resource use efficiency including lighting electricity (Graamans et al., 2018). Simulation-based analysis made it possible to find out the optimal lighting arrangement and distance for maximal light use efficiency for photosynthesis in lettuce canopies (Kim et al., 2020b). For the production of high-value-added plants, uniform quality is as important as efficient production. Several novel LED lighting systems have been proposed to provide light more evenly to all leaves by combining downward, horizontal, and upward lighting in plant factories (Kozai et al., 2016; Joshi et al., 2017). However, the UV-B lighting factors related to phenolic production and their UV-B radiation use efficiency have not been optimized. The objectives of this study were to predict phenolic contents in kale plants exposed to pre-harvest UV-B with UV-B radiation interception on individual leaves using optical simulation, and to evaluate the simulation-based scenarios of UV-B LED arrangements in plant factories.

MATERIALS AND METHODS

Plant materials and experimental conditions

The experimental procedure is described in Fig. 3-1. Kale (*Brassica oleracea* L. var. *acephala*) seeds were sown on sponge cubes and germinated in water culture systems with florescent lamps at a photosynthetic photon flux density (PPFD) of 150 µmol m^{-2} s^{-1} over the waveband 400-700 nm for 16-h light periods. At 1 week after germination, a nutrient solution for *Brassica*: N 137.8, P 30.9, K 140.9, Ca 104.6, Mg 54.8, Fe 2.76, Cu 0.02, Zn 0.05, Mn 0.68, B 0.50, and Mo 0.01 mg L^{-1} was supplied with an electrical conductivity (EC) of 0.6 dS m^{-1}. After 4 weeks, seedlings of uniform size were transplanted into plant factory modules with a deep flow technique system, each 150 L $\times$ 80 W $\times$ 50 H (cm) in size. Air temperature, relative humidity, CO_2 concentration, and EC of the nutrient solution in the modules were maintained at 20°C, 70%, 500 µmol mol^{-1}, and 1.2 dS m^{-1}, respectively. The transplanted plants were irradiated with red, blue, and white LEDs at a PPFD of 255 µmol m^{-2} s^{-1} (at 7 cm from the center of the ground) for 16-h light periods. The spectrum and intensity of growth LEDs were measured using a spectroradiometer (Blue-Wave spectrometer, StellarNet Inc., Tampa, FL, USA) in the range of 400-900 nm (Fig. 3-2a).

For UV-B treatment, UV-B LEDs with a spectrum peak at 310 nm, which consisted of five bar module arrays each containing twelve chips (Ericsong Co.,

126
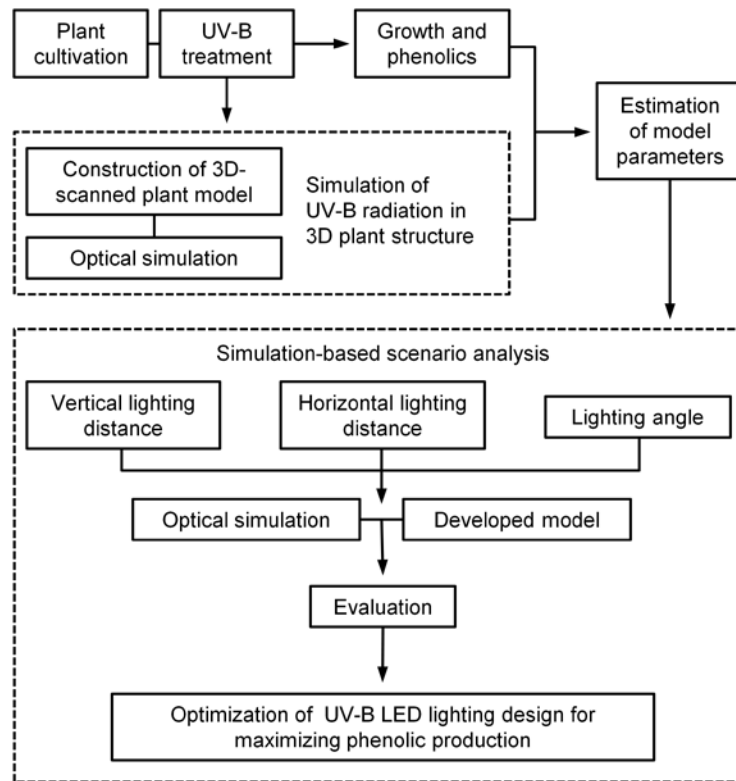
Fig. 3-1. Experimental procedure to optimize UV-B lighting design for maximizing phenolic production in this study. To estimate model parameters, three-dimensional (3D)-scanned plant models were constructed from the plant leaves exposed to UV-B radiation at harvest. The simulated UV-B radiation interception and the measured phenolics were used to estimate the model parameters. In simulation-based scenario analysis, the UV radiation interception were obtained according to lighting distance or angle of UV-B light-emitting diodes (LEDs) and used to predict phenolic production with the developed models.
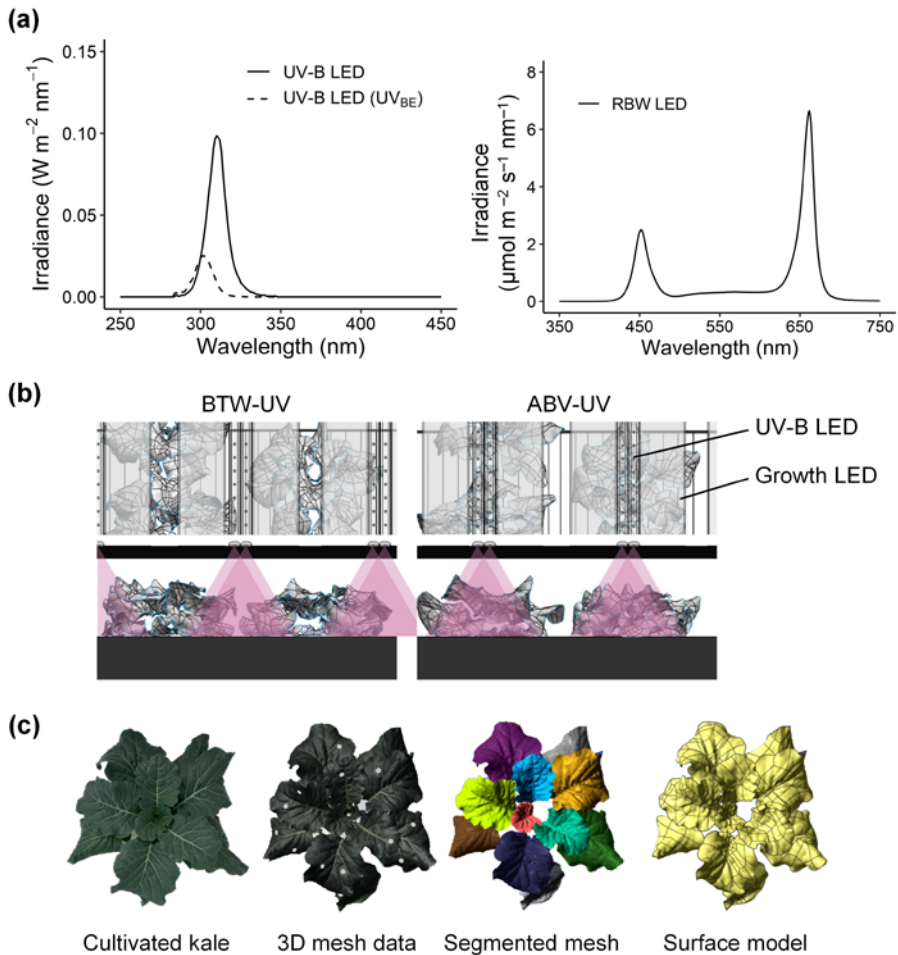
Fig. 3-2. Experimental setup for UV-B treatment to kale plants for estimating model parameters. Light spectra (a) of the UV-B light-emitting diode (LED) with a spectrum peak at 310 nm and growth LEDs consisting of red, blue, and white LEDs (RBW LED), arrangement of UV-B LED bars (b) between the plant rows (BTW-UV) and above the plant rows (ABV-UV), and representative models at each step (c) to construct the 3D-scanned plant model. UV-B$_{BE}$ indicates biologically effective UV-B calculated using a biological spectral weighting function for plants (Flint and Caldwell, 2003), and thereby its spectral peak was at about 302 nm.

Ltd., Bucheon, Korea) were used. The UV-B treatment was divided into UV-B LED bar arrangement between the plant rows (BTW-UV) and above the plant rows (ABV-UV), as shown in Fig. 3-2b. The plants were exposed to UV-B LEDs for 12 h and harvested after recovery for 4 h. The UV-B dose was 15.6 kJ m^{-2} d^{-1} biologically effective UV-B (UV-B$_{BE}$), calculated using a biological spectral weighting function for plants (Flint and Caldwell, 2003). The spectrum and intensity of UV-B LEDs were measured at 7 cm from the ground between the bars using the spectroradiometer in the range of 250-400 nm (Fig. 3-2a).

Growth characteristics

The plants were harvested at 28 days after transplanting (DAT). Fresh masses of individual leaves were measured separately at harvest with four plants per treatment. After photographing all leaves, the areas of individual leaves were calculated with an image analysis software (ImageJ 1.53, National Institutes of Health, Bethesda, MD, USA).

Photosynthetic pigment, phenolic content, and antioxidant capacity (AOC)
Sample preparation

Seventh to eleventh true leaves per plant were sampled at harvest, and lyophilized using a freeze dryer (FD8512, Ilshin Biobase Co., Yangju, Korea) at −80°C under a vacuum of 0.007 mmHg for 120 h. The 50-mg freeze-dried samples were pulverized and resuspended with 1 mL of appropriate solvent and

2.8-mm ceramic beads using a bead mill homogenizer (Beadruptor 4, Omni International, Kennesaw, GA, USA).

Photosynthetic pigment content

The extract with 80% (v/v) acetone was incubated in the dark at room temperature for 24 h, and then centrifuged at $11,000 \times g$ for 10 min. Chlorophyll a and b, and carotenoid contents were calculated based on absorbance at 663, 647, and 470 nm according to the method of Lichtenthaler and Buschmann (2001), and expressed as milligrams of chlorophyll or carotenoid per gram of dry mass (mg g^{-1} DM).

Total phenolic content (TPC) and total flavonoid content (TFC)

The extract with 80% (v/v) methanol was incubated in the dark at 4°C for 18 h, and then centrifuged at $11,000 \times g$ at 4°C for 10 min. TPC was determined according to the Folin-Ciocalteu colorimetric method (Ainsworth and Gillespie, 2007). A mixture of 100-μL supernatant with 200 μL of 10% (v/v) Folin–Ciocalteu reagent (Junsei Chemical Co., Ltd., Tokyo, Japan) and 400 μL of distilled water was vortexed, and then 800 μL of 700 mM Na_2CO_3 was added. After shaken for 10 s, the mixture was incubated in a water bath at 45°C for 15 min. The absorbance was read at 765 nm using a spectrophotometer (Photolab 6100vis, WTW, Weilheim, Germany), and the results were expressed as milligrams of gallic acid (Sigma–Aldrich Chemical Corp., St. Louis, MO, USA)

equivalent per gram of dry mass (mg GAE g^{-1} DM).

TFC was determined according to the aluminum chloride colorimetric method (Dewanto et al., 2002). The supernatant of 100 μL was mixed with 500 μL of distilled water and 30 μL of 5% (w/v) $NaNO_2$. After 6 min, 60 μL of 10% (w/v) $AlCl_3$ was added. After 5 min, 200 μL of 1 M NaOH and 110 μL of distilled water were added. All reactants were thoroughly mixed followed by incubation for 5 min. The absorbance was read at 510 nm and the results were expressed as milligrams of catechin acid (Supelco, Bellefonte, PA, USA) equivalent per gram of dry mass (mg CE g^{-1} DM).

Total anthocyanin content (TAC) and UV-absorbing pigment content (UAPC)

The extract with 1% acidified methanol was incubated in the dark at 4°C for 48 h, and then centrifuged at 11,000 × g at 4°C for 15 min. For determining TAC, the supernatant was diluted 2-fold, and the absorbance was read at 530 (A_{530}) and 657 nm (A_{657}) and corrected to $A_{530} - 0.25A_{657}$ (Sytar et al., 2018). The results were expressed as milligrams of cyanidin 3-glucoside (Sigma–Aldrich Chemical Corp.) equivalent per gram of dry mass (mg C3GE g^{-1} DM). For determining UAPC, the supernatant was diluted 20-fold, and the absorbance was read at 285 (A_{285}) and 330 nm (A_{285}) and corrected as ($A_{285}+A_{330}$)/2 (Si et al., 2015; Khudyakova et al., 2019). The results were expressed as absorbance per gram of dry mass (OD g^{-1} DM).

AOC

AOC was determined using both the 2, 2'-azino-bis (3-ethylbenzothiazoline-6-sulfonic acid)-diammonium salt (ABTS) and the 2, 2-diphenyl-1-picrylhydrazyl (DPPH) assays (AOC_{ABTS} and AOC_{DPPH}, respectively). The extract with 80% (v/v) methanol was incubated in the dark at 4°C for 42 h, and then centrifuged at $11,000 \times g$ at 4°C for 10 min. The ABTS radical scavenging activity was determined according to the method of Re et al. (1999). The ABTS radical cation ($ABTS^{•+}$) reagent was produced by reacting 7 mM ABTS solution (Sigma–Aldrich Chemical Corp.) with 2.45 mM $K_2S_2O_8$ (1:1, v/v), and stored at 4°C in the dark for 18 h before use. The $ABTS^{•+}$ solution was diluted with 80% methanol to obtain appropriate absorbance. A mixture of 50-μL supernatant with 1.8 mL of the diluted $ABTS^{•+}$ solution was incubated in the dark at room temperature for 6 min, and the absorbance was read at 734 nm. DPPH radical scavenging activity was determined according to the method of Brand-Williams et al. (1995). The DPPH solution was freshly made using DPPH (Alfa Aesar, Ward Hill, MA, USA) and methanol before use. A mixture of 100-μL supernatant with 1.8 mL of 0.12 mM DPPH methanol solution was incubated in the dark at room temperature for 30 min, and the absorbance was read at 517 nm. Calibration curves for ABTS and DPPH assays were constructed using L-ascorbic acid (Samchun Pure Chemical Co., Ltd., Pyeongtaek, Korea). The AOC_{ABTS} and AOC_{DPPH} were expressed as milligrams of ascorbic acid equivalent per gram of dry mass (mg AAE g^{-1} DM).

Simulation of UV-B radiation interception

Construction of 3D models

UV-B radiation interception analysis was performed with a 3D-scanned plant model and ray-tracing simulation (Kim et al., 2020b; Yoon et al., 2021a). The virtual plant factory modules based on the dimensions measured were constructed using a 3D computer-aided design (CAD) software (Solidworks, Dassault Systèmes, Vélizy-Villacoublay, France). Plant models were directly obtained using a high-resolution portable 3D scanner (Go! SCAN50TM, Creaform Inc., Lévis, Quebec, Canada) and its software (Vxelement, Creaform Inc.). Four plants per treatment were 3D-scanned after UV-B exposure. The 3D mesh data were fixed for holes and noise, segmented into leaf mesh data, and reconstructed to individual surface models using a reverse engineering software (Geomagic Design X, 3D Systems, Rock Hill, SC, USA). The surface models were transferred to the 3D CAD software for optical simulation. All 3D models were placed in the same position and orientation as actual materials and plants (Fig. 3-2b). The representative kale models at each step are shown in Fig. 3-2c.

Optical simulation

The optical properties of plants and plant factory modules were measured and included in each model. Spectral power distributions of UV-B LEDs were set as the measured spectra in the range of 280-400 nm, and the physical light distribution was set as a Lambertian distribution with a half angle of 60°. The

ray-tracing simulation was performed using a ray-tracing software (Optisworks, Optis Inc., La Farlède, France) with a total of 1 giga-ray. All leaf surface models were set up as separate detectors. The UV-B radiation interception values were obtained for each 3D coordinate constituting the plant model.

Prediction of TPC and TFC from simulation results

TPC and TFC per leaf were calculated by multiplying the measured concentrations (mg eq. g^{-1} DM) by the leaf dry mass (g DM). A model for predicting the TPC and TFC per leaf was obtained by multiple regression analysis based on previously developed model equation in the range of all leaves at 30 DAT as follows:

$$M(L,U) = \beta_0 + \beta_1 L + \beta_2 L^2 + (\beta_3 L + \beta_4 L^2)\, U \qquad \text{Eq. 3-1}$$

where M is TPC or TFC per leaf (mg eq. per leaf), L is leaf order numbered as absolute order of leaf emergence, U is daily UV-B radiation interception per leaf (kJ d^{-1} per leaf), and β_0-β_4 are regression coefficients obtained by the regression analysis. The accuracy of the developed models was analyzed with randomly selected test data not used for model development. The test data were corresponded to 12 data points among a total of 48 data points.

Scenario analysis

Scenario analysis: LED arrangement and angle

Based on the optical simulation and developed model, scenarios were employed to evaluate the effect of lighting manipulation on UV-B radiation interception and phenolic accumulation. For optical simulation, four 3D-scanned plant models were arranged in a row, and all leaf surface models were set as detectors. The plant height (H) and width (W) were 18.4 and 40 cm, respectively, and were obtained as the mean of the four plants used for the simulation. UV-B LED bars with the LED chips embedded in 5-cm intervals were used. The scenario settings for simulation are described in Fig. 3-3. The two UV-B bars were arranged according to three scenarios: (1) vertical lighting distances of 0.5-, 1.0-, 1.5-, and 2.0-fold H from the top of plant (0.5, 1.0, 1.5, and 2.0H); (2) horizontal lighting distances of 0-, 1/3-, 2/3-, and 1-fold W from the center of plant row (0, 1/3, 2/3, and 1W); (3) lighting angles of 0, 30, 60, and 90° at the ellipse towards the center of plant (0, 30, 60, and 90AE). In scenarios 2 and 3, the vertical distance of the LED bar from the top of plant was determined as the optimal vertical distance from scenario 1. The simulation results were used to predict the TPC and TFC per leaf of kale plants in virtual environments using the developed model.

Evaluation of scenarios

The simulation results of the scenarios were evaluated with the total UV radiation interception, TPC, and TFC per plant, the coefficient of variance (CV),

(a) Scenario 1 (vertical lighting distance)
Distance between UV-B LED bar and plant height (H)

UV-B LED →

Case
2.0H
1.5H
1.0H
0.5H

H

Plant

(b) Scenario 2 (horizontal lighting distance)
Distance between UV-B LED bars based on plant width (W)

1W
2/3W
1/3W
0W

Case
0, 1/3, 2/3, 1W

H1

H1 = Optimal
vertical distance
from scenario 1

Plant

(c) Scenario 3 (lighting angle on ellipse)
UV-B LED lighting angle at the ellipse towards the center of the plant

H1
H1

0°   30°
60°
90°

Plant 30°

Case
0, 30, 60, 90AE

Fig. 3-3. Scenario analysis scheme and models in simulation. In scenario 1 (a), UV-B light-emitting diode (LED) bars were located in the center of the plant row at 0.5-, 1.0-, 1.5-, and 2.0-fold plant height (H) from the top of the plant (0.5, 1.0, 1.5, and 2.0H). In scenario 2 (b), UV-B LED bars were located at 0-, 1/3-, 2/3-, and 1-fold plant width (W) from the center of the plant row (0, 1/3, 2/3, and 1W). In scenario 3 (c), UV-B LED bars were located at angles of 0, 30, 60, and 90° at the ellipse towards the center of the plant (0, 30, 60, and 90AE). In scenarios 2 and 3, the distance of the LED bar from the top of the plant (H1) was determined as the optimal vertical distance

136

from scenario 1. In this study, the H and W were 18.4 and 40 cm, respectively, obtained as the mean of four plants used for the simulation.

and UV-B radiation use efficiency for TPC and TFC. The CV means variability between leaves, calculated by dividing the standard deviation by the total average value for each leaf. The UV-B radiation use efficiency was determined as a ratio of the changes in phenolic contents per plant relative to those without UV-B to the radiant energy emitted from the light source (RUE) or absorbed by the plants (RUE_{int}).

The annual production of total phenolics and total flavonoids in kale plants was estimated in virtual plant factories. The annual production per unit area (g eq. m^{-2} yr^{-1}) was calculated as (the TPC or TFC per plant, g eq. per plant) × (planting density, plant m^{-2}) × (cultivation cycles per year, yr^{-1}) according to a previous method (Yoon et al., 2019). In the present study, kale plants were assumed to be planted at a density of 6.25 plants m^{-2} based on a planting distance of 40 cm and harvested at 28 DAT with a size of 0.4 × 0.4 × 0.18 m (W × L × H). For example, when a virtual plant factory consists of a growing bed with a size of 4 × 4 × 0.3 m (W × L × H) and five floors, the total growing area and the growing area for daily harvest will be 2,240 and 80 m^2, respectively, with a cultivation cycle of 28 days. Under the applied assumptions, number of harvested plants will be 500 plants per day and 182,500 plants per year. The annual productivity and energy consumption were compared according to additional pre-harvest UV-B radiation. The biomass, plant size, growth condition, and energy for growth were assumed to be the same with and without UV-B radiation.

Statistical analysis

For experimental data, the homogeneity of variance was evaluated by Levene's test, and the normality was evaluated by Shapiro–Wilk test. The mean values were compared with one-way ANOVA and Tukey's honestly significant difference (HSD) test at $P < 0.05$ to assess the effects of the UV-B treatment. Model accuracy was evaluated with the coefficient of determination (R^2) and normalized root mean squared error (NRMSE).

RESULTS

Effect of UV-B radiation on growth, photosynthetic pigment contents, phenolic contents, and antioxidant capacity

The two UV-B radiation arrangements for parameter estimation enhanced TPC, TFC, and AOC without reducing growth and photosynthetic pigment contents (Tables 3-1, 3-2). The growth and photosynthetic pigment contents did not differ among the treatments. Both TPC and TFC were significantly higher in the order of ABV-UV, BTW-UV, and the control. The ABV-UV treatment significantly increased the TPC and TFC by 39.0 and 79.0%, respectively, compared to the control. The BTW-UV treatment significantly increased the TPC and TFC by 20.9 and 37.0%, respectively, compared to the control. Across all data, TPC was positively correlated with TFC, and their Pearson's correlation coefficient was 0.94 at $P < 0.001$. TAC did not differ among the treatments. UAPC was significantly higher by 22.0% in BTW-UV and by 32.7% in ABV-UV than in the control. AOC_{ABTS} and AOC_{DPPH} were significantly increased by 21.2-25.1% in BTW-UV and by 28.6-34.6% in ABV-UV compared to the control. Across all data, UAPC was positively correlated with AOC_{ABTS} and AOC_{DPPH}, and their Pearson's correlation coefficients were 0.84 and 0.85, respectively, at $P < 0.001$.

UV-B radiation interception according to UV-B LED arrangement

140

Table 3-1. Growth and photosynthetic pigment contents in kale plants according to UV-B lighting arrangement.

Treatment	Total fresh mass (g)	Total leaf area (cm^2)	Chlorophyll a (mg g^{-1} DM)	Chlorophyll b (mg g^{-1} DM)	Carotenoid (mg g^{-1} DM)
Control	137.7 ± 19.4	2,206.2 ± 249.7	10.1 ± 0.54	4.0 ± 0.26	2.5 ± 0.08
BTW-UV	149.4 ± 21.6	2,220.1 ± 275.5	10.6 ± 0.48	4.2 ± 0.24	2.6 ± 0.10
ABV-UV	118.2 ± 15.6	1,838.2 ± 232.8	10.6 ± 0.08	4.2 ± 0.06	2.8 ± 0.05

UV treatment indicates UV-B lighting arrangement between the plant rows (BTW-UV) and above the plant rows (ABV-UV).
Mean ± SD for growth parameters, ± SE for photosynthetic pigment contents (n = 4).

Table 3-2. Phenolic content and antioxidant capacity in kale plants according to UV-B lighting arrangement.

Treatment	TPC (mg GAE g⁻¹ DM)	TFC (mg CE g⁻¹ DM)	TAC (mg C3GE g⁻¹ DM)	UAPC (OD g⁻¹ DM)	AOC (mg AAE g⁻¹ DM)	
					ABTS	DPPH
Control	7.8 ± 0.14 c	4.0 ± 0.14 c	0.7 ± 0.04 a	0.7 ± 0.04 b	4.3 ± 0.18 b	3.9 ± 0.24 b
BTW-UV	9.5 ± 0.33 b	5.4 ± 0.41 b	0.7 ± 0.03 a	0.9 ± 0.02 a	5.2 ± 0.12 a	4.9 ± 0.15 a
ABV-UV	10.9 ± 0.27 a	7.1 ± 0.32 a	0.6 ± 0.06 a	1.0 ± 0.03 a	5.5 ± 0.09 a	5.3 ± 0.09 a

UV treatment indicates UV-B lighting arrangement between the plant rows (BTW-UV) and above the plant rows (ABV-UV).

TPC, total phenolic content; TFC, total flavonoid content; TAC, total anthocyanin content; UAPC, UV-absorbing pigment content; AOC, antioxidant capacity using ABTS or DPPH assay.

Mean $\pm$ SE ($n = 4$).

Different letters within columns indicate significant differences by one-way ANOVA and Tukey's HSD test at $P < 0.05$.

The spatial distribution of UV-B radiation interception was simulated with 3D-scanned plant models (Fig. 3-4a). The UVR_{int} values at the center and upper leaves (leaf orders of 11-13) were 2.3-fold higher in ABV-UV than in BTW-UV (Fig. 3-4b). In ABV-UV treatment, the average UVR_{int} value was 0.71 ± 0.13 W m^{-2} (equivalent to 7.71 ± 1.45 kJ UV_{BE} m^{-2} d^{-1}), and the total UVR_{int} per plant was 1.43 ± 0.27 kJ UV_{BE} d^{-1} per plant. In BTW-UV treatment, the average UVR_{int} value was 0.48 ± 0.13 W m^{-2} (equivalent to 5.20 ± 1.37 kJ UV_{BE} m^{-2} d^{-1}), and the total UVR_{int} per plant was 1.28 ± 0.41 kJ UV_{BE} d^{-1} per plant.

Model for predicting TPC and TFC

Model parameters for predicting TPC and TFC per leaf were estimated using measured TPC and TFC, and simulated UVR_{int} as follows:

$$\text{TPC per plant} = -2.27 + 2.68\,L - 0.13\,L^2 + (10.16\,L - 0.88\,L^2)U$$

$$\text{TFC per plant} = -2.94 + 1.92\,L - 0.10\,L^2 + (6.83\,L - 0.56\,L^2)U$$

The P-values of the TPC and TFC models were significant at $P = 0.003$ and $P = 0.002$, respectively. The accuracy of the models was tested with $R^2 > 0.6$ (Fig. 3-5). The relative error of the TPC model was approximately 16.9%, meaning that the model could predict TPC with 83.1% accuracy. Likewise, the TFC model could predict TFC with 81.1% accuracy. From the developed model, the spatial and intraindividual distributions of TPC and TFC were estimated on
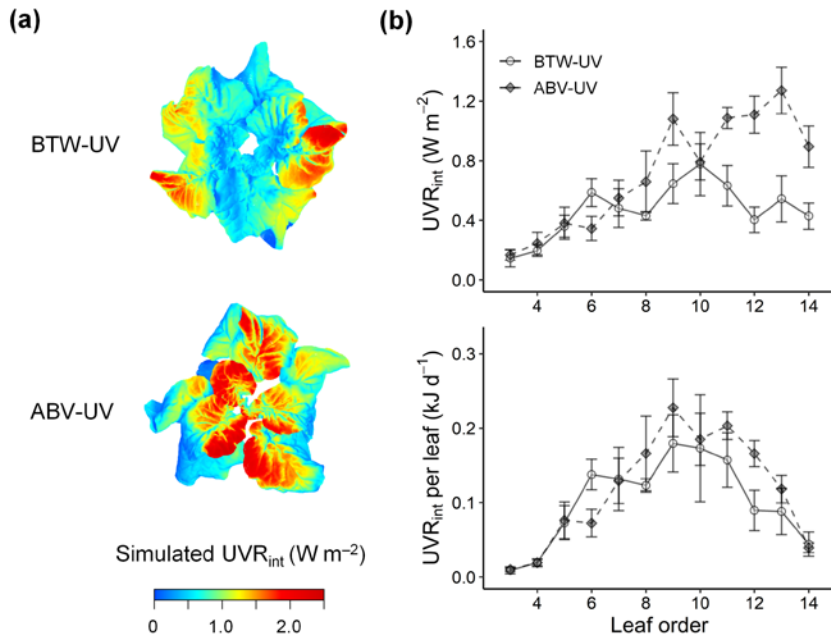
Fig. 3-4. Representative simulated distribution (a) and intraindividual distribution (b) of UV-B radiation interception (UVR_{int}) on 3D-scanned kale models according to UV-B lighting arrangement (BTW-UV, between the plant rows; ABV-UV, above the plant rows). The intraindividual distribution indicates the average value of UVR_{int} and daily UVR_{int} per leaf (kJ UV_{BE} d^{-1} per leaf) according to leaf order. Vertical bars indicate SE, $n = 4$.
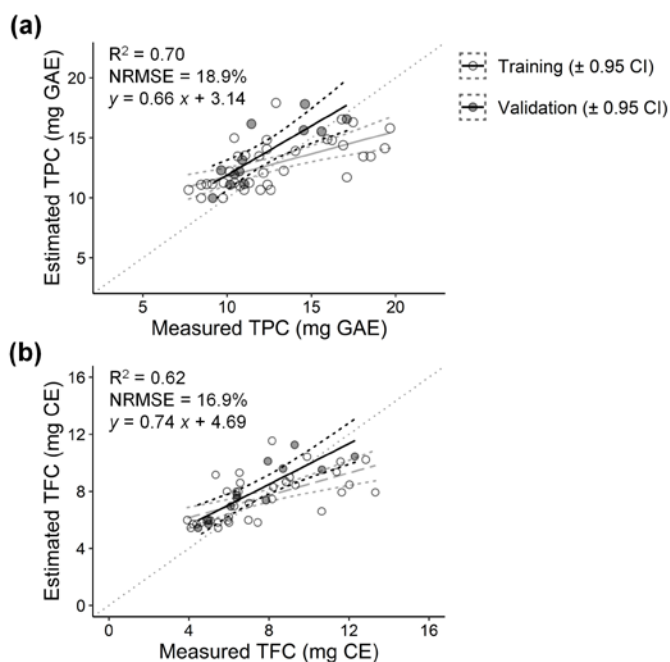
Fig. 3-5. Comparison between measured and estimated values of total phenolic content (TPC) per leaf (a) and total flavonoid content (TFC) per leaf (b) of kale plants derived from the developed TPC and TFC models. Closed circles are test data not used for model development, while open circles are training data for model development. Solid lines indicate linear regression lines, and dashed lines indicate the range of the 95% confidence interval (CI). The coefficient of determination (R^2), the normalized root mean squared error (NRMSE), and the linear regression equation of the test data are presented inside each panel.

3D-scanned kale plant models (Fig. 3-6). Both the TPC and TFC in the middle and upper leaves (8-14th leaf order) were 1.4-fold higher in ABV-UV treatment than in BTW-UV treatment. On the other hand, the TPC and TFC per leaf were similar between UV-B treatments. Calculated by the coefficient of UVR_{int} (U) at each leaf order (L), the effect of UVR_{int} was higher in the lower and middle leaves (3rd-9th leaves) than in the upper leaves (10-14th leaves).

Simulation results of scenarios for LED arrangement and angle

The simulated UVR_{int} and predicted TPC and TFC in kale leaves differed markedly with the UV-B LED arrangement and angle. In scenario 1, the simulated UVR_{int} on individual leaves increased with shorter vertical lighting distance, which was 2.0-fold higher at 0.5H than at 2.0H (Fig. 3-7). In 2.0H, the simulated UVR_{int}, predicted TPC and TFC were lower by 46.7, 2.8, and 7.3%, respectively, on average than those at 0.5H. The inversion in predicted TPC and TFC in upper leaves was caused by the negative effect of UVR_{int} from the developed model. In scenario 2, the simulated UVR_{int} on individual leaves decreased with a longer horizontal lighting distance only on the middle and upper leaves (Fig. 3-8). The simulated UVR_{int} in 1/3W was 7.0% lower than that at 0.5H on average, but that of the predicted TPC was 2.5% higher. In scenario 3, the different lighting angles of UV-B LEDs on the ellipse surrounding the plant most affected the leaf-to-leaf deviation of UVR_{int} among all scenarios (Fig. 3-9). With a greater lighting angle, the simulated UVR_{int} on

146
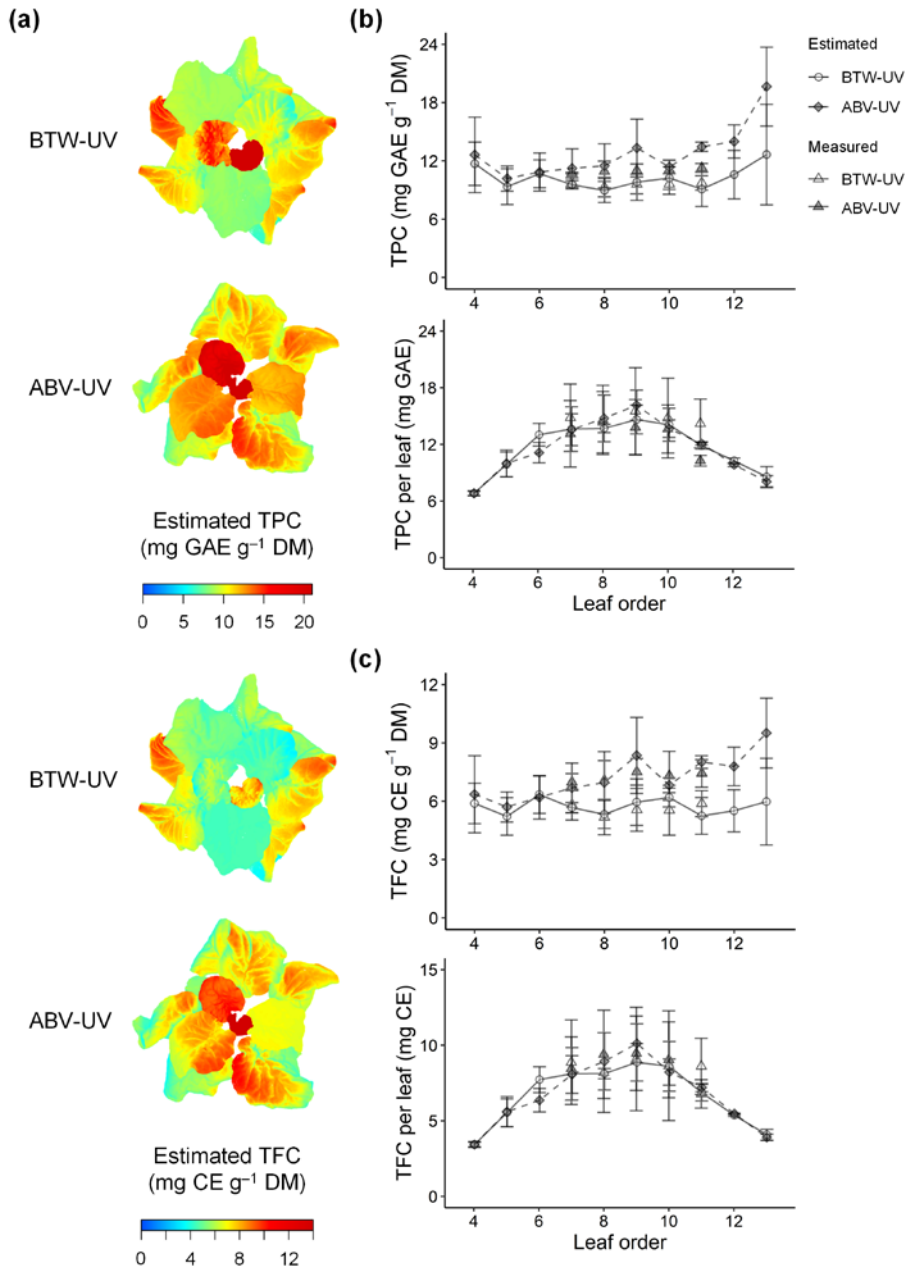
Fig. 3-6. Representative spatial distribution (a) and intraindividual distribution of estimated total phenolic content (TPC, b) and total flavonoid content (TFC, c) on 3D-scanned kale models according to UV-B lighting

arrangement (BTW-UV, between the plant rows; ABV-UV, above the plant rows). The intraindividual distribution indicates estimated TPC (b) and TFC (c) per dry mass (left) and per leaf (right) according the UV-B lighting arrangement. Gray points indicate measured contents. Vertical bars indicate SE, $n = 4$.
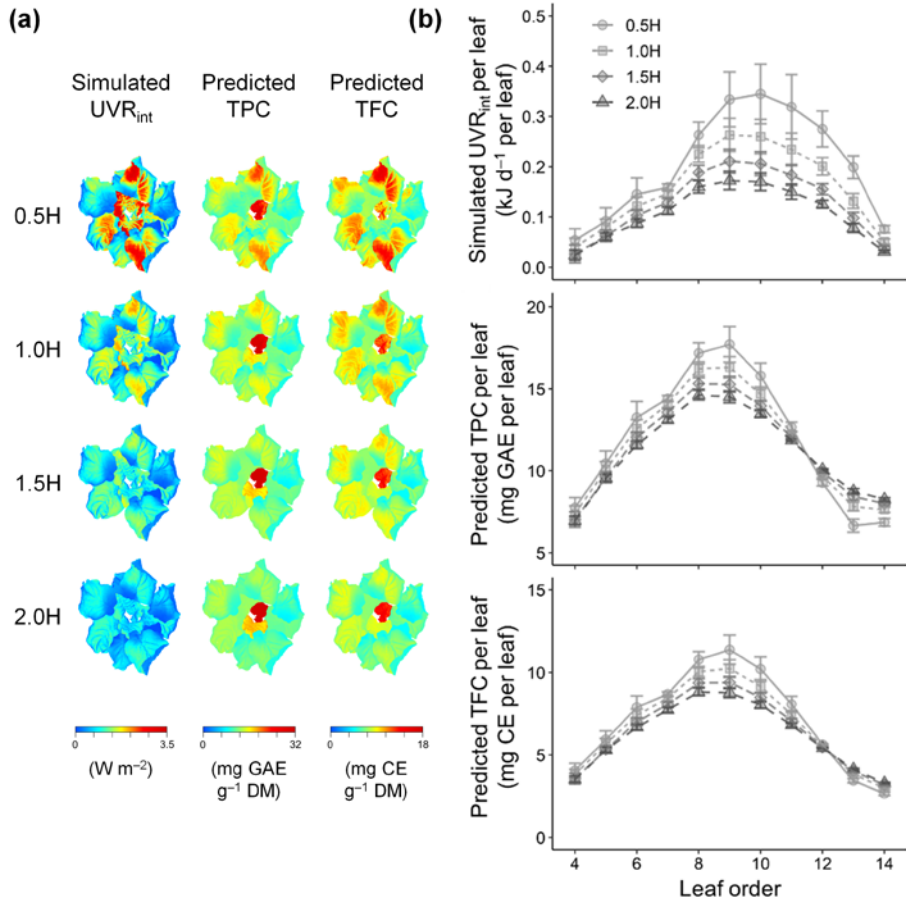
Fig. 3-7. Results of scenario 1, vertical lighting distance of UV-B lighting at 0.5-, 1.0-, 1.5-, and 2.0-fold plant height (H) from the top of the plant (0.5, 1.0, 1.5, and 2.0H). Representative spatial distribution (a) and intraindividual distribution (b) of simulated UV-B radiation interceptions (UVR$_{int}$), predicted total phenolic content (TPC), and total flavonoid content (TFC) on 3D-scanned kale models. Vertical bars indicate SE, $n = 4$. Detailed scenario settings refer to Fig. 3-3.
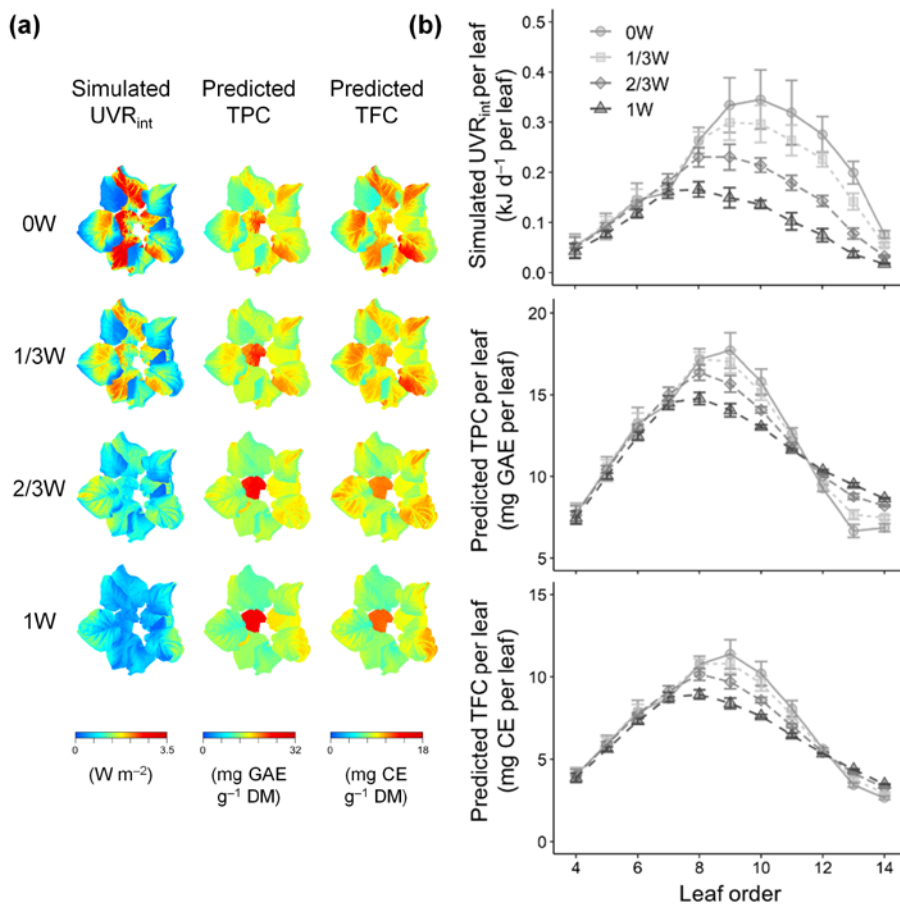
Fig. 3-8. Results of scenario 2, horizontal lighting distance of UV-B lighting at 0-, 1/3-, 2/3-, and 1-fold plant width (W) from the center of the plant row (0, 1/3, 2/3, and 1W). Representative spatial distribution (a) and intraindividual distribution (b) of simulated UV-B radiation interceptions (UVR_{int}), predicted total phenolic content (TPC), and total flavonoid content (TFC) on 3D-scanned kale models. Vertical bars indicate SE, $n = 4$. Detailed scenario settings refer to Fig. 3-3.
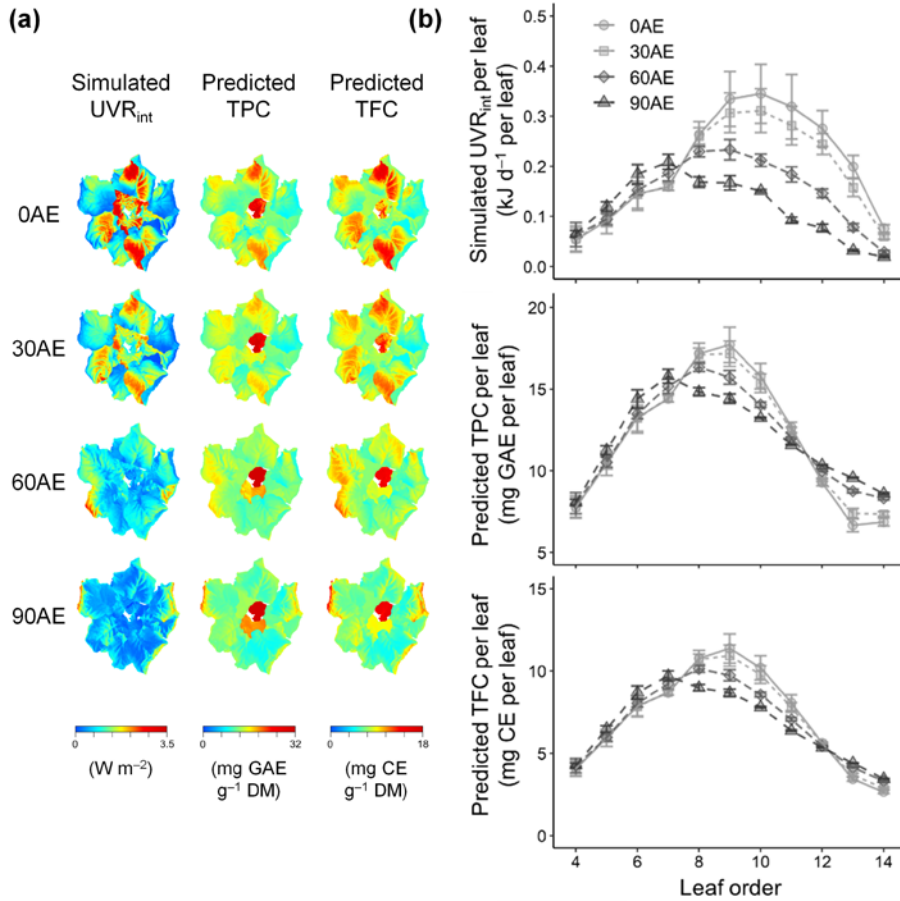
Fig. 3-9. Results of scenario 3, lighting angle of UV-B lighting with 0, 30, 60, and 90° at the ellipse surrounding the plant (0, 30, 60, and 90AE). Representative spatial distribution (a) and intraindividual distribution (b) of simulated UV-B radiation interceptions (UVR_{int}), predicted total phenolic content (TPC), and total flavonoid content (TFC) on 3D-scanned kale models. Vertical bars indicate SE, $n = 4$. Detailed scenario settings refer to Fig. 3-3.

individual leaves decreased in the middle and upper leaves and increased in the lower leaves. Thereafter, the predicted TPC and TFC in the lower and upper leaves were higher with greater lighting angles. The simulated UVR_{int} at 90AE was 4.1% lower than that at 0AE on average. However, the predicted TPC and TFC were 5.6 and 2.3% higher, respectively, at 90AE than at 0AE.

The shorter vertical lighting distance from the plant in scenario 1 increased the total UVR_{int}, TPC, and TFC per plant (Tables 3-3). The total UVR_{int}, TPC, and TFC per plant were highest at 0.5H, which was 1.9-, 1.1-, and 1.2-fold higher, respectively, than those at 2.0H. The RUE_{TPC} and RUE_{TFC} were also highest at 0.5H, which was 1.6- and 1.7-fold higher than those at 2.0H (Table 3-4). From the results, the distance of UV-B LED bars from the plant in scenarios 2 and 3 was determined to be half of the plant height (0.5H).

The horizontal lighting distance and lighting angle on the ellipse surrounding the plant remarkably affected both total UVR_{int} and RUE_{int} in scenarios 2 and 3 (Tables 3-3, 3-4). The total UVR_{int} was reduced by 51.4% at 1W and 41.5% at 90AE when compared to that at 0W (the same case as at 0AE). The RUE_{int} for TPC and TFC were highest both at 1W and 90AE. While the RUE_{TPC} in scenario 2 was highest at 1/3W (1.3-fold higher than at 1W), the RUE_{TPC} in scenario 3 was similar among the angles (highest at 60AE). The RUE_{TFC} was highest at 0W (the same case as at 0AE), which was corresponded to 1.5- and 1.2-fold higher than at 1W and 90AE, respectively. The CV_{UVR} was lowest at 1W and 60AE, which corresponded with reductions of 43.5 and 51.3%,

Table 3-3. Simulated total biologically effective UV radiation interception (UVR_{int}), the coefficient of variance for UVR_{int} (CV_{UVR}), predicted total phenolic content (TPC) per plant, and predicted total flavonoid content (TFC) per plant in kale plants according to UV-B lighting arrangement and angle.

Scenario	Case	Total UVR_{int} (kJ UVR_{BE} d^{-1} per plant)	CV_{UVR} (%)	Predicted TPC per plant (mg GAE per plant)	Predicted TFC per plant (mg CE per plant)
1	0.5H	2.25 ± 0.11	60.2 ± 4.86	137.4 ± 1.04	81.0 ± 0.88
	1.0H	1.75 ± 0.08	51.4 ± 4.91	133.9 ± 1.27	76.8 ± 1.01
	1.5H	1.38 ± 0.07	47.1 ± 5.46	129.6 ± 2.07	72.6 ± 1.46
	2.0H	1.17 ± 0.05	45.6 ± 4.35	127.8 ± 1.16	70.6 ± 0.88
2	0W	2.25 ± 0.11	60.2 ± 4.86	137.4 ± 1.04	81.0 ± 0.88
	1/3W	2.01 ± 0.07	47.4 ± 3.55	138.1 ± 1.56	80.3 ± 1.13
	2/3W	1.57 ± 0.02	35.0 ± 3.42	136.3 ± 1.22	77.3 ± 0.81
	1W	1.09 ± 0.01	34.0 ± 5.32	131.6 ± 0.83	72.4 ± 0.47
3	0AE	2.25 ± 0.11	60.2 ± 4.88	137.4 ± 1.05	81.0 ± 0.88
	30AE	2.07 ± 0.08	50.9 ± 3.43	137.6 ± 1.46	80.3 ± 1.05
	60AE	1.63 ± 0.05	29.4 ± 3.63	137.7 ± 1.35	78.3 ± 0.95
	90AE	1.32 ± 0.06	30.3 ± 5.71	137.7 ± 1.91	76.8 ± 1.32
Without UV-B		-	-	112.0 ± 0.0	56.3 ± 0.0

Scenario 1, vertical lighting distance of UV-B lighting at 0.5-, 1.0-, 1.5-, and 2.0-fold plant height (H) from the top of the plant; Scenario 2, horizontal lighting distance of UV-B lighting at 0-, 1/3-, 2/3-, and 1-fold plant width (W) from the center of the plant; Scenario 3, lighting angle of UV-B lighting with angles (AE) of 0, 30, 60, and 90° on ellipse surrounding the plant. Detailed scenario settings refer to Fig. 3-3.
Data represent mean ± SD (n = 3).

Table 3-4. UV-B radiation use efficiency (RUE) and the coefficient of variance (CV) for total phenolic content (TPC) and total flavonoid content (TFC) in kale plants according to UV-B lighting arrangement and angle.

Scenario	Case	RUE$_{TPC}$ (mg GAE / emitted UV$_{BE}$)	RUE$_{TFC}$ (mg CE / emitted UV$_{BE}$)	RUE$_{int, TPC}$ (mg GAE / absorbed UV$_{BE}$)	RUE$_{int, TFC}$ (mg CE / emitted UV$_{BE}$)	CV$_{TPC}$ (%)	CV$_{TFC}$ (%)
1	0.5H	1.10 ± 0.05	1.07 ± 0.04	11.3 ± 0.69	11.0 ± 0.45	39.3 ± 1.65	48.8 ± 2.25
	1.0H	0.95 ± 0.05	0.89 ± 0.04	12.5 ± 0.68	11.7 ± 0.44	34.4 ± 0.76	44.0 ± 1.50
	1.5H	0.76 ± 0.09	0.71 ± 0.06	12.7 ± 1.08	11.8 ± 0.63	31.5 ± 1.01	41.1 ± 1.49
	2.0H	0.68 ± 0.05	0.62 ± 0.04	13.5 ± 0.74	12.2 ± 0.47	29.5 ± 1.14	38.7 ± 1.43
2	0W	1.10 ± 0.05	1.07 ± 0.04	113 ± 0.69	11.0 ± 0.45	39.3 ± 1.65	48.8 ± 2.25
	1/3W	1.13 ± 0.07	1.04 ± 0.05	13.0 ± 0.74	11.9 ± 0.47	36.0 ± 1.11	45.5 ± 2.02
	2/3W	1.05 ± 0.05	0.91 ± 0.04	15.5 ± 0.71	13.3 ± 0.44	31.9 ± 1.85	41.5 ± 2.41
	1W	0.85 ± 0.04	0.70 ± 0.02	17.9 ± 0.82	14.7 ± 0.49	27.9 ± 1.49	37.1 ± 1.64
3	0AE	1.10 ± 0.05	1.07 ± 0.04	11.3 ± 0.69	11.0 ± 0.45	39.3 ± 1.66	48.8 ± 2.24
	30AE	1.11 ± 0.06	1.04 ± 0.05	12.4 ± 0.75	11.6 ± 0.47	36.6 ± 1.13	46.0 ± 2.08
	60AE	1.11 ± 0.06	0.95 ± 0.04	15.8 ± 0.52	13.5 ± 0.33	31.2 ± 1.56	40.6 ± 1.93
	90AE	1.11 ± 0.08	0.89 ± 0.06	19.4 ± 0.84	15.5 ± 0.47	27.9 ± 0.96	37.3 ± 1.90

Scenario 1, vertical lighting distance of UV-B lighting at 0.5-, 1.0-, 1.5-, and 2.0-fold plant height (H) from the top of the plant; Scenario 2, horizontal lighting distance of UV-B lighting at 0-, 1/3-, 2/3-, and 1-fold plant width (W) from the center of the plant; Scenario 3, lighting angle of UV-B lighting with angles (AE) of 0, 30, 60, and 90° on ellipse surrounding the plant. UV-B radiation use efficiency was calculated as the difference in the content per plant with and without UV-B radiation divided by the biologically effective UV radiant energy (UV$_{BE}$) emitted from the light source (RUE) or absorbed by the plants (RUE$_{int}$). Detailed scenario settings refer to Fig. 3-3.

respectively, when compared to that at 0W (the same case as at 0AE). At both 1W and 90AE, the CV_{TPC} and CV_{TFC} were reduced by 29 and 24%, respectively, when compared to those at 0W (the same case as at 0AE). Across all scenarios, Pearson's correlation coefficients between CV_{UVR} and CV_{TPC} or CV_{TFC} were 0.71-0.77 at $P < 0.001$ (data not shown). A low CV means more uniform distribution within the 3D plant structure.

From the prediction model, the annual productions of total phenolics and total flavonoids in kale plants grown in virtual plant factory were estimated and compared according to UV-B radiation (Table 3-5). The estimate was calculated based on the TPC and TFC per plant in ABV-UV and 0.5H cases with the developed prediction model (Figs. 3-6, 3-7). Under the applied assumptions, additional UV-B radiation increased the annual total phenolics and total flavonoids production per unit area by 15.2-22.6 and 28.9-43.9%, respectively, compared to the control. In the virtual plant factory, the application of UV-B radiation for 12 h at the harvest date was effective enough to achieve annual production scale increases of 17.4 and 31.5% for TPC and TFC, respectively.

Table 3-5. Assumption and comparison for estimating annual production of total phenolics and total flavonoids in kale plants grown in a virtual plant factory according to pre-harvest additional UV-B lighting.

Assumption		Value	Unit
Growth condition	Cultivation cycle	28	day
	Planting density	6.25	plant m^{-2}
Plant factory	Module	16	m^2
	Number of modules	28	
	Layer	5	layer
	Total growing area	2,240	m^2
	Total plant	182,500	plant yr^{-1}
Daily harvest	Plant	500	plant d^{-1}
	Growing area	80	m^2
TPC per plant	Without UV-B	112.0	mg GAE per plant
	UV-B (experiment)	129.0	
	UV-B (scenario)	137.4	
TFC per plant	Without UV-B	56.3	mg CE per plant
	UV-B (experiment)	72.6	
	UV-B (scenario)	81.0	
Estimated annual production per unit area			
TPC	Without UV-B	255.6	g GAE m^{-2} yr^{-1}
	UV-B (experiment)	294.4	
	UV-B (scenario)	313.4	
TFC	Without UV-B	128.5	g CE m^{-2} yr^{-1}
	UV-B (experiment)	165.6	
	UV-B (scenario)	184.8	
Estimated annual production in the virtual plant factory			
TPC	Without UV-B	20.4	kg GAE yr^{-1}
	UV-B (experiment)	23.6	
	UV-B (scenario)	25.1	
TFC	Without UV-B	10.3	kg CE yr^{-1}
	UV-B (experiment)	13.2	
	UV-B (scenario)	14.8	

The values of TPC and TFC per plant were obtained from the developed model. The UV-B cases indicate the experimental condition (pre-harvest UV-B lighting above the plant rows, the same as in ABV-UV in Fig. 3-6) and the scenario condition (pre-harvest UV-B lighting at 0.5-fold plant height from the top of the plant, the same as at 0.5H in Fig. 3-7).

DISCUSSION

Variables affecting plant responses to UV-B radiation

Plant responses to UV-B radiation are affected by manipulation factors, and are consequently multifaceted. Most of the current literatures agree regarding the dependence on the UV-B dose for triggering the biosynthesis of phenolics, especially flavonoids, but not all are consistent (Santin et al., 2021). In general, plants perceive UV-B radiation by a specific receptor UV RESISTANCE LOCUS 8 (UVR8) and respond to frequently varying levels of UV-B in natural environments by UV-B-specific (commonly UVR8-mediated) or nonspecific signaling pathways (Jenkins, 2009). In addition to the intensity or dose, the variation in the sources (wavelength, broad-band, or narrow-band), manipulation (timing or duration), and setup (greenhouse or chamber) can affect the plant's perception of UV-B radiation, triggering different signaling pathways (Meyer et al., 2021).

In the present study, the UV-B LED used was narrow-banded with a peak at 310 nm and was supplemented at pre-harvest (Fig. 3-2). Rechner et al. (2016) reported that quercetin and kaempferol glycosides in broccoli were highest after supplementation with UV-B radiation at 310 nm among different short-wavelengths from 310 to 420 nm. Both ABV-UV and BTW-UV treatments significantly increased the phenolic contents, except for TAC, and AOC in kale leaves (Table 3-2). In blueberry leaves, the anthocyanin content under UV-B

157

exposure increased only at long durations or high intensities (Inostroza-Blancheteau et al., 2014). These results might be caused by the time sequence in the expression of anthocyanin biosynthesis-related genes (Su et al., 2016). In the flavonoid biosynthesis, early biosynthesis genes (such as chalcone synthase, chalcone isomerase, and flavanone 3-hydroxylase) are induced prior to late biosynthesis genes (such as dihydroflavonol 4-reductase and anthocyanidin synthase) directly related to anthocyanin synthesis. Therefore, the TAC in the present study might have increased with higher UV-B doses or longer recovery times. The AOC was more strongly correlated with UAPC than with TPC or TFC ($r = 0.63$ or 0.57, respectively, at $P < 0.01$). These results were caused by the difference in reactivities of determination methods to various polyphenols as reported by Csepregi et al. (2013, 2016). On the other hand, the pre-harvest and short-term UV-B treatment in the present study did not decrease the growth or photosynthetic pigment contents (Table 3-1). Mosadegh et al. (2019) showed that the chlorophyll contents in basil were maintained after short-term UV-B exposure but decreased after longer UV-B exposure as the recovery time prolonged. Therefore, short-term pre-harvest UV-B exposure is effective in enhancing the phenolic content in kale plants without growth reduction.

Variables affecting UV-B radiation distribution in controlled environments

In controlled environments, lighting systems should ensure sufficient light and efficient energy use and be optimized with a methodology combining numerous

optical and physical factors (Kozai, 2018). To evaluate the light environment with consideration of the relevant factors, optical simulation methods with 3D models have been used (Kim et al., 2016, 2020a; Shin et al., 2021). Especially in plant factories, the number of light sources, the distance between them and the physical light distribution have significant impacts on the uniformity and utilization efficiency of light absorption in the plant canopy (Saito et al., 2020).

In the scenarios of the present study, similarly, the lighting distance and angle of UV-B LEDs affected the distribution of UV-B radiation interception in kale plants (Figs. 3-3, 3-7, 3-8, 3-9). A lower CV_{UVR} means more uniform UVR_{int} between the leaves (Table 3-3). When uniform radiation interception was a priority, the optimal horizontal lighting distance was two-thirds of the plant width (2/3W), and the optimal lighting angle was 60° located at the ellipse surrounding the plant (60AE). Since the scenarios were employed with one row of plants, however, the results may vary depending on the cultivation space or plant canopy. The total UVR_{int} per plant was highest with the UV-B LED arrangement placed at half of the plant height in the center of the plant row (0.5H, 0W, and 0AE). Similarly, Kim et al. (2020b) reported that light sources arranged vertically above the plant increased the light interception more greatly in lettuce plants, but decreased the uniformity compared to those arranged between the plants. This result might be due to the formation of the plant structure with a wide leaf inclination angle depending on the growth lighting located at the top and the low planting density. In addition to maximizing light

interception, the LED arrangement and lighting distance could be optimized to maximize canopy photosynthesis (Kim et al., 2020b). For the use of UV-B radiation, the lighting system targeted the specific bioactive compounds in plants. In this study, ABV-UV and BTW-UV treatments differed only in the LED bar arrangement (Fig. 3-2b). Although the total UVR_{int} per plant differed by 12.0% between UV-B treatments, the difference in TFC was 30.7% (Fig. 3-4, Table 3-2). Since the effect of UVR_{int} depended on the leaf position, the increase in total UVR_{int} cannot entirely lead to the increases in TPC or TFC. In scenarios 2 and 3, the increased UVR_{int} in mid-lower leaves induced increases in RUE_{int} for TPC and TFC, although the total UVR_{int} was decreased (Tables 3-3, 3-4). Therefore, the UV-B lighting system, including the light source arrangement, should be optimized to maximize phenolic production rather than radiation interception.

Prediction of phenolic content with UV-B radiation interception

Exploring specific variables influencing the accumulation of bioactive compounds and their quantitative relationships can serve as a starting point for the optimization of the compound production. The intraindividual distribution of UV-B-induced phenolic content in kale plants grown under the same growth conditions could be explained by both leaf developmental age and UVR_{int} as physical and physiological bases (Yoon et al., 2021a). The effect of UVR_{int}, i.e., UV-B energy yield for phenolic accumulation, depended on the leaf position

160

and growth stage (Yoon et al., 2021b). Previous studies and empirical data (unpublished) showed a linear pattern of phenolic accumulation with short-term UV-B dose or a quadratic pattern with leaf age (Dou et al., 2019; Yoon et al., 2021a, b). Such optimizations have mostly been reported in studies of in vitro plant tissue culture (Ghorbani et al., 2015; Farjaminezhad and Garoosi, 2021). The tissue culture provides a number of advantages similar to plant factories, including independence from external variation, uniform quality and yield, and relatively short cycle without pesticide use (Espinosa-Leal et al., 2018). The production of bioactive compounds was optimized with statistical modeling or machine learning (García-Pérez et al., 2020; Farjaminezhad and Garoosi, 2021).

In the present study, the models for predicting TPC or TFC per leaf in kale plants were developed using multiple regression analysis based on the previously developed model structures (Figs. 3-5, 3-6). As a limitation, these models were based on the relationship in non-acclimated plants exposed to pre-harvest short-term UV-B radiation. Due to the dynamics of UVR8 signaling depending on whether the plants are acclimated to UV-B radiation, the response in UV-B-acclimated plants could not be estimated accurately (Liao et al., 2020). Phenolic content is affected by various environmental factors, such as light intensity and spectrum, drought, salinity, and UV-B radiation (Li et al., 2020). The UV-B-induced responses also depended on interactions with those factors (Escobar-Bravo et al., 2017). Therefore, the models used in the present study were applicable only to kale plants grown under the same growth conditions

with pre-harvest short-term UV-B exposure. The prediction models could extensively be applied with various physical scopes. Optical simulation can analyze numerous variables of the lighting system mentioned above (Kozai, 2018; Kim et al., 2020b; Saito et al., 2020). Therefore, the prediction of TPC and TFC based on the simulation is applicable to various types of plant factories implemented with a 3D model.

Optimization of UV-B LED lighting design for total phenolic production

The variables of UV-B LED arrangements could be optimized to enhance efficiency or uniformity of total phenolic production, represented by low CV or high RUE, respectively (Table 3-4). The priority for the optimization may vary depending on the purpose, but in general, how much the content has increased relative to the input energy, i.e., the yield, is important. Across all scenarios, the maximum TPC yield (RUE_{TPC}) was obtained with UV-B LED bars arranged at one-third of the plant width from the center of the plant row (1/3W) or with a lighting angle of 60° at the ellipse surrounding the plant (60AE). For maximum TFC yield (RUE_{TFC}), the optimal UV-B LED arrangement was employed at half of the plant height in the center of the plant row (0.5H, 0W, and 0AE). This simulation-based scenario analysis could be applied to numerous parameters related to cultivation space, plants, and LED spacing (Kozai et al., 2016). Ultimately, these optimization methods will allow us to design UV-B lighting strategies and to achieve efficient, uniform, and stable production of bioactive

162

compounds in various plant factories.

The addition of UV-B lighting to plant factories increased the annual productivity of total phenolics and total flavonoids when compared to those without UV-B radiation (Table 3-5). The estimation can help make decisions about the introduction of artificial UV-B light sources in commercial plant factories. The electric input power of RBW LEDs was 24.1 W per plant in the experiment, requiring 10.8 kWh of electrical energy per plant for 28 days with 16-h light period. Under the experiment (ABV-UV) or scenario (0.5H) conditions, the electric input power of UV-B LEDs was 49.7 or 66.3 W per plant, so the electrical energy was 0.6 or 0.8 kWh per plant for 12 h at harvest, respectively. Under the virtual plant factory conditions, UV-B LEDs will incur an additional cost equivalent to 5.5-7.4% of the total electrical energy for LEDs. However, the yields per electrical energy consumed for producing total phenolics and total flavonoids will be increased by 9.2-14.2 and 22.1-34.0%, respectively, compared to those without UV-B radiation. The wall-plug efficiency of LED, which is the ratio of optical output power to electric input power, is much lower for UV LEDs than for visible light LEDs and is expected to be approximately 10% (Kneissl et al., 2019). Since the distance and number of LED chips were set based on the plant row, they can be reduced and optimized depending on the planting spacing. For UV-B LED application to plant factories, therefore, the optical efficiency should be improved through material and packaging technology development, and investment costs should

be saved through commercialized UV-B LED module production.

In summary, short-term pre-harvest UV-B exposure was an effective photo-elicitor to enhance the phenolic contents in kale plants. Even with the same dose, the UV-B LED arrangement caused a difference in the spatial distribution of UV radiation interception, inducing different phenolic accumulation. UV-B-induced phenolic accumulation was predicted with combination of structural and physiological factors, i.e., UV-B radiation interception in plant structures and leaf order (related leaf age). The simulation-based analysis of scenarios could optimize the UV-B LED lighting system for phenolic accumulation in plants. The estimated annual productivity of total phenolics in a virtual plant factory confirmed that the addition of UV-B lighting was effective enough to be commensurate with the increase at the plant factory scale. These results will contribute to increasing the commercial application of UV-B lighting for phenolic production in plant factories.

LITERATURE CITED

Ainsworth EA, Gillespie KM (2007) Estimation of total phenolic content and other oxidation substrates in plant tissues using Folin-Ciocalteu reagent. Nat Protoc 2:875–877.

Brand-Williams W, Cuvelier ME, Berset C (1995) Use of a free radical method to evaluate antioxidant activity. LWT Food Sci Technol 28:25–30.

Csepregi K, Kocsis M, Hideg É (2013) On the spectrophotometric determination of total phenolic and flavonoid contents. Acta Biol Hung 64:500–509.

Csepregi K, Neugart S, Schreiner M, Hideg É (2016) Comparative evaluation of total antioxidant capacities of plant polyphenols. Molecules 21:208.

Dewanto V, Xianzhong W, Adom KK, Liu RH (2002) Thermal processing enhances the nutritional value of tomatoes by increasing total antioxidant activity. J Agric Food Chem 50:3010–3014.

Dou H, Niu G, Gu M (2019) Pre-harvest UV-B radiation and photosynthetic photon flux density interactively affect plant photosynthesis, growth, and secondary metabolites accumulation in basil (*Ocimum Basilicum*) plants. Agronomy 9:434.

Escobar-Bravo R, Klinkhamer PGL, Leiss KA (2017) Interactive effects of UV-B light with abiotic factors on plant growth and chemistry, and their consequences for defense against arthropod herbivores. Front Plant Sci 8:1–

14.

Espinosa-Leal CA, Puente-Garza CA, García-Lara S (2018) In vitro plant tissue culture: Means for production of biological active compounds. Planta 248:1–18.

Farjaminezhad R, Garoosi G (2021) Improvement and prediction of secondary metabolites production under yeast extract elicitation of *Azadirachta indica* cell suspension culture using response surface methodology. AMB Express 11:43.

Flint SD, Caldwell MM (2003) A biological spectral weighting function for ozone depletion research with higher plants. Physiol Plant 117:137–144.

García-Pérez P, Lozano-Milo E, Landín M, Gallego PP (2020) Combining medicinal plant in vitro culture with machine learning technologies for maximizing the production of phenolic compounds. Antioxidants 9:210.

Ghorbani M, Ghorbani A, Omidi M, Hashemi SM (2015) Response surface modeling of noradrenaline production in hairy root culture of purslane (*Portulaca oleracea* L.). Turkish J Agric Food Sci Technol 3:349.

Graamans L, Baeza E, van den Dobbelsteen A, Tsafaras I, Stanghellini C (2018) Plant factories versus greenhouses: Comparison of resource use efficiency. Agric Syst 160:31–43.

Inostroza-Blancheteau C, Reyes-Díaz M, Arellano A, Latsague M, Acevedo P, Loyola R, Arce-Johnson P, Alberdi M (2014) Effects of UV-B radiation on anatomical characteristics, phenolic compounds, and gene expression of the

phenylpropanoid pathway in highbush blueberry leaves. Plant Physiol Biochem 85:85–95.

Isah T (2019) Stress and defense responses in plant secondary metabolites production. Biol Res 52:39.

Jenkins GI (2009) Signal transduction in responses to UV-B radiation. Annu Rev Plant Biol 60:407–431.

Joshi J, Zhang G, Shen S, Supaibulwatana K, Watanabe CKA, Yamori W (2017) A combination of downward lighting and supplemental upward lighting improves plant growth in a closed plant factory with artificial lighting. HortScience 52:831–835.

Khudyakova AY, Kreslavski VD, Shmarev AN, Lyubimov VY, Shirshikova GN, Pashkovskiy PP, Kuznetsov VV, Allakhverdiev SI (2019) Impact of UV-B radiation on the photosystem II activity, pro-/antioxidant balance, and expression of light-activated genes in *Arabidopsis thaliana hy4* mutants grown under light of different spectral composition. J Photochem Photobiol B Biol 194:14–20.

Kim D, Kang WH, Hwang I, Kim J, Kim JH, Park KS, Son JE (2020a) Use of structurally-accurate 3D plant models for estimating light interception and photosynthesis of sweet pepper (*Capsicum annuum*) plants. Comput Electron Agric 177:105689.

Kim J, Kang WH, Son JE (2020b) Interpretation and evaluation of electrical lighting in plant factories with ray-tracing simulation and 3D plant

modeling. Agronomy 10:1545.

Kim JH, Lee JW, Ahn TI, Shin JH, Park KS, Son JE (2016) Sweet pepper (*Capsicum annuum* L.) canopy photosynthesis modeling using 3D plant architecture and light ray-tracing. Front Plant Sci 7:1–10.

Kneissl M, Seong T-Y, Han J, Amano H (2019) The emergence and prospects of deep-ultraviolet light-emitting diode technologies. Nat Photonics 13:233–244.

Kozai T (2018) Smart plant factory. Springer, Singapore.

Kozai T, Fujiwara K, Runkle ES (2016) LED lighting for urban agriculture. Springer, Singapore.

Kozai T, Niu G, Takagaki M (2019) Plant factory: An indoor vertical farming system for efficient quality food production, 2nd Edn., Academic Press, New York, NY, USA.

Li Y, Kong D, Fu Y, Sussman MR, Wu H (2020) The effect of developmental and environmental factors on secondary metabolites in medicinal plants. Plant Physiol Biochem 148:80–89.

Liao X, Liu W, Yang H, Jenkins GI (2020) A dynamic model of UVR8 photoreceptor signaling in UV-B-acclimated *Arabidopsis*. New Phytol 227:857–866.

Lichtenthaler HK, Buschmann C (2001) Chlorophylls and carotenoids: Measurement and characterization by UV-VIS spectroscopy. Curr Protoc Food Anal Chem 1:F4.3.1-F4.3.8.

Loconsole D, Santamaria P (2021) UV lighting in horticulture: A sustainable tool for improving production quality and food safety. Horticulturae 7:9.

Matsuura HN, de Costa F, Yendo ACA, Fett-Neto AG (2013) Photoelicitation of bioactive secondary metabolites by ultraviolet radiation: Mechanisms, strategies, and applications. In: Chandra S, Lata H, Varma A (Eds.) Biotechnology for medicinal plants. Springer, Berlin, pp 171–190.

Meyer P, Van de Poel B, De Coninck B (2021) UV-B light and its application potential to reduce disease and pest incidence in crops. Hortic Res 8:194.

Mosadegh H, Trivellini A, Lucchesini M, Ferrante A, Maggini R, Vernieri P, Sodi AM (2019) UV-B physiological changes under conditions of distress and eustress in sweet basil. Plants 8:396.

Neugart S, Schreiner M (2018) UVB and UVA as eustressors in horticultural and agricultural crops. Sci Hortic 234:370–381.

Re R, Pellegrini N, Proteggente A, Pannala A, Yang M, Rice-Evans C (1999) Antioxidant activity applying an improved ABTS radical cation decolorization assay. Free Radic Biol Med 26:1231–1237.

Rechner O, Neugart S, Schreiner M, Wu S, Poehling H-M (2016) Different narrow-band light ranges alter plant secondary metabolism and plant defense response to aphids. J Chem Ecol 42:989–1003.

Robson TM, Aphalo PJ, Banaś AK, Barnes PW, Brelsford CC, Jenkins GI, Kotilainen TK, Łabuz J, Martínez-Abaigar J, Morales LO, Neugart S, Pieristè M, Rai N, Vandenbussche F, Jansen MAK (2019) A perspective on

ecologically relevant plant-UV research and its practical application. Photochem Photobiol Sci 18:970–988.

Saito K, Ishigami Y, Goto E (2020) Evaluation of the light environment of a plant factory with artificial light by using an optical simulation. Agronomy 10:1663.

Šamec D, Urlić B, Salopek-Sondi B (2019) Kale (*Brassica oleracea* var. *acephala*) as a superfood: Review of the scientific evidence behind the statement. Crit Rev Food Sci Nutr 59:2411–2422.

Santin M, Ranieri A, Castagna A (2021) Anything new under the sun? An update on modulation of bioactive compounds by different wavelengths in agricultural plants. Plants 10:1485.

SharathKumar M, Heuvelink E, Marcelis LFM (2020) Vertical farming: Moving from genetic to environmental modification. Trends Plant Sci 25:724–727.

Shin J, Hwang I, Kim D, Moon T, Kim J, Kang WH, Son JE (2021) Evaluation of the light profile and carbon assimilation of tomato plants in greenhouses with respect to film diffuseness and regional solar radiation using ray-tracing simulation. Agric For Meteorol 296:108219.

Si C, Yao XQ, He XL, Chu JZ, Ma CH, Shi XF (2015) Effects of enhanced UV-B radiation on biochemical traits in postharvest flowers of medicinal chrysanthemum. Photochem Photobiol 91:845–850.

Su N, Lu Y, Wu Q, Liu Y, Xia Y, Xia K, Cui J (2016) UV-B-induced anthocyanin

accumulation in hypocotyls of radish sprouts continues in the dark after irradiation. J Sci Food Agric 96:886–892.

Sytar O, Bośko P, Živčák M, Brestic M, Smetanska I (2018) Bioactive phytochemicals and antioxidant properties of the grains and sprouts of colored wheat genotypes. Molecules 23:2282.

Thakur M, Bhattacharya S, Khosla PK, Puri S (2019) Improving production of plant secondary metabolites through biotic and abiotic elicitation. J Appl Res Med Aromat Plants 12:1–12.

Toscano S, Trivellini A, Cocetta G, Bulgari R, Francini A, Romano D, Ferrante A (2019) Effect of preharvest abiotic stresses on the accumulation of bioactive compounds in horticultural produce. Front Plant Sci 10:1–17.

Yoon HI, Kim D, Son JE (2020) Spatial and temporal bioactive compound contents and chlorophyll fluorescence of kale (*Brassica oleracea* L.) under UV-B exposure near harvest time in controlled environments. Photochem Photobiol 96:845–852.

Yoon HI, Kim HY, Kim J, Oh MM, Son JE (2021a) Quantitative analysis of UV-B radiation interception in 3D plant structures and intraindividual distribution of phenolic contents. Int J Mol Sci 22:2701.

Yoon HI, Kim HY, Kim J, Son JE (2021b) Quantitative analysis of UV-B radiation interception and bioactive compound contents in kale by leaf position according to growth progress. Front Plant Sci 12:667456.

Yoon HI, Kim JS, Kim D, Kim CY, Son JE (2019) Harvest strategies to

maximize the annual production of bioactive compounds, glucosinolates, and total antioxidant activities of kale in plant factories. Hortic Environ Biotechnol 60:883–894.

CONCLUSIONS

This study confirmed the quantitative relationship between total phenolic accumulation and UV-B radiation interception in three-dimensional plant structure in a plant factory. The pre-harvest UV-B radiation was an effective photo-elicitor to enhance the phenolic content and antioxidant capacity without noticeable damage in kale plants. The quantification of UV-B radiation interceptions in the plant structure confirmed their contribution to the heterogeneous distribution of total phenolic content. In the plant structure at different growth stages, the UV-B-induced phenolic content in individual leaves could be predicted with multiple regression models based on daily UV-B radiation interception and developmental age. From the models, the UV-B energy yield was found to depend on the plant and leaf developmental ages. These results provided the fundamental data and models required for the optimization process. The factors of UV-B lighting systems were evaluated and optimized through the model-based simulation. This study first proposed the statistical models for predicting UV-B-induced phenolic content in plants. This approach could be used to find out optimal UV-B condition and will contribute to increasing the commercial application of UV-B lighting for phenolic production in plant factories.

ABSTRACT IN KOREAN

280–315nm 영역대의 자외선(UV–B)은 식물의 생리 활성 화합물을 증진시키는 광 유도원으로 이용되어 왔다. 식물 구조 내에서 잎 위치별 불균일한 UV–B 노출과 UV–B에 대한 발달 연령 의존적 민감도로 인한 페놀 화합물의 국소적 축적은 예측할 수 없었다. 본 연구에서는 식물 구조에서 UV–B에 의해 유발된 페놀 화합물 함량과 UV–B 수광량 사이의 관계를 분석하고, 그 함량 분포의 추정을 위한 통계적 모델을 개발하고 시뮬레이션 기반의 시나리오 분석을 통해 식물공장의 UV–B 발광 다이오드(LED) 조명 시스템을 평가하고 최적화하였다. 케일(*Brassica oleracea* L. var. *acephala*)은 식물공장에서 3, 4, 5주간 재배하였으며 310nm 피크의 UV–B LED를 수확 전 1일 또는 2일 동안 하루 12시간씩 조사하였다. 케일에서 UV–B 수광량(UV–B radiation interception, UVR_{int})의 공간 분포는 3차원 스캔 식물 모델과 함께 광 추적 시뮬레이션을 사용하여 정량화하였다. 수확 시기에 따른 페놀 화합물 함량에 대한 다중 회귀 모델은 2차 다항식을 사용하여 각 잎의 일 누적 UVR_{int} 및 발달 연령을 기반으로 개발하였으며 UV–B LED 배열에 따른 회귀 분석을 수행하여 매개변수를 추정하였다. 시나리오 분석은 UV–B의 수직 또는 수평 거리, 조사 각도와 같은 조명 시스템 요인에 대해 수행하였다. 단기 UV–B 조사로 케일의 생육 및 광화학적 활성, 엽록소 함량에 유의한 변화가 나타나지 않았으나 총 페놀 화합물(total phenolic content, TPC)과 총 플라보노이드 화합물(total flavonoid content, TFC) 및 UV–B 흡수 색소의 함량과 항산화능은 UV–B를 조사한 잎에서 유의하게 증가하였다. 한 식물 개체 수준에서 TPC 또는 TFC의 개체 내 분포는 일 누적 UVR_{int} 및 엽 순서에 의해 결정할 수 있었으며, UV–B를 조사하지 않은 경우보다 더 이질적으로 나타났다. 개발된 모델은 테스트 데이터에서 0.78

이상의 R^2 값과 약 30%의 오차율로 높은 정확성을 나타내었다. 모델 결과에서 UV-B 에너지 수율이 식물 및 엽 발달 연령에 의존한다는 것을 확인하였다. 대부분의 시나리오 분석 결과에서 TPC 또는 TFC 생산량의 균일성과 효율성은 반대 경향을 나타내었다. 본 연구에서 개발한 UV-B 수광량에 따른 추정 모델은 UV-B 이용 효율을 높이고 조명 시스템을 최적화하는 데 활용할 수 있을 것으로 판단하였다. 또한 본 연구 결과는 식물공장에서 생리 활성 화합물 생산을 위한 UV-B 광원의 적용을 증가시키는 데 기여할 것으로 기대하였다.

추가 주요어: 광 추적 시뮬레이션, 비생물적 스트레스, 생리 활성 화합물, 식물공장, 이차대사산물, 플라보노이드, 항산화

학번: 2018-35422

Determination of leaf group according to growth stage based on relative growth rates

Leaf groups at each growth stage were characterized with the changes of leaf fresh mass and leaf area over a time span of 7-8 days. Leaf fresh mass and leaf area were measured separately for kale plants harvested at 15, 23, 30, and 38 days after transplanting (DAT) with four plants per treatment (Fig. A2-1).
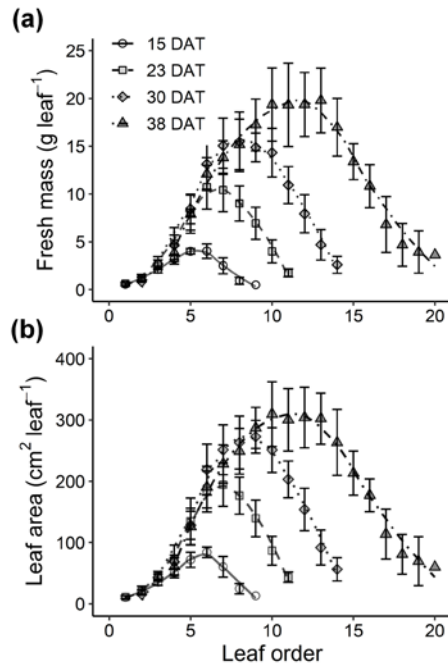
The relative growth rate (RGR) and relative expansion rate (RER) were calculated as (Behn et al., 2011; Pontarin et al., 2020):

$$\text{RGR (g g}^{-1}\text{ d}^{-1}\text{)} = [\ln(FM_{t2}) - \ln(FM_{t1})]/(t_2 - t_1) \qquad \text{Eq. A2-1}$$

$$\text{RER (cm cm}^{-1}\text{ d}^{-1}\text{)} = [\ln(LA_{t2}) - \ln(LA_{t1})]/(t_2 - t_1) \qquad \text{Eq. A2-2}$$

where FM is the individual leaf fresh mass (g), LA is the individual leaf area (cm^2) at DAT = t, and t is the time span (day). In this study, leaf RGR and RER were calculated between sampling days at 15-23, 23-30, and 30-38 DAT. When the leaf did not appear at the prior time, their RGR and RER values were inferred by interpolation by fitting a regression. The values were regressed with quadratic function of leaf order (L), and all R^2 was 0.99 (Fig. A2-2).

$$\text{RGR (23 DAT)} = 0.119 + 0.318\,L + 0.100\,L^2$$

Fig. A2-1. Leaf fresh mass (a) and leaf area (b) of kale plants according to leaf order and growth stage at 23, 30, and 38 days after transplanting (DAT).
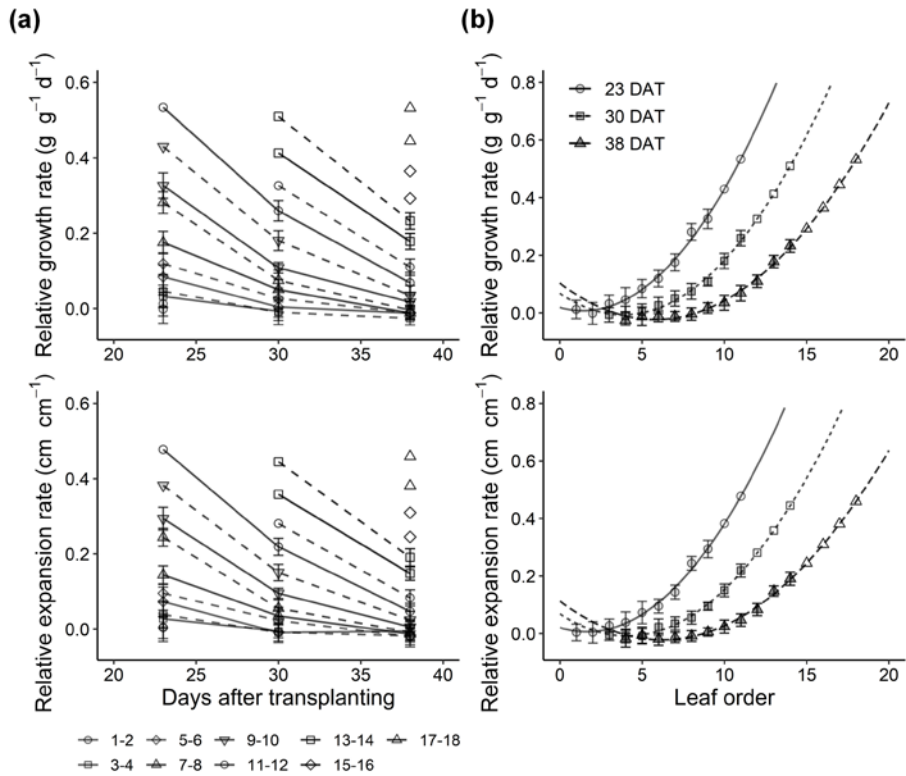
Fig. A2-2. Leaf relative growth rate and expansion rate of leaf populations in kale plants according to 23, 30, and 38 days after transplanting (DAT, a) and leaf order (b). Open points indicate interpolated values by fitting a regression since the leaf did not appear at the prior time. All R^2 of regression lines with leaf order in the left panels were 0.99. The solid and dashed lines in the right panels indicate odd and even leaf orders (the absolute order of leaf emergence), respectively.

RGR (30 DAT) = 0.076 + 0.244 L + 0.088 L^2

RGR (38 DAT) = 0.052 + 0.249 L + 0.110 L^2

RER (23 DAT) = 0.103 + 0.280 L + 0.094 L^2

RER (30 DAT) = 0.062 + 0.208 L + 0.081 L^2

RER (38 DAT) = 0.040 + 0.202 L + 0.102 L^2

On all these dates, the older leaves presented RGR and RER values close to zero, and their values did not change between the dates. As the growth progressed, the gaps in both RGR and RER values between the leaves narrowed. Based on these patterns, the leaf populations at each growth stage were divided into three leaf groups. The RGR and RER values of leaf groups and the assigned leaf order at each growth stage are shown in Table A2-1.

Total growth parameter

Total fresh mass, leaf area, and root dry mass were measured separately for kale plants harvested at 15, 23, 30, and 38 DAT with four plants per treatment (Fig. A2-3). All parameters were not significantly different among the treatments by one-way ANOVA at $P < 0.05$.

Phenolic contents per leaf according to UV-B radiation and growth stage

Total phenolic content (TPC), total flavonoid content (TFC), total anthocyanin content (TAC), UV-absorbing pigment content (UAPC), and ascorbic acid

Table A2-1. The relative growth rate (RGR), relative expansion rate (RER) of leaf groups and the assigned leaf order in kale plants at 23, 30, and 38 days after transplanting (DAT).

DAT	Leaf group	RGR (g g^{-1} d^{-1})	RER (cm cm^{-1} d^{-1})	Leaf order
23	1	< 0.04	< 0.3	1-3
	2	0.05-0.18	0.04-0.15	4-7
	3	0.28-0.53	0.24-0.48	8-11
30	1	< 0.03	< 0.03	3-6
	2	0.05-0.11	0.04-0.10	7-9
	3	0.18-0.51	0.15-0.45	10-14
38	1	< 0.01	< 0.01	4-8
	2	0.02-0.11	0.01-0.08	9-12
	3	0.18-0.53	0.15-0.46	13-18

RGR and RER values were obtained at 15-23, 23-30, and 30-38 DAT, and referred to Eqs. A2-1, A2-2, and Figs. A2-1, A2-2.
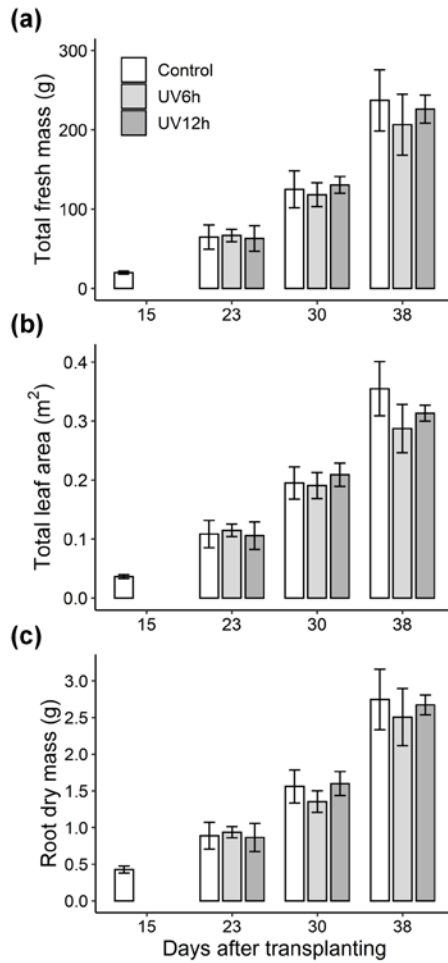
Fig. A2-3. Total fresh mass (a), leaf area (b), and root dry mass (c) of kale plants according to UV-B radiation and growth stage at 15, 23, 30, and 38 days after transplanting. Vertical bars indicate SD, $n = 4$.

equivalent antioxidant capacities using ABTS (AOC_{ABTS}) and DPPH assays (AOC_{DPPH}) per leaf were calculated by multiplying their concentrations (mg eq. g^{-1} DM) by the leaf dry mass (g DM). The phenolic contents per leaf were compared according to UV-B radiation by one-way ANOVA and Tukey's HSD test and compared according to leaf groups and growth stages by two-way ANOVA and post-hoc test referring to Materials and Methods in Chapter 2.

The TPC, TFC, TAC, UAPC, AOC_{ABTS}, and AOC_{DPPH} per leaf were significantly higher on the order of 38, 30, and 23 DAT, with the values affected by the leaf dry mass (Fig. A2-4). All of the values were significantly higher in leaf groups 2 and 3 than in the group 1, except for TAC, and were higher with UV-B radiation at each leaf group, except for the group 1 at 30 DAT.
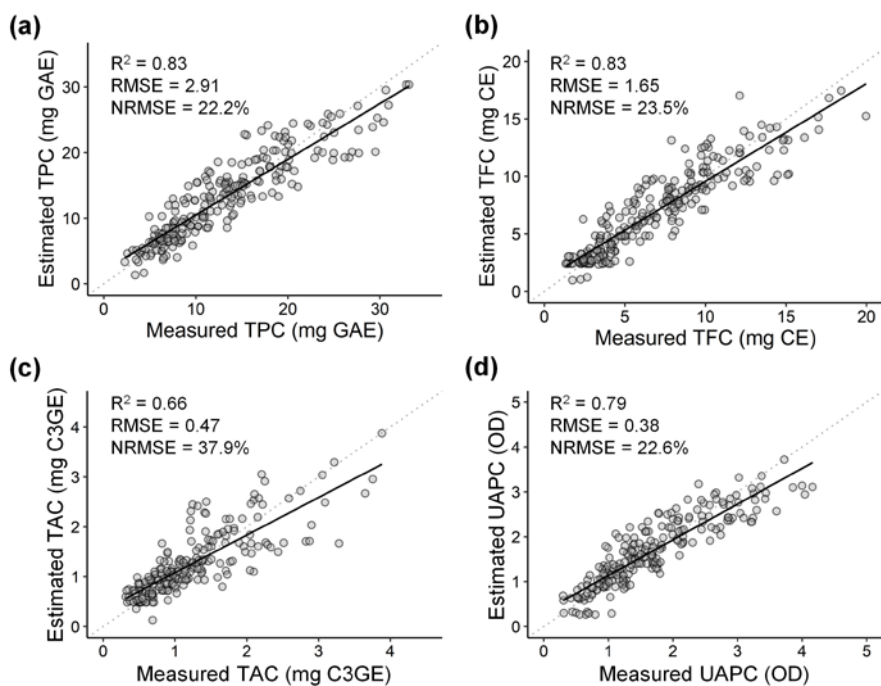
Comparisons of measured and estimated phenolic contents per leaf

Multiple regression models for predicting the phenolic contents were obtained by stepwise regression using backward elimination method based on a second-order multi-polynomial model in Eq. 2-1. The regression models were selected with significance of all independent variables, and finally developed models are shown in Fig. 2-4 and Table 2-3. In the data set using the model development, the measured and estimated contents were compared across all growth stages (Fig. A2-5). The R^2 for the four models was higher in the data set integrated from the models across whole growth stage than in the models at each growth stage (Table 2-3).
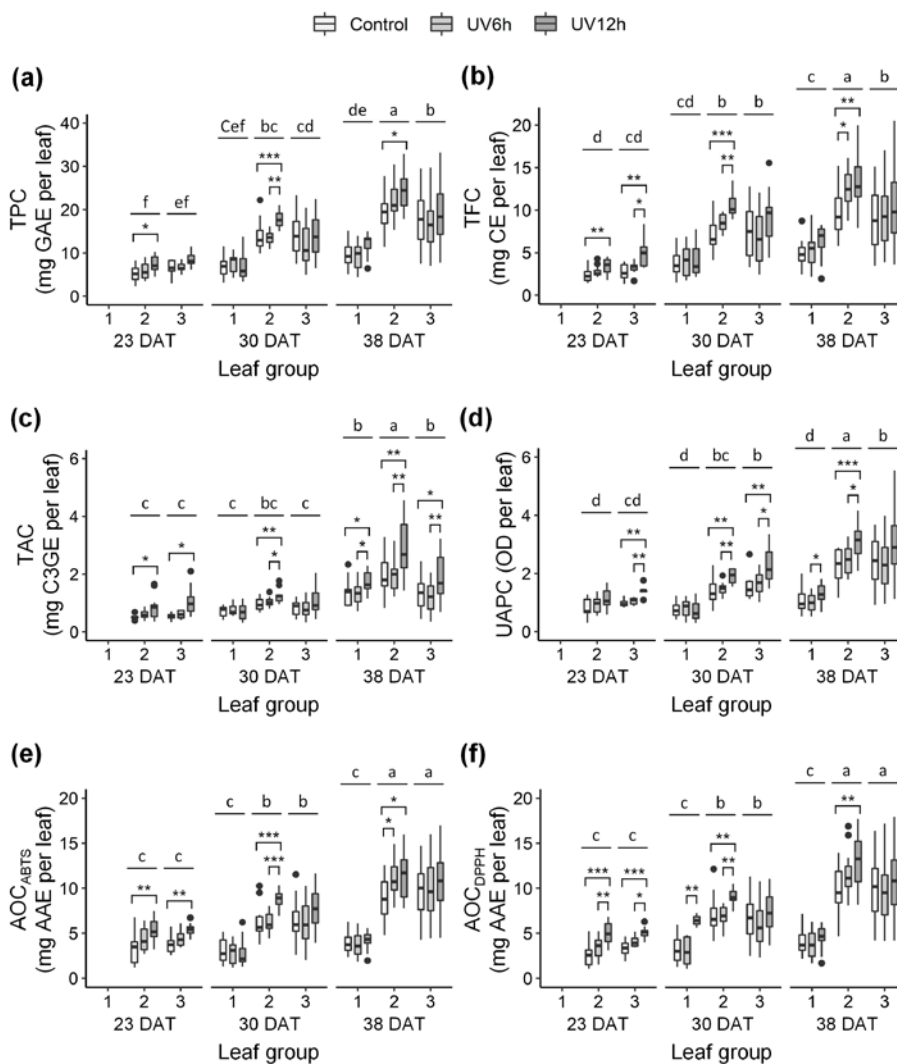
Fig. A2-4. Total phenolic content (TPC, a), total flavonoid content (TFC, b), total anthocyanin content (TAC, c), UV-absorbing pigment content (UAPC, d), and antioxidant capacity using ABTS (AOC_{ABTS}, e) and DPPH assays (AOC_{DPPH}, f) per leaf of kale plants according to UV-B radiation and leaf group at 23, 30, and 38 days after transplanting (DAT). Asterisks indicates significant differences between UV-B treatments at each growth stage and leaf group by one-way ANOVA and Tukey's HSD test, *, $P < 0.05$; **, $P < 0.01$; ***, $P < 0.001$; ($n = 7$-13). Different letters indicate significant

differences among growth stage and leaf group at $P < 0.05$ by two-way ANOVA and post-hoc test ($n = 20\text{-}50$) referring to Materials and Methods.

Fig. A2-5. Comparison between measured and estimated phenolic contents per leaf of kale plants in the data set integrated from the models across all growth stages. TPC, total phenolic content (a); TFC, total flavonoid content (b); TAC, total anthocyanin content (c); UAPC, UV-absorbing pigment content (d). The coefficient of determination (R^2), root mean squared error (RMSE), and the normalized RMSE (NRMSE) are presented inside each panel.